



Czech University of Life Sciences Prague  
Faculty of Environmental Sciences  
*Department of Water Resources and Environmental modelling*  
Environmental Modelling Program

---

# Semi-distributed Hydrological Model of Amalie Site

Master thesis of:  
**Hossein Abbasizadeh**

Supervisor:  
**doc. Ing. Petr Maca, Ph.D.**

30.03.2022



Czech University of Life Sciences Prague

Faculty of Environmental Sciences

### DIPLOMA THESIS TOPIC

Author of thesis:	MSc. Hossein Abbasizadeh, MSc
Study programme:	Environmental Modelling
Thesis supervisor:	doc. Ing. Petr Máca, Ph.D.
Supervising department:	Department of Water Resources and Environmental Modeling
Language of a thesis:	English
Thesis title:	<b>Semi-distributed hydrological model of Amalie site</b>
Objectives of thesis:	The aim of the thesis is to develop a semi distributed hydrological model for Amalie site. The Amalie site is formed of two small watersheds. Use available observations for constructing different semi distributed hydrological models and compare the calibration results for both watersheds.
Methodology:	The methodology consists of: <ol style="list-style-type: none"><li>1. Preparation of input data sets on Amalie site using different types of information</li><li>2. Derivation of different types of spatial discretizations of both Amalie watersheds</li><li>3. Creating semi distributed models using the dHRUM modeling framework</li><li>4. Calibration of semi distributed models using hydrological signatures and available observations</li></ol>
The proposed extent of the thesis:	standard
Keywords:	runoff, prediction, ungauged basins, dHRUM
Recommended information sources:	<ol style="list-style-type: none"><li>1. BEVEN, K J. <i>Rainfall-runoff modelling : the primer</i>. Chichester: Wiley-Blackwell, 2012. ISBN 978-0-470-71459-1.</li><li>2. Blöschl, G. and Blöschl, G. and Sivapalan, M. and Wagener, T. and Savenije, H. and Viglione, A.: <i>Runoff Prediction in Ungauged Basins: Synthesis Across Processes, Places and Scales</i>. Cambridge University Press,2013.</li><li>3. Web Science, Scopus and others</li></ol>
Expected date of thesis defence:	2021/22 SS - FES

# Author's Statement

Hereby declare that I have independently elaborated the diploma thesis with the topic of: **Semi-distributed hydrological model of Amalie site** and that I have cited all the information sources that I used in the thesis and that are also listed at the end of the thesis in the list of used information sources.

I am aware that my diploma thesis is subject to Act No. 121/2000 Coll., on copyright, on rights related to copyright and on amendment of some acts, as amended by later regulations, particularly the provisions of Section 35(3) of the act on the use of the thesis.

I am aware that by submitting the diploma thesis I agree with its publication under Act No. 111/1998 Coll., on universities and on the change and amendments of some acts, as amended, regardless of the result of its defence.

With my own signature, I also declare that the electronic version is identical to the printed version and the data stated in the thesis has been processed in relation to the GDPR.

**Hossein Abbasizadeh**

# Acknowledgement

I would like to thank my supervisor, doc. Ing. Petr Maca for his guidance and help throughout this project.

**Hossein Abbasizadeh**

# Abstract

In order to simulate the rainfall-runoff processes accurately in a catchment, it is essential to calibrate our hydrological model properly. A well-calibrated hydrological model can give us a profound insight into different hydrological processes and consequently enhance water management, floods and droughts prediction and risk assessment in the study area. In this study, a semi-distributed hydrological model of the Amalie site is developed. The model parameters are constrained and identified using expert knowledge and available information in the study area, like soil moisture content and groundwater level. The catchments in the study area are divided into two main basins, namely *Brejlský Potok* (BP) and *Karluv Luh* (KL), and each basin is discretized according to the soil type and drainage system. The obtained results show that constraining the solution space of the model parameters based on expert knowledge and available data can increase the model accuracy and decrease the level of equifinality in finding effective parameters. In addition, using *Groundwater* (GW) and *Soil Moisture* (SM) information can increase the accuracy of the simulated water balance and reduce the effects of different discretizations, *Hydrological Response Unit* (HRU) configurations, on fluxes and storage variables.

# Contents

<b>List of Figures</b>	<b>iv</b>
<b>List of Tables</b>	<b>ix</b>
<b>List of Acronyms</b>	<b>xi</b>
<b>1 Introduction</b>	<b>1</b>
1.1 Rainfall-Runoff Modelling . . . . .	1
1.2 Calibration of Hydrological Models . . . . .	4
1.3 Aims and Goals . . . . .	6
<b>2 Methodology</b>	<b>8</b>
2.1 Study Area . . . . .	8
2.2 Data . . . . .	12
2.2.1 Time Series . . . . .	13
2.2.2 Point information . . . . .	16
2.2.3 GIS Data . . . . .	17
2.3 Distributed Hydrological Response Unit Model (dHRUM) .	18
2.3.1 Discretization of Study Area . . . . .	19
2.4 Estimation of Model's Parameters . . . . .	23
2.4.1 Global Optimization by Differential Evolution . . . .	25
2.4.2 Objective Functions . . . . .	25
2.4.3 Soil Parameters . . . . .	26

2.4.4	Runoff Parameters . . . . .	29
2.4.5	Constraining Parameters . . . . .	31
<b>3</b>	<b>Results</b>	<b>36</b>
3.1	Expert Calibration . . . . .	36
3.1.1	Manual Sensitivity Analysis . . . . .	37
3.1.2	The Effects of Parameters on Model outputs . . . . .	37
3.1.3	The Effects Parameters on FDC . . . . .	39
3.2	Applying Expert Knowledge to Calibration Procedure . . . . .	41
3.3	Adding Soil moisture and Groundwater data to the Calibration Procedure . . . . .	46
3.3.1	Calibration Using Groundwater Information . . . . .	48
3.3.2	Calibration Using Soil Moisture Information . . . . .	56
3.3.3	Calibration Using Both Groundwater Level and Soil Moisture Information . . . . .	65
3.4	The Effects of Catchment Discretization on Water Balance . . . . .	76
3.4.1	State Variables . . . . .	76
3.4.2	Fluxes . . . . .	78
3.4.3	Storages . . . . .	89
<b>4</b>	<b>Discussion</b>	<b>99</b>
<b>5</b>	<b>Conclusion</b>	<b>103</b>
	<b>Bibliography</b>	<b>107</b>
	<b>Appendix A: Outputs from Expert Calibration</b>	<b>112</b>
	The model outputs for BP_S_FG catchment . . . . .	112
	The model outputs for KL_D_FG catchment . . . . .	114
	The model outputs for KL_S_FG catchment . . . . .	116
	<b>Appendix B: Calibration Results Using SM and GW Information</b>	<b>119</b>

BP\_D\_FG catchment . . . . . 119  
    Calibration Results Using GW . . . . . 119  
    Calibration Results Using SM . . . . . 121  
    Calibration Results Using Both GW and SM . . . . . 123  
BP\_S\_FG catchment . . . . . 124  
    Calibration Results Using GW . . . . . 124  
    Calibration Results Using SM . . . . . 126  
    Calibration Results Using Both GW and SM . . . . . 128  
KL\_D\_FG catchment . . . . . 129  
    Calibration Results Using GW . . . . . 129  
    Calibration Results Using SM . . . . . 131  
    Calibration Results Using Both GW and SM . . . . . 133  
KL\_S\_FG catchment . . . . . 135  
    Calibration Results Using GW . . . . . 135  
    Calibration Results Using SM . . . . . 138  
    Calibration Results Using Both GW and SM . . . . . 140

# List of Figures

2.2	Land cover in Amalie's arable land . . . . .	10
2.3	Land cover in Amalie's forested areas . . . . .	11
2.4	Hillshade map of study area . . . . .	12
2.5	Sensors' location . . . . .	15
2.6	TONST TDR . . . . .	16
2.7	Soil field capacity and wilting points . . . . .	17
2.8	Discretization based on drainage system . . . . .	21
2.9	Discretization based on soil retention capacity . . . . .	22
2.10	Amalie's drainage channel . . . . .	23
2.11	HRUs 1 and 8 . . . . .	27
2.12	C_max, C_min and B_soil . . . . .	28
3.1	Total runoff in BP_D_FG catchment . . . . .	42
3.2	Direct runoff in BP_D_FG catchment . . . . .	42
3.3	Baseflow in BP_D_FG catchment . . . . .	43
3.4	Interception storage in BP_D_FG catchment . . . . .	44
3.5	Canopy storage in BP_D_FG catchment . . . . .	44
3.6	Stem Storage in BP_D_FG catchment . . . . .	45
3.7	FDC of BP catchment (Expert calibration) . . . . .	45
3.8	FDC of KL catchment (Expert calibration) . . . . .	46
3.9	Sensor coverage in BP . . . . .	47
3.10	Sensor coverage in KL . . . . .	48

3.11	GW level variations in BP_D_FG . . . . .	49
3.12	GW level variations in BP_S_FG . . . . .	49
3.13	GW level variations in KL_D_FG . . . . .	50
3.14	GW level variations in KL_S_FG . . . . .	50
3.15	Scatter plots of BP for GW . . . . .	52
3.16	Scatter plots of KL . . . . .	53
3.17	FDC of BP catchment using GW data . . . . .	54
3.18	FDC of KL catchment using GW data . . . . .	55
3.19	SM variations in BP_D_FG . . . . .	56
3.20	SM variations in BP_S_FG . . . . .	57
3.21	SM variations in KL_D_FG . . . . .	57
3.22	SM variations in KL_S_FG . . . . .	58
3.23	Scatter plots of BP for SM . . . . .	60
3.24	Scatter plots of KL for SM . . . . .	61
3.25	FDC of BP catchment using SM data . . . . .	63
3.26	FDC of KL catchment using SM data . . . . .	64
3.27	GW and SM variations in BP_D_FG . . . . .	66
3.28	GW and SM variations in BP_S_FG . . . . .	66
3.29	GW and SM variations in KL_D_FG . . . . .	66
3.30	GW and SM variations in KL_S_FG . . . . .	67
3.31	Scatter plots of BP_D_FG for GW and SM . . . . .	70
3.32	Scatter plots of BP_S_FG for GW and SM . . . . .	71
3.33	Scatter plots of KL_D_FG for GW and SM . . . . .	72
3.34	Scatter plots of KL_L_FG for GW and SM . . . . .	73
3.35	FDC of BP catchment using GW and SM data . . . . .	74
3.36	FDC of KL catchment using GW and SM data . . . . .	75
3.37	Scattered plots of snow . . . . .	77
3.38	Scattered plots of baseflow . . . . .	79
3.39	Heatmap of baseflow . . . . .	80
3.40	Scattered plots of direct runoff . . . . .	81
3.41	Heatmap of direct runoff . . . . .	82

3.42	Scatted plots of percolation . . . . .	83
3.43	Heatmap of percolation . . . . .	84
3.44	Scatted plots of percolation . . . . .	85
3.45	Heatmap of total runoff . . . . .	86
3.46	Scatted plots of melting . . . . .	87
3.47	Heatmap of melting . . . . .	88
3.48	Scatted plots of GW storage . . . . .	90
3.49	Heatmap of GW storage . . . . .	91
3.50	Scatted plots of interception storage . . . . .	92
3.51	Heatmap of interception storage . . . . .	93
3.52	Scatted plots of soil storage . . . . .	94
3.53	Heatmap of soil storage . . . . .	95
3.54	Scatted plots of surface retention . . . . .	96
3.55	Heatmap of surface retention . . . . .	97
4.1	Modified FDCs of KL_D_FG catchment using coefficient 1 . .	101
4.2	Modified FDCs of KL_D_FG catchment using coefficient 2 . .	101
1	Total runoff in BP_S_FG catchment . . . . .	112
2	Direct runoff in BP_S_FG catchment . . . . .	113
3	Baseflow in BP_S_FG catchment . . . . .	113
4	Interception in BP_S_FG catchment . . . . .	114
5	Total runoff in KL_D_FG catchment . . . . .	114
6	Direct runoff in KL_D_FG catchment . . . . .	115
7	Baseflow in KL_D_FG catchment . . . . .	115
8	Interception in KL_D_FG catchment . . . . .	116
9	Total runoff in KL_S_FG catchment . . . . .	116
10	Direct runoff in KL_S_FG catchment . . . . .	117
11	Baseflow in KL_S_FG catchment . . . . .	117
12	Interception in KL_S_FG catchment . . . . .	118
13	GW variation in BP_D_FG catchment, in HRU 1 . . . . .	119

14 GW variation in BP\_D\_FG catchment, in HRU 2 . . . . . 120

15 GW variation in BP\_D\_FG catchment, in HRU 3 . . . . . 120

16 GW variation in BP\_D\_FG catchment, in HRU 4 . . . . . 121

17 SMvariation in BP\_D\_FG catchment, in HRU 1 . . . . . 121

18 SM variation in BP\_D\_FG catchment, in HRU 3 . . . . . 122

19 SM variation in BP\_D\_FG catchment, in HRU 8 . . . . . 122

20 GW and SM variation in BP\_D\_FG catchment, in HRU 1 . . 123

21 GW and SM variation in BP\_D\_FG catchment, in HRU 3 . . 123

22 GW and SM variation in BP\_D\_FG catchment, in HRU 4 . . 124

23 GW variation in BP\_S\_FG catchment, in HRU 6 . . . . . 124

24 GW variation in BP\_S\_FG catchment, in HRU 33 . . . . . 125

25 GW variation in BP\_S\_FG catchment, in HRU 34 . . . . . 125

26 GW variation in BP\_S\_FG catchment, in HRU 35 . . . . . 126

27 SM variation in BP\_S\_FG catchment, in HRU 33 . . . . . 126

28 SM variation in BP\_S\_FG catchment, in HRU 34 . . . . . 127

29 SM variation in BP\_S\_FG catchment, in HRU 35 . . . . . 127

30 GW and SM variation in BP\_S\_FG catchment, in HRU 33 . . 128

31 GW and SM variation in BP\_S\_FG catchment, in HRU 34 . . 128

32 GW and SM variation in BP\_D\_FG catchment, in HRU 35 . . 129

33 GW variation in KL\_D\_FG catchment, in HRU 2 . . . . . 129

34 GW variation in KL\_D\_FG catchment, in HRU 3 . . . . . 130

35 GW variation in KL\_D\_FG catchment, in HRU 4 . . . . . 130

36 GW variation in KL\_D\_FG catchment, in HRU 20 . . . . . 131

37 SM variation in KL\_D\_FG catchment, in HRU 1 . . . . . 131

38 SM variation in KL\_D\_FG catchment, in HRU 2 . . . . . 132

39 SM variation in BP\_S\_FG catchment, in HRU 3 . . . . . 132

40 SM variation in KL\_D\_FG catchment, in HRU 4 . . . . . 133

41 GW and SM variation in KL\_D\_FG catchment, in HRU 2 . . 133

42 GW and SM variation in KL\_D\_FG catchment, in HRU 3 . . 134

43 GW and SM variation in KL\_D\_FG catchment, in HRU 4 . . 134

44 GW and SM variation in KL\_D\_FG catchment, in HRU 20 . . 135

45 GW variation in KL\_S\_FG catchment, in HRU 10 . . . . . 135

46 GW variation in KL\_S\_FG catchment, in HRU 22 . . . . . 136

47 GW variation in KL\_S\_FG catchment, in HRU 23 . . . . . 136

48 GW variation in KL\_S\_FG catchment, in HRU 24 . . . . . 137

49 GW variation in KL\_S\_FG catchment, in HRU 28 . . . . . 137

50 SM variation in KL\_S\_FG catchment, in HRU 22 . . . . . 138

51 SM variation in KL\_S\_FG catchment, in HRU 23 . . . . . 138

52 SM variation in KL\_S\_FG catchment, in HRU 24 . . . . . 139

53 SM variation in KL\_S\_FG catchment, in HRU 27 . . . . . 139

54 SM variation in KL\_S\_FG catchment, in HRU 28 . . . . . 140

55 GW and SM variation in KL\_S\_FG catchment, in HRU 10 . . 140

56 GW and SM variation in KL\_S\_FG catchment, in HRU 22 . . 141

57 GW and SM variation in KL\_S\_FG catchment, in HRU 23 . . 141

58 GW and SM variation in KL\_S\_FG catchment, in HRU 24 . . 142

59 GW and SM variation in KL\_S\_FG catchment, in HRU 28 . . 142

# List of Tables

2.1	Flow duration curves of BP and KL catchments . . . . .	14
2.2	State Variables ( <i>distributed Hydrological Response Unit Model</i> (dHRUM) output) . . . . .	18
2.3	Fluxes (dHRUM output) . . . . .	19
2.4	Storages (dHRUM output) . . . . .	19
2.5	Different types of discretization of study Area . . . . .	20
2.6	dHRUM Parameters (Turk, 2020) . . . . .	24
2.7	Estimated range of parameters for forested areas . . . . .	32
2.8	Estimated range of parameters for arable lands . . . . .	33
2.9	Estimated range of parameters for wetlands . . . . .	34
2.10	Estimated range of parameters for built-up area . . . . .	35
3.1	Correlation coefficients between standardized GW storage and measured GW level in BP . . . . .	51
3.2	Correlation coefficients between standardized GW storage and measured GW level in KL . . . . .	51
3.3	correlation coefficients between simulated soil storage and mea- sured SM in BP . . . . .	59
3.4	Correlation coefficients between simulated soil storage and mea- sured SM in KL . . . . .	59
3.5	Correlation coefficients derived from calibration using both GW and SM data in BP catchment . . . . .	68

3.6	Correlation coefficients derived from calibration using both GW and SM data in KL catchment . . . . .	69
3.7	Comparison of fluxes in BP and KL catchments for four different types of calibrations . . . . .	89
3.8	Comparison of storages in BP and KL catchments for four different types of calibrations . . . . .	98
4.1	Mean absolute error of <i>Flow Duration Curves</i> (FDCs) derived from simulations . . . . .	99
4.2	Parameters and their applied coefficients for producing more accurate FDCs in KL_D_FG catchment . . . . .	100

# List of Acronyms

<b>dHRUM</b> distributed Hydrological Response Unit Model . . . . .	ix
<b>FDC</b> Flow Duration Curve . . . . .	x
<b>SUMMA</b> Unifying Multiple Modeling Alternatives . . . . .	2
<b>MARRMoT</b> Modular Assessment of Rainfall-Runoff Model Toolbox	2
<b>PDM</b> Probability Distributed Model . . . . .	3
<b>mRM</b> Multiscale Routing Model . . . . .	4
<b>LSM</b> Land Surface Model . . . . .	4
<b>MPR</b> Multiscale Parameter Regionalization . . . . .	4
<b>GW</b> Groundwater . . . . .	5
<b>SM</b> Soil Moisture . . . . .	5
<b>BP</b> Brejlský Potok . . . . .	5
<b>KL</b> Karluv Luh . . . . .	5
<b>HRU</b> Hydrological Response Unit . . . . .	5
<b>HMH</b> Distributed Mesoscale Hydrologic Model . . . . .	5

*LIST OF ACRONYMS*

xii

<b>SR</b> Standard Regionalization . . . . .	5
<b>GIS</b> Geographic Information Systems . . . . .	12
<b>DEM</b> Digital Elevation Model . . . . .	11
<b>DEoptim</b> Differential Evolution Optimization Algorithm . . . . .	25
<b>CDF</b> Cumulative Distribution Function . . . . .	27
<b>DSC</b> Depression Storage Capacity . . . . .	30
<b>RR</b> Random Roughness . . . . .	30

# Introduction

## 1.1 Rainfall-Runoff Modelling

Rainfall-runoff hydrological models are proper tools to understand a region's hydrology beyond measurement (Beven, 2009, 2012). These models can be used to investigate the behaviour of the catchments using hypothesis testing (Beven, 2002; Clark et al., 2011; Fenicia et al., 2008; Kirchner, 2016, 2006), and to model the changes in catchments' characteristics and climatic conditions (Bathurst et al., 2004; Ewen and Parkin, 1996; Klemes, 1986; Peel and Bloeschl, 2011; Seibert and van Meerveld, 2016; Wagener et al., 2010). Rainfall-runoff models are divided into many categories based on their assumptions, structures, and input data, ranging from simple conceptual models to spatially distributed models. Each type of these models has its own benefits and drawbacks regarding spatial resolution, representation of hydrological processes, computational efforts, and data requirement.

According to the study of Beven (2001), nonlinearity, uniqueness, and uncertainty, which is also mentioned in (Bloeschl et al., 2019), are the

some of the challenges in hydrological modelling. Even recently-developed process-based hydrological models have not adequately tackled these problems. These problems arise due to our poor understanding of several issues such as soil and vegetation properties, spatial variability of hydrological processes at different scales, uncertainty in hydrological modelling etc. (Bloeschl et al., 2008; Samaniego et al., 2010).

In recent years, different process-based hydrological modeling frameworks have been developed. These frameworks have their philosophy and assumptions in representation of processes in the catchment trying to address these problems. Clark et al. (2015) developed a modelling framework by combining various hydrologic and thermodynamic models to simulate different physical processes in a catchment, based on multiple hypotheses about hydrologic processes and spatial scaling behaviour which is called *Unifying Multiple Modeling Alternatives* (SUMMA). The modelling framework can represent different physical processes in different hydrological model structures. This framework helps solve significant hydrology challenges like finding the optimum model's complexity, solving the conservation equations across a hierarchy of spatial scales, choosing the best flux parameterisations, enhancing the computational efficiency and numerical accuracy, and identifying different sources of uncertainty.

Knoben et al. (2019) developed a modelling framework called *Modular Assessment of Rainfall-Runoff Model Toolbox* (MARRMoT) to investigate the inter-comparison of conceptual hydrological models with different structures. The model consists of two parts: the mathematical model in which the underlying equations are defined and the numerical models, which uses the implicit Euler time-stepping scheme to solve the ordinary differential equations. The authors defined these two parts separately to adjust and debug the codes quickly. The MARRMoT consists of 46 different hydrologic lumped models with 100 flux equations and eight different types of unit hydrographs. The model inputs are precipitation, potential evapotranspiration, and temperature. This model is developed to help users to select the

best choice among multi-model frameworks considering different storage combinations. These storages are mostly representing snow storage, interception storage, surface depression storage, soil moisture storage, deficit storage, groundwater storage, routing storage, and channel storage. The model performance is tested in the study area using all 46 models to identify the most successful combination of modeling approaches. Also, the Kling-Gupta efficiency is applied as the objective function to calibrate the model. They investigated the structural uncertainty of lumped and deterministic conceptual models to identify the best model for the considered catchment. They showed that the number of parameters is not related to the model performance. Also, the obtained results from the most successful model showed that a specific saturation excess mechanism played a crucial role in achieving accurate calibration results. This mechanism was the flashy reaction of the catchment during the rainfall event due to the low available soil storage. They found that the runoff mechanism alone cannot fully explain the hydrologic behaviour of the catchment, and a higher number of parameters does not mean higher model accuracy (Knoben et al., 2019).

The *Probability Distributed Model* (PDM), (Moore, 2007), is another widely used hydrological model which is developed to be used as a toolkit for rainfall-runoff modelling and forecasting. This model is based on the distribution of soil absorption capacity using the probability distribution function of chosen theoretical form. The probability distribution of soil moisture store is derived using a mass balance equation. The terms of this equation are precipitation, evaporation, groundwater recharge, and direct runoff. A tension threshold is defined based on the water content to control the soil drainage to the groundwater store. However, the model has no explicit soil drainage function to separate slow and fast runoff responses. Instead, the total flow is divided into surface runoff and based flow components, and they are routed using the Horton Izzard equation. A transfer function is also an alternative routing method using two linear reservoirs. The PDM model has been used for many design and operational

cases, and the results showed the efficacy of the model in terms of runoff modelling and predicting.

Another challenge in hydrological modelling is the simulation of lateral water fluxes to show the spatial heterogeneity at the sub-grid level. In the study of (Thober et al., 2019), a *Land Surface Model* (LSM) was developed to simulate lateral water fluxes in multiple spatial scales. Land surface models are methods to simulate streamflows using the exchange of fluxes of water and energy at the earth surface and atmosphere. The model is called *Multiscale Routing Model* (mRM). They applied the finite difference method with an adaptive time-stepping scheme to solve kinematic wave equations. The major objective of this research is to design an LSM that can work with user-defined spatial resolution without any need for modifying the model setups. The model performance is evaluated using two datasets, the high spatial resolution German dataset and the European dataset with lower resolution to simulate streamflow. The obtained results showed the model worked more accurately with the coarser dataset compared to the high-resolution one.

## 1.2 Calibration of Hydrological Models

Model calibration is a crucial part of hydrological modelling. It means finding a unique set of parameters that results in an acceptable system behaviour compared to actual measurements in the real system (Judd, 2010). Calibration guarantees the model's accuracy, and helps to represent the underlying physics of the processes more realistically. Therefore, modellers acquire various types of data to be able to find effective parameters using calibration, but there are always problems with providing such data. Such models transform into "overparameterized conceptual models" (Beven, 2001; Kirchner, 2006; Thober et al., 2019).

Many studies have been conducted to investigate the effective parameters of the model of interest. Samaniego et al. (2010) developed a *Multiscale*

*Parameter Regionalization* (MPR) method to deal with high resolution remotely sensed data and integrate the spatial heterogeneity of physiographic features. MPR technique avoids problems of over parameterization, non-transferability of parameters at different spatial scales and heterogeneity of soil, vegetation, and topography into the model. This technique links the parameters at the coarser scale to a finer one using upscaling operation to correspond to the input data scale. A non-linear transfer function connects the predictors on a local scale to global parameters. The performance of MPR is compared to the *Standard Regionalization* (SR) method. Both methods are implemented within a spatially *Distributed Mesoscale Hydrologic Model* (HMH) in a basin located in Germany. MPR outperformed the SR method and successfully tackled the mentioned deficiencies of the distributed hydrologic model.

Jahanshahi et al. (2021) investigate the effect of three types of parameter transfer on simulating streamflow in 576 ungauged catchments in Iran. The parameter transfer comprises the spatial transfer across different regions, temporal transfer across different calibration periods and spatiotemporal transfer across both different areas and periods. The model rainfall-runoff model used in this study is HBV. This model is a semi-distributed conceptual model which is developed by Bergström (1976). The obtained results showed that the temporal parameter transfer results in the best goodness of fit, and the spatial and spatiotemporal transfer lead to almost the same results. They showed that parameters related to the runoff component have the highest, and the ones related to snow have the lowest uncertainties. They also concluded that the model performs better in humid catchments compared to arid catchment and elevation significantly affect parameter estimation.

In many modelling cases like this study, the measured runoff hydrograph is unavailable and the model calibration is problematic (Nijzink et al., 2018). Therefore, it is reasonable to use alternative methods rather than using a pure optimization algorithm to calibrate the runoff component

parameters. Gharari et al. (2014b) developed an method to constrain the model parameters based on the expert knowledge which comprises two steps. First, limiting the solution space by constraining the parameters based on the realistic relationships between parameters and second, checking if there are realistic relationships between state variables and fluxes which is called process constraints. To do so, they proposed an algorithm to search for acceptable solution space and satisfy the two steps. The algorithm results in providing more conceptually realistic parameter sets, however, it should be tested by different hydrological models to investigate its performance more accurately.

Despite all the efforts to calibrate hydrological models, these models still lack prediction power due to inadequate representation of underlying processes. Therefore, Hrachowitz et al. (2014) combined expert knowledge and systematic use of hydrological signatures to enhance the model's consistency. The obtained results showed that it is possible to reproduce the hydrograph in the calibration period using a simple conceptual model constrained by four calibration objective functions. They tested the constraining scheme on 11 models from simple to complex and showed that expert knowledge could help modellers reach the adequate models' behaviour, system representation and predicting power.

### 1.3 Aims and Goals

In this study, the hydrological model of the Amalie site using a semi-distributed hydrological model is represented. The model used in this study called *distributed Hydrological Response Unit Model* (dHRUM) and can be used as a lumped or semi-distributed model that will be explained in section 2.3. This study put a lot of emphasis on finding effective parameters for dHRUM by constraining the solution space and investigating the effects of different catchment discretization on the model's performance. In the following chapters, first the methodology 2 will be explained. This chapter

explains the study area, data availability, hydrological and optimization models. Then, the obtained results are presented in chapter 3 and the discussed in chapter 4.

# CHAPTER 2

## Methodology

In this chapter, the method and the data used to model the water balance in the study area are explained. First, the study area and the data are explained in sections 2.1 and 2.2. Then the hydrological model and its parameters are described in sections 2.3 and 2.4.

### 2.1 Study Area

The study area, Amalie, is located in the western part of Czech Republic and, it is a part of Středočeský Kraj region. This region is divided into two catchments, *Brejlský Potok* (BP) and *Karlův Luh* (KL) catchments. The area of BP is  $4.65 \text{ km}^2$  and KL is  $3.32 \text{ km}^2$ . The study area is mainly covered by forested and arable lands. Figure 2.1 shows the boundary of study area, and the delineation of both underlying watersheds.

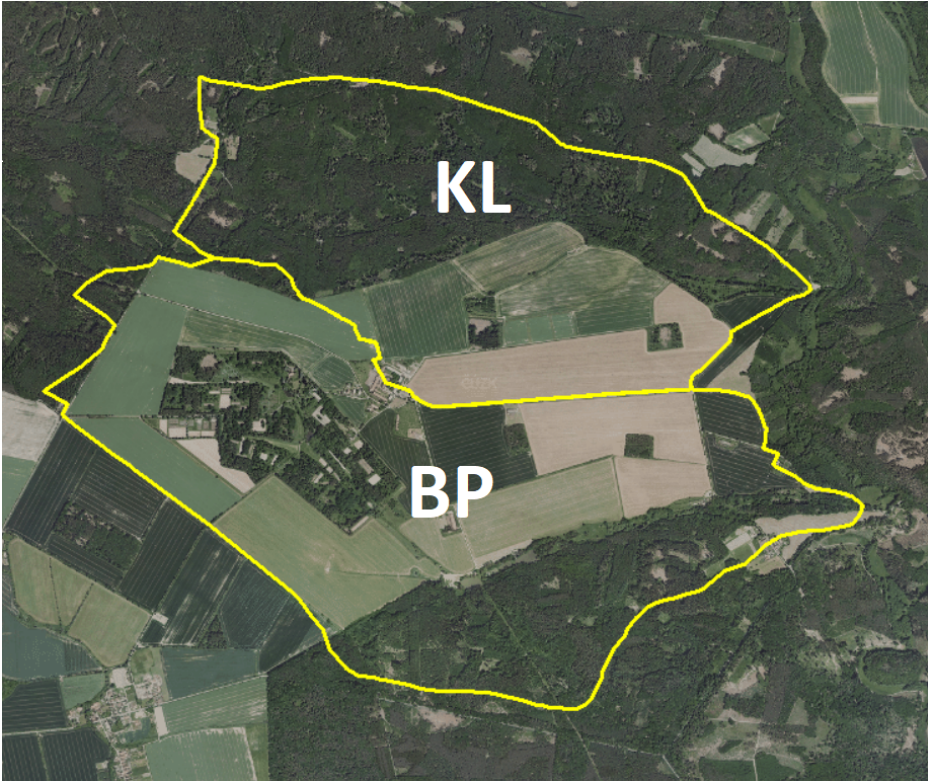


Fig. 2.1: Study Area, BP (down) and KL (up)

As it can be seen in the figure above, the area of both forested and arable lands are comparable. acBP catchment is approximately 40 percent forested and 60 percent arable lands, and acKL is opposite. Figures 2.2 and 2.3 show the vegetation cover of the arable and forested lands in the Amalie site during October 2021.



Fig. 2.2: Land cover in Amalie's arable land (October 2021)



Fig. 2.3: Land cover in Amalie's forested areas (October 2021)

According to the figures 2.1, 2.2 and 2.3, there are few buildings and roads in this region which their areas are negligible compared to the whole catchment. Therefore, it can be assumed that almost the entire catchment is permeable and contributes to the percolation mechanism and baseflow generation. Figure 2.4 shows the hillshade map of study area which is derived from *Digital Elevation Model* (DEM). This picture can give us a visual idea of the places with steep slopes like northern parts of KL catchments or plateaus like southern part of BP catchment. Slope is an

important factor to determine the value of direct runoff and baseflow which will be explained in section 2.4.4.

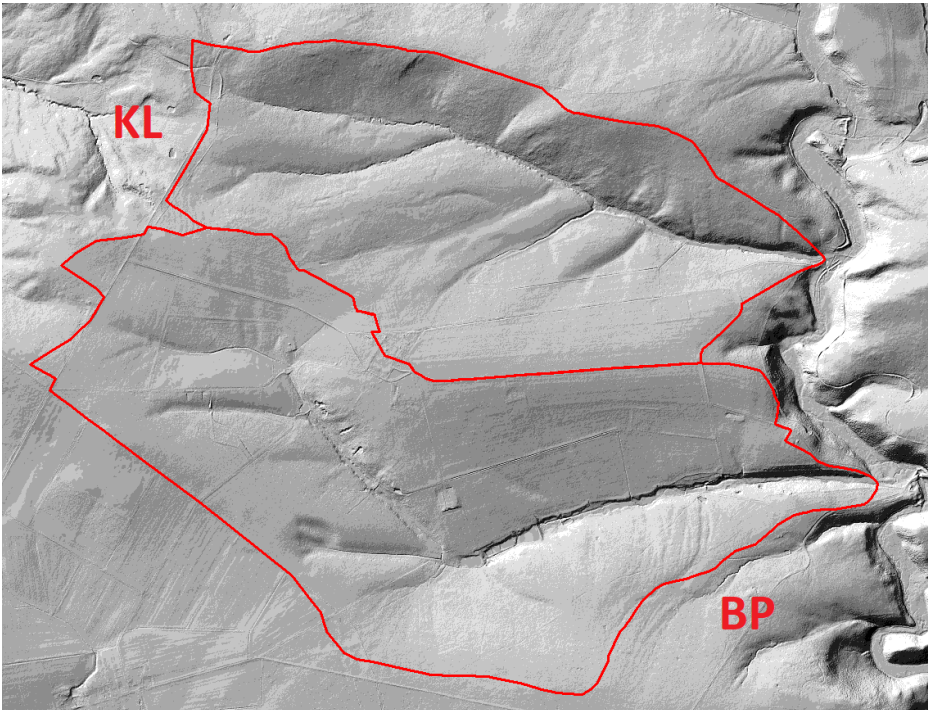


Fig. 2.4: Hillshade map of study area

## 2.2 Data

In this study, different types of data have been used to run and calibrate the hydrological model. General, three types of data have been used in this study, including time-series, point data, and *Geographic Information Systems* (GIS) data which are explained in the next sections.

### 2.2.1 Time Series

The daily precipitation and mean daily temperature time series of study area, from 1960 to 2021, are used as inputs to the model. These data are derived from rasters produced by Czech Hydrometeorological institute, and the time series are calculated for each *Hydrological Response Unit* (HRU) which will be explained in section 2.3.1.

The *Flow Duration Curve* (FDC) curves estimated for both watersheds using regionalization approach of CHMI are used as a streamflow benchmark to calibrate the model. The FDCs show the cumulative frequency of mean daily discharges at the outlet points of BP and KL catchments and are provided by Czech Hydrometeorological Institute. The data for both basins are represented in table 2.1.

The *Soil Moisture* (SM) and *Groundwater* (GW) sensors record soil relative water content in a layer of the particular depth and groundwater level, respectively. The sensors are installed in the site recently, and the period of measurements are between 6 to 12 months. The GW sensors record the daily GW fluctuates over time. The SM sensors, TONST TDR, measure soil moisture in 5 minutes intervals in the upper 15cm of soil layer. The SM sensors are calibrated in laboratory before installing in the catchment. The daily average value of recorded SM is considered in this study. Figure 2.5 shows the maps of GW and SM sensors in the catchment.

Tab. 2.1: Flow duration curves of BP and KL catchments

Day	30.00	60.00	90.00	120.00	150.00	180.00	210.00	240.00	270.00	300.00	330.00	355.00	364.00
BP [ $m^3/day$ ]	26.00	18.00	14.00	12.00	10.00	8.00	7.00	6.00	4.50	3.50	2.50	1.00	0.50
KL [ $m^3/day$ ]	22.00	15.00	12.00	10.00	8.50	6.50	6.00	5.00	3.50	3.00	2.00	1.00	0.50

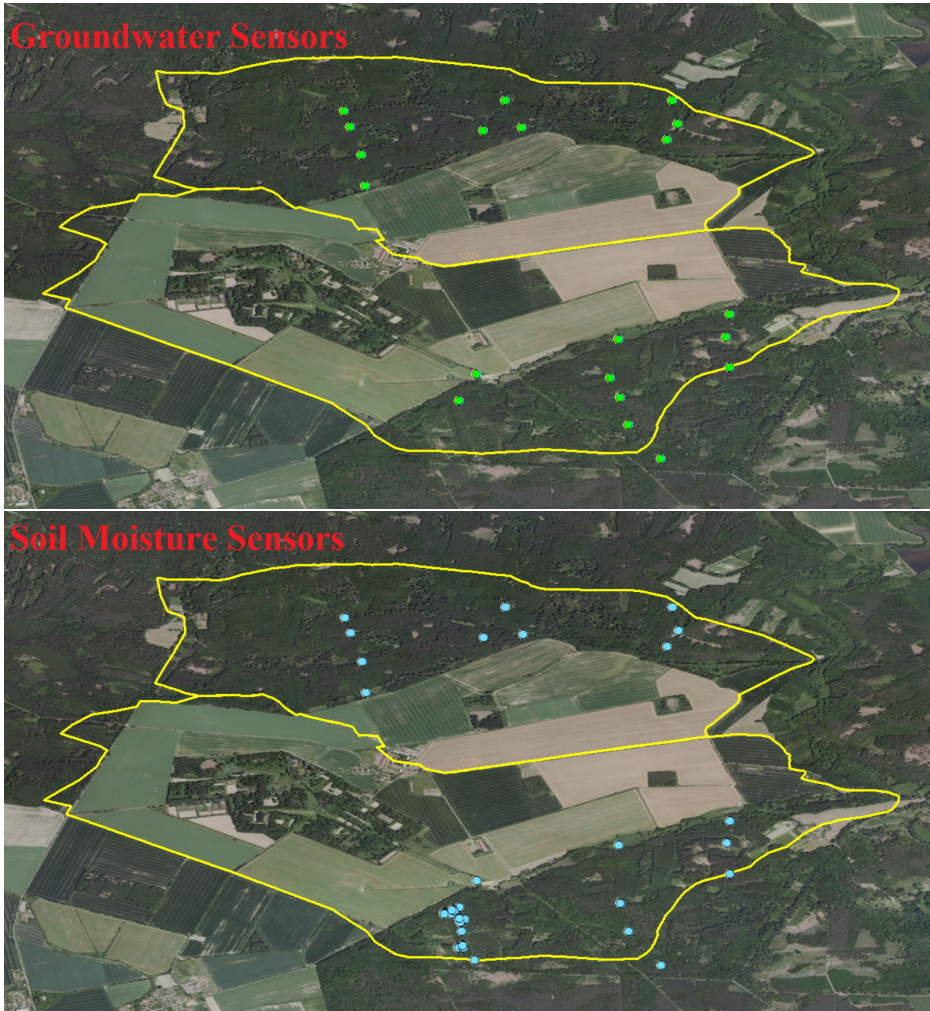


Fig. 2.5: The locations of GW and SM sensors in the catchment

Figure 2.6 shows the some of the soil moisture sensors, TONST TDR, in the study area.



Fig. 2.6: Soil moisture sensors (TONST TDR)

### 2.2.2 Point information

The other available data used to calibrate the hydrological model is the soil field capacity and wilting point information. Figure 2.7 shows the points at which these information are measured and recorded. This data is used to estimate the parameters of the soil bucket model, which will be explained in section 2.4.3.

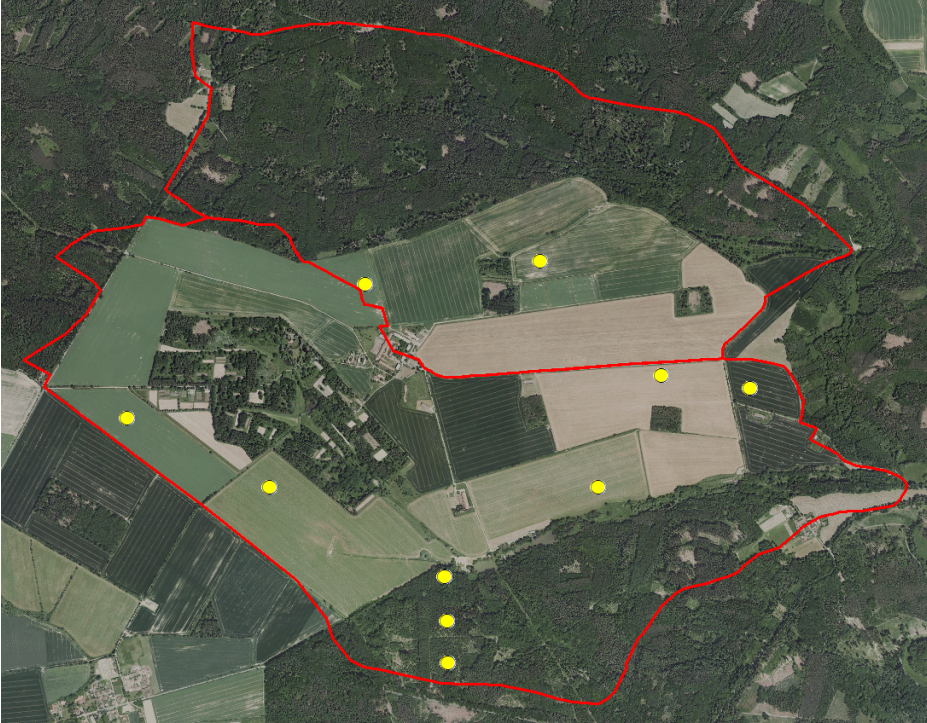


Fig. 2.7: The locations of measured soil field capacity and wilting points

### 2.2.3 GIS Data

Different types of spatial data (GIS) have been used in this study. A DEM of the study area with the resolution of 2 meters have been used to derive the catchment delineations in the frosted parts and the slope map of the study area. The produced slope map is of the same resolution as DEM and used to estimate and constrain the runoff parameters of the hydrological model.

## 2.3 Distributed Hydrological Response Unit Model (dHRUM)

The hydrological model used in this study is called *distributed Hydrological Response Unit Model* (dHRUM). This model is a physical semi-distributed hydrological model which follows tipping-bucked and HRU philosophies.

There are two main assumptions in physically-based hydrological models states 1) the complexity and spatial resolution of the models are determined by available data and 2) the catchment response at each scale is the aggregation of smaller-scale processes. However, in many modelling processes, these assumptions are violated, and consequently, the prediction power and representation of hydrological processes of these models is limited. Therefore, To overcome these challenges, the concept of HRU has been introduced to satisfy both model simplicity which is adequate for parameters identification and an acceptable level of process heterogeneity (Gharari et al., 2014a).

There are six main storages inside the dHRUM, namely groundwater storage, surface retention, canopy storage, stem storage, interception storage and soil storage. The model takes precipitation and temperature as inputs as well as sixteen parameters for different storages and processes and produces twenty-two components of the water balance equation (Turk, 2020). The outputs are divided into 3 categories which are shown in tables 2.2, 2.3 and 2.4.

Tab. 2.2: State Variables (dHRUM output)

Num	Output name	Definition
1	PREC [mm]	Precipitation
2	SNOW [mm]	Snow depth
4	PET [mm]	Potential evapotranspiration
5	TEMP [C]	Temperature

Tab. 2.3: Fluxes (dHRUM output)

Num	Output name	Definition
1	TOTR [mm]	Total-runoff
2	BASF [mm]	Base-flow
3	DIRR [mm]	Direct Runoff
4	PERC [mm]	Percolation
5	TROF [mm]	Through fall
6	STEF [mm]	Stem flow
7	CANF [mm]	Canopy drainage
8	AET [mm]	Actual evapotranspiration
7	PREF [mm]	Effective precipitation
12	EVAC [mm]	Canopy Evaporation
13	EVAS [mm]	Stem-evaporation
13	EVBS [mm]	Bare soil evapotranspiration
14	MELT [mm]	Melting

Tab. 2.4: Storages (dHRUM output)

Num	Output name	Definition
1	INTS [mm]	Interception storage
2	SOIS [mm]	Soil storage
3	GROS [mm]	Groundwater storage
4	SURS [mm]	Surface retention

### 2.3.1 Discretization of Study Area

In order to model the study area using semi-distributed version of dHRUM, it is necessary to divide the catchments into a number of HRUs. These units can be determined according to various criteria, such as drainage system, geomorphological features or hydro-pedological characteristics. In this study, The arable lands in BP and KL catchments are discretized based on the drainage system and soil retention capacity, and the forested

areas are discretized based on geomorphological features. The catchments are named based on the discretization criteria which can be found in table 2.5

Tab. 2.5: Different types of discretization of study Area

Num	Name	Description
1	BP_D_FG	Discretization is based on the drainage system in arable lands and geomorphology in forested areas.
2	BP_S_FG	Discretization is based on soil properties in arable lands and geomorphology in forested areas.
3	KL_D_FG	Discretization is based on the drainage system in arable lands and geomorphology in forested areas.
4	KL_S_FG	Discretization is based on soil properties in arable lands and geomorphology in forested areas.

The figures 2.8 and 2.9 shows the discretization based on drainage system and soil retention capacity.

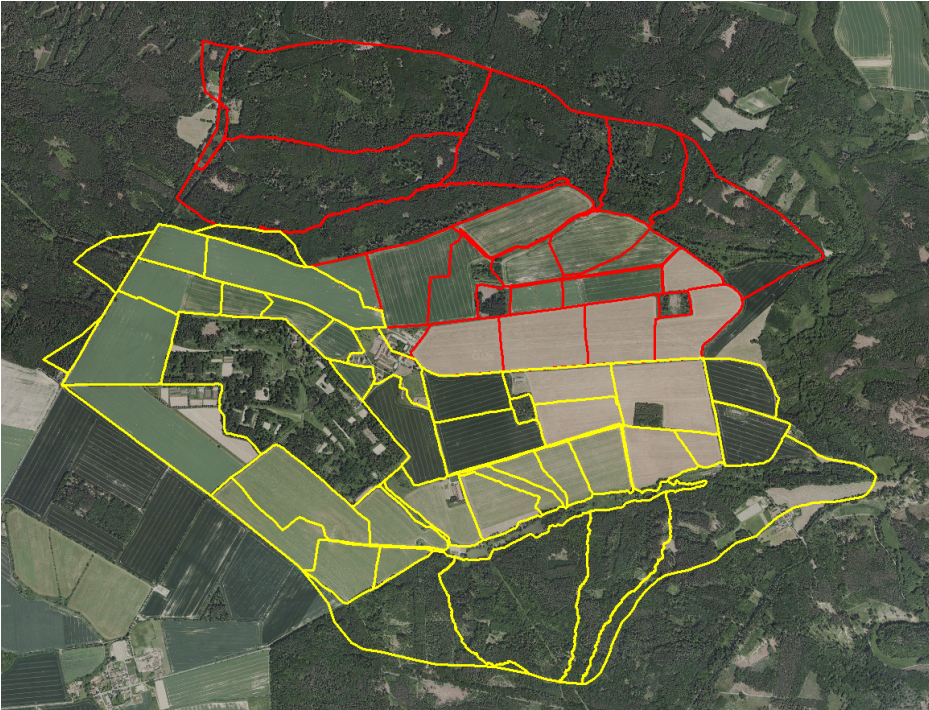


Fig. 2.8: BP\_D\_FG (yellow) and KL\_D\_FG (red) catchments, discretized based on drainage system

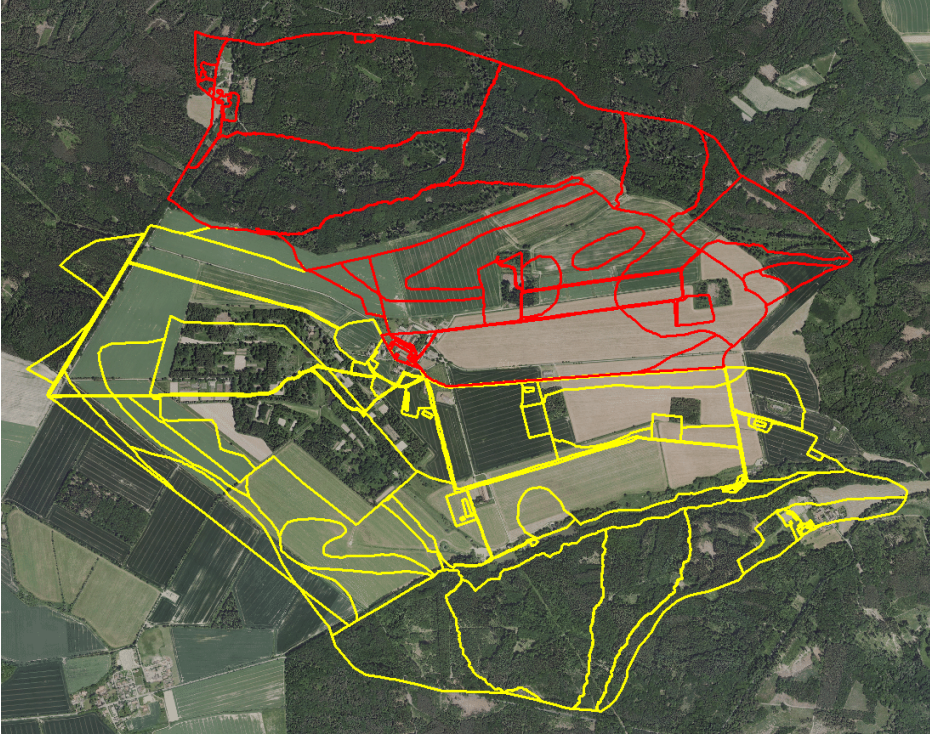


Fig. 2.9: BP\_S\_FG (yellow) and KL\_S\_FG (red) catchments, discretized based on soil retention capacity

Figure 2.10 shows one of the drainage channels on Amalie site. These channels are connected to the underground drainage network, where water from irrigation or precipitation is collected and transferred to these channels. The water moves to natural streams through these channels and flows to the catchment outlet.



Fig. 2.10: A drainage channel in Amalie site BP watershed

## 2.4 Estimation of Model's Parameters

dHRUM has sixteen different parameters which control storages and fluxes during simulation. Table 2.6 shows the parameters' names and definitions.

Tab. 2.6: dHRUM Parameters (Turk, 2020)

Num	Parameter	Role and range
1	B_SOIL	Shape of Pareto distribution of soil storage [0,inf]
2	C_MAX [mm]	Maximum storage in Pareto distribution [0,inf]
3	B_EVAP [mm]	Soil evapotranspiration rate [0,inf]
4	KS [-]	Storage coefficient of groundwater storage [0,1]
5	KF [-]	Storage coefficient of runoff response [0,1]
6	ADIV [-]	Divider of percolation into the direct runoff and groundwater
7	CDIV [-]	Divider of gross rainfall as a canopy input [0,1]
8	SDIV [-]	Divider of gross rainfall as a trunk input [0,1]
9	CANS_ST [mm]	The Max canopy storage [0,inf]
10	STEM_ST [mm]	The Max stem and trunk storage
11	CSDIV [-]	Divider of canopy outflow to through fall and stem flow [0,1]
12	TETR [C]	Threshold temperature for when rainfall becomes snow [-inf,inf] better [-5,5]
13	DDFA [C]	The day degree model for snow melt [0, inf]
14	TMEL [C]	Threshold temperature for determining melting process [-inf, inf]
15	RETCAP [C]	The maximum capacity of surface retention [0, inf]
16	CMIN [mm]	Minimum storage in Pareto distribution [0,inf]

In order to simulate the hydrological behaviour of the study area accurately, it is necessary to identify the effective values of model parameters. In this study, these parameters are identified using an optimization algorithm, expert judgment and available data. Next section, 2.4.1, describes the optimization algorithm used in this study.

### 2.4.1 Global Optimization by Differential Evolution

The optimization algorithm used in this study is called *Differential Evolution Optimization Algorithm* (DEoptim) (Storn and Price, 1997) which is a global optimization algorithm. DEoptim belongs to the evolutionary algorithms family which are population-based methods. The methods in this family are inspired by biological evolution and use mathematical and stochastic methods to find the optimum solution.

DEoptim package in R, (Ardia et al., 2011) is used to calibrate the model parameters. DEoptim parameters are set to  $itermax = 3$ , population size (NP) = 5000,  $trace = 7$ , crossover probability = 0.25, and step-size = 0.7 and strategy = 6 for calibrating SM and GW storages and 2 for FDC. The upper and lower boundaries of each parameter are determined according to tables 2.7, 2.8, 2.9 and 2.10 which will be explained in next sections.

### 2.4.2 Objective Functions

In order to run DEoptim an objective function is needed to be minimized. In this study, different types of objective functions have been used for different purposes. To calibrate the model based on FDC or SM data, the Mean Absolute error has been used which is shown in equation 2.1:

$$MEA = \frac{\sum_{i=1}^n obs_i - sim_i}{n}, \quad (2.1)$$

where  $MAE$  is mean absolute error,  $obs$  is the measured value,  $sim$  is the simulated value and  $n$  is the total number of data points.

To calibrate semi-distributed dHRUM model using the information of groundwater storage, the linear correlation is used. This function calculates the dependencies between the normalized value of groundwater fluctuations (measured data) and groundwater storage (simulation). The reason why we use normalized data is that the observation and simulation GW data

better describes dependencies on groundwater fluctuations than raw data.. The observed data shows GW fluctuation based on location of groundwater measurement sensor, and the simulated data shows the acGW storage at the HRU of interest. The Pearson correlation coefficient is calculated using equation 2.2.

$$r = \frac{(obs_i - \overline{obs})(sim_i - \overline{sim})}{\sqrt{\sum (obs_i - \overline{obs})^2 \sum (sim_i - \overline{sim})^2}} \quad (2.2)$$

where  $r$  is the Pearson correlation coefficient,  $obs$  and  $sim$  is the measured and simulated values,  $\overline{obs}$  and  $\overline{sim}$  is the mean value of measured and simulated data, respectively. As the best value for  $r$  is one and the DEoptim method calculates the minimum value of function,  $1 - r$  is used as the objective function.

### 2.4.3 Soil Parameters

The soil bucket in dHRUM is modelled using *Probability Distributed Model* (PDM) which is based on Pareto distribution function. In order to estimate the values of  $C\_max$ ,  $C\_min$  and  $B\_Soil$ , the following steps are applied.

1. Extracting the field capacity (RVK) data from interpolated RVK raster file for each polygon.
2. Calculating the probability of each extracted data point using Pareto cumulative distribution function which is shown in equation 2.3.

$$F(c) = \left( \frac{C\_max - C}{C\_max - C\_min} \right)^b \quad (2.3)$$

where  $C\_max$  is field capacity,  $C\_min$  is the wilting point, and  $C$  is soil capacity which  $C\_max > C > C\_min$ , and  $F(c)$  is the exceedance probability of  $C$ .

3. Calculating the *Cumulative Distribution Function* (CDF) of observed RVK values (percentile).
4. Using DEoptim method to estimate the best fit to the data using optimized values of  $C_{max}$ ,  $C_{min}$  and  $B_{soil}$ . DEoptim minimizes the difference between CDF curves of measured data and Pareto CDF function (equation 2.3).

As an example, figure 2.12 shows the results of fitting curves for the HRUs number 1 and 8 for BP\_D\_FG catchment which are shown in figure 2.11.

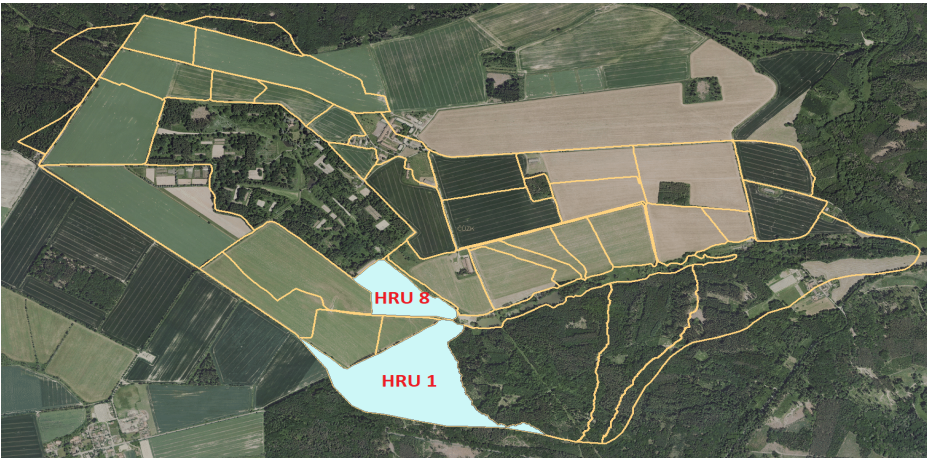


Fig. 2.11: The position of HRUs 1 and 8 in BP\_D\_FG catchment

The optimized values for HRU 1 are  $C_{max} = 449.90$ ,  $C_{min} = 434.94$  and  $B_{soil} = 0.89$  and for HRU 8 are  $C_{max} = 450.05$ ,  $C_{min} = 430.71$  and  $B_{soil} = 1.83$ . These values are the coefficients of equation 2.3 and produce the red graphs in figure 2.12. This procedure has been done for all HRUs and discretizations of BP and KL catchments.

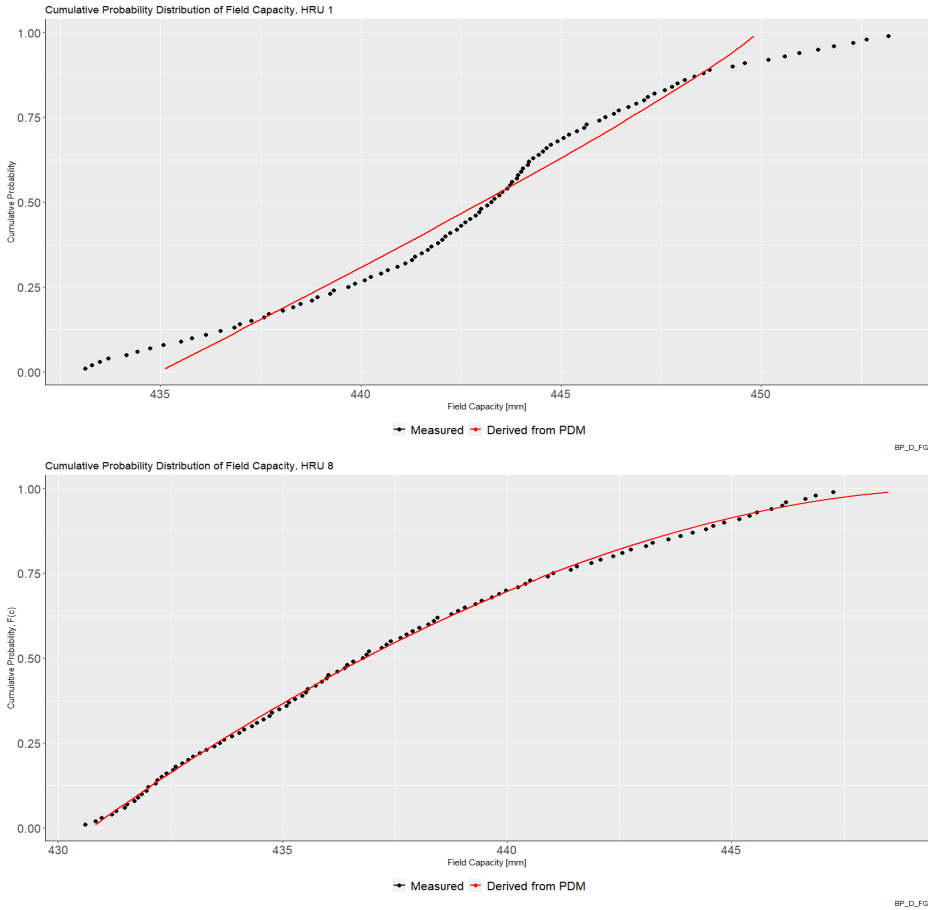


Fig. 2.12: Fitting Pareto cumulative distribution function to the soil field capacity data for HRUs 1 and 8

The derived values from this procedure are considered as an acceptable estimation of the parameters mentioned above. Using these values, we can constraint the soil bucket parameters of PDM soil bucket in our optimization model.

#### 2.4.4 Runoff Parameters

The parameters that affect runoff in the model, direct runoff, baseflow and total runoff, are KS, KF, ADIV and RETCAP. The KS, KF and ADIV values are constrained based on the normalized mean values of slope in each polygon and the distance from the catchment's outlet. In order to calculate the mean value of slope the following procedure have been done:

1. Creating slope raster of the study area using the DEM raster.
2. Extracting the pixel values of slope within each polygon/HRU which is done using "terra" package in R.
3. calculating the mean value of the cell (pixel) values in each polygon/HRU.

After calculating the mean slope for each polygon, the normalized value of slope is calculated using equation 2.4:

$$nrmSlope = \frac{S_i}{1.1S_{max}} \quad (2.4)$$

where  $nrmSlope$  is the normalized slope,  $S_i$  is the mean slpe at HRU i amd  $S_{max}$  is the largest slope. The equation 2.4 normalizes the slope values between zero and one in a way that the slope equal to 0 refers to as a horizontal surface and the slope near 1 belongs to the HRUs with the maximum slope. The term 1.1 in the denominator prevents the  $nrmSlope$  becoming absolute 1 for the HRU with maximum slope. As the formula is used to estimate KS and AVID,  $nrmSlope$  equal to 1 means all water from precipitation percolates to the groundwater or contributes to fast runoff response which is not valid in reality. Therefore, this term is added to the formula.

The value of ADIV is constrained using  $nrmSlope$ . To define the constraints for KS, another criterion is defined which is the normalized distance of the considered HRU from the catchment's outlet. The distances

from the outlet is calculated and the normalized value of them is calculated the same as  $nrmSlope$  which is shown in equation 2.5:

$$nrmDist = \frac{D_i}{1.1D_{max}} \quad (2.5)$$

where  $nrmDist$  normalized distance from outlet,  $D_i$  is the distance of  $i$ th HRU from the outlet and  $D_{max}$  is the maximum distance. Adding distance to estimate the KS parameter help us to consider the baseflow lag time in simulating total runoff which is shown in equation 2.6:

$$meanDS = \frac{nrmDist + nrmSolpe}{2} \quad (2.6)$$

where  $meanDS$  is the mean value of normalized distance and slope and  $nrmDist$  is normalized value of distance from the catchment outlet.

The maximum value of surface retention, RETCAP, is estimated using *Depression Storage Capacity* (DSC) model which is developed by Abd Elbasit et al. (2020). DSC model is a conceptual model which estimates surface depression storage using soil surface roughness and slope values. The model is built to estimate DSC in rainwater harvesting when precipitation occurs on the bare soil in the arid regions. To do so, Abd Elbasit et al. (2020) applied precipitation on a square surface with the area of  $900 \text{ cm}^2$  which is constructed with four sizes of gravel, low, medium and high roughness, and perform the experiment for nine different slope values. They used a mass balance equation to calculate the DSC. Then they built a regression model and derived an empirical formula which is based on *Random Roughness* (RR) which is defined as equation 2.7:

$$RR = \left[ \frac{1}{k} \sqrt{\sum_{k=1}^{i=1} Z_i - \bar{Z}} \right]^{1/2} \quad (2.7)$$

where  $RR$  is random roughness,  $Z_i$  is elevation at point  $i$ ,  $\bar{Z}$  average elevation and  $k$  is number of points or pixels. The DSC is calculated using equation 2.8

$$DSC = 0.0157 \sqrt{\frac{RR}{slope}} \quad (2.8)$$

where  $DSC$  is the depression storage capacity,  $RR$  is random roughness and  $slope$  is the slope of the surface in degree.

In this study, the equations 2.7 and 2.8 are used to estimate RETCAP parameter. To do so, the DEM map of the study area is used instead of the small square surface used in the work of Abd Elbasit et al. (2020). According to the obtained results in this research, the equation 2.8 should be multiplied by ten to give more accurate results. Therefore,  $10DSC$  is used to constrain the RETCAP parameter.

#### 2.4.5 Constraining Parameters

Other parameters  $CAN\_ST$ ,  $STEM\_ST$ ,  $CDIV$ ,  $SDIV$ ,  $B\_EVAP$ ,  $TMEL$  and  $DDF$  are constrained based on our obtained knowledge from visiting the study area like land cover and forest canopy density, and there is no specific method used to calculate them. Tables 1, 2 and 3 show all the obtained range of parameters, upper and lower bound, for forested areas, arable lands and wetlands, respectively.

Tab. 2.7: Estimated range of parameters for forested areas

Parameter	Upper bound	Lower bound
B_SOIL	$Bsoil_{est}^1 + 0.1Bsoil_{est}$	$Bsoil_{est} - 0.1Bsoil_{est}$
C_MAX	$Cmax_{est}^2 + 0.8Cmax_{est}$	$Cmax_{est} - 0.05C_{diff}$
B_EVAP	5.0	0.01
KS	$meanDS - 0.1meanDS$	$meanDS - 0.7meanDS$
KF	0	1.0
ADIV	$nrmSlope - 0.2nrmSlope$	$nrmSlope - 0.8nrmSlope$
CDIV	0.9	0.3
SDIV	0.3	0.01
CANS_ST	3.0	1.0
STEM_ST	2.0	1.0
CSDIV	0.5	0
TETR	4.0	1.0
DDFA	0.01	0
TMEL	-5.0	-20
RETCAP	$DSC^3 - 0.2DSC$	$DSC - 0.4DSC$
CMIN	$Cmin_{est}^4 + 0.05C_{diff}$	$Cmin_{est} - 0.8Cmin_{est}$

<sup>1</sup> The estimated value of B\_SOIL calculated in section 2.4.3

<sup>2</sup> The estimated value of C\_MAX calculated in section 2.4.3

<sup>3</sup> DSC is derived from equation 2.8 multiplied by 10

<sup>4</sup> The estimated value of CMIN calculated in section 2.4.3

Tab. 2.8: Estimated range of parameters for arable lands

Parameter	Upper bound	Lower bound
B_SOIL	$B_{soil_{est}}+0.1B_{soil_{est}}$	$B_{soil_{est}}-0.1B_{soil_{est}}$
C_MAX	$C_{max_{est}}+0.8C_{max_{est}}$	$C_{max_{est}}-0.05C_{diff}$
B_EVAP	8.0	0.01
KS	$meanDS+0.3meanDS$	$meanDS-0.3meanDS$
KF	0	1.0
ADIV	$nrmSlope+0.4nrmSlope$	$nrmSlope-0.05nrmSlope$
CDIV	0.4	0.01
SDIV	0.2	0.01
CANS_ST	1.5	0.5
STEM_ST	1.3	0.1
CSDIV	0.5	0
TETR	4.0	1.0
DDFA	0.01	0
TMEL	0	-5.0
RETCAP	$DSC+0.2DSC$	$DSC-0.2DSC$
CMIN	$C_{min_{est}}+0.05C_{diff}$	$C_{min_{est}}-0.8C_{min_{est}}$

Tab. 2.9: Estimated range of parameters for wetlands

Parameter	Upper bound	Lower bound
B_SOIL	$B_{soil_{est}}+0.1B_{soil_{est}}$	$B_{soil_{est}}-0.1B_{soil_{est}}$
C_MAX	$C_{max_{est}}+0.8C_{max_{est}}$	$C_{max_{est}}$
B_EVAP	6.0	0.01
KS	$meanDS$	$meanDS-0.8meanDS$
KF	0	1.0
ADIV	$nrmSlope-0.2nrmSlope$	$nrmSlope-0.8nrmSlope$
CDIV	0.4	0.1
SDIV	0.4	0.01
CANS_ST	1.3	0.5
STEM_ST	1.1	0.1
CSDIV	0.5	0
TETR	4.0	1.0
DDFA	0.01	0
TMEL	-2.0	-8.0
RETCAP	$DSC-0.2DSC$	$DSC-0.4DSC$
CMIN	$C_{min_{est}}-0.2C_{diff}$	$C_{min_{est}}-0.8C_{min_{est}}$

Tab. 2.10: Estimated range of parameters for built-up area

Parameter	Upper bound	Lower bound
B_SOIL	5	0
C_MAX	800	401
B_EVAP	20	0.6
KS	0.5	0.001
KF	0.1	0
ADIV	1.0	0.8
CDIV	0.1	0
SDIV	0.1	0
CANS_ST	1.0	0.01
STEM_ST	0.5	0.001
CSDIV	0.5	0
TETR	4.0	1.0
DDFA	0.01	0
TMEL	-1.0	-2.0
RETCAP	20	5.0
CMIN	400	300

# CHAPTER 3

## Results

In this chapter, the obtained results from the hydrological simulation are represented. First, the calibration using expert knowledge is explained in sections 3.1 and 3.2. Then, the GW level, SM content are incorporated in the modelling procedure and the results are explained in section 3.3. Finally, the effects of different catchment discretizations are discussed in section 3.4.

### 3.1 Expert Calibration

In this chapter, the calibration results are represented. As there is no stream-flow observation available, the model calibration is done using DEoptim and expert knowledge of the study area which are explained in sections 2.2 and 2.4. The required knowledge about hydrological characteristics is gathered through visiting the site, talking to experienced people and available data like DEM , SM and GW information. This knowledge is applied to define feasible upper and lower boundaries for the model parameters.

### 3.1.1 Manual Sensitivity Analysis

To use apply our knowledge of the catchments to the model properly, we should first know how each parameter affects the model's output through manual sensitivity analysis. To do so, the value of parameters are changed and dHRUM is executed multiple times to investigate how each parameter affects model's output and FDC. The following results are obtained by this investigation:

### 3.1.2 The Effects of Parameters on Model outputs

This part shows the effects of parameters on some of the important model's outputs. This analysis is done using the semi-distributed version of dHRUM.

#### **Soli storage**

Soli storage variation depends on the difference between  $C\_max$  and  $C\_min$  ( $C\_diff = C\_max - C\_min$ ). The higher the  $C\_diff$ , the higher the soil storage.

#### **Groundwater storage:**

- The lower the  $B\_Evap$ , the higher the GW storage.
- The lower the  $KS$ , the higher the GW storage.
- The lower the  $ADIV$ , the higher the GW storage.
- The lower the  $RETCAP$ , the higher the GW storage.

#### **Baseflow:**

- The lower the  $ADIV$ , the higher the Baseflow.

- The higher the CDIV, the higher the Baseflow.
- The higher the SDIV, the higher the Baseflow.
- The lower the TMELT, the higher the Baseflow.
- The lower the RETCAP, the considerably higher the Baseflow.
- The lower KS and TETR, slightly higher Basedflow.

**Direct Runoff:**

- The higher the ADIV, the higher the Direct Runoff.
- The lower the CDIV, the higher the Direct Runoff.
- The lower the SDIV, the higher the Direct Runoff.
- The higher CAN\_ST, STEM\_ST and DDFA, the higher Direct Runoff.
- The lower the TMEL, the higher Direct Runoff.
- The lower the RETCAP the higher the Direct Runoff, especially in summer.

**Percolation:**

- The lower the B\_EVAP, SDIV, TETR, the higher the Percolation.
- The higher the CSDIV, DDFA, the slightly higher the Percolation.
- The lower the CDIV, the considerably higher the Percolation.
- The lower the CAN\_ST, the higher the Percolation.
- The lower the RETCAP, the considerably higher the Percolation.

- The higher the TMEL, the higher the Percolation during spring and the lower Percolation during winter.

### 3.1.3 The Effects Parameters on FDC

The only available information about the streamflow in this study is FDC. Therefore, the FDC is calculated using simulated total runoff hydrograph to be compared with observed FDC. The same procedure is done to analyse the effects of parameters on FDC, but here we run the lumped version of dHRUM. The FDC is divided into high, mid and low flows and the effects on parameters on each part are investigated. The obtained results are as follows:

- The low value of the KF increases the low and mid flows and decreases the high flows and Total Runoff (whole runoff volume).
- The low value of the KS increases the low and mid flows and decreases the high flows.
- The low values of the KS and KF shift the FDC up but keep the shape of simulated FDC the same.
- The low value of the RETCAP increases Total Runoff.
- The high value of the RETCAP increases low flows and decreases mid, high flows and Total Runoff.
- The low value of ADIV increases high flows and decreases low flows and vice versa.
- The high value of CDIV significantly increases high flows and slightly increases low flows.
- The low value of CDIV significantly decreases high and low flows.

- The high value of the SDIV significantly increases high flows
- The low value of the SDIV does not affect Total Runoff
- The high value of the CAN\_ST slightly decreases high flows
- The low value of the CAN\_ST does not affect Total Runoff
- The high value of the STEM\_ST very slightly decreases high flows
- The low value of the STEM\_ST decreases high flows and slightly decreases low flows
- The high or low value of CSDIV does not affect Total Runoff.
- The high value of the TETR decreases high flows
- The low value of the TETR increases high flows.
- The low value of the DDFA decrease low and high flows and vice versa.
- The high value of the DDFA increases runoff in cold seasons.
- The high value of the TMEL increases high flows.
- The low value of the TMEL slightly decreases high flows and increases Total Runoff.
- The high value of the C\_MAX slightly decreases Total Runoff.
- The high value of the C\_MAX the slightly decreases Total Runoff.
- The low value of the CMIN decreases the high flow.

## 3.2 Applying Expert Knowledge to Calibration Procedure

Having known the effects of each parameter on the FDC we can take the following steps to calibration the semi-distributed model.

1. Running the optimization model and saving the obtained parameters.
2. Identifying parameters with non-physical values produced in the optimization procedure, like the higher value of canopy storage in arable land compared to forested areas.
3. Modifying the parameters considering their initial/previous optimized values and our knowledge about the study area, like the land cover and slope, and defining lower and higher boundaries for parameters.
4. Comparing the obtained FDC with the observation and finding the parts with the most significant error (high, middle or low flows)
5. Repeating steps 3 and 4.

This procedure is applied for all 4 catchment discretizations, BP\_D\_FG, BP\_S\_FG, KL\_D\_FG and KL\_S\_FG. The results of this procedure for BP\_D\_FG, distribution of fluxes and storages over the catchment, are presented. The results for other discretizations are presented in appendix 5.

Figures 3.2 to 3.3 show the mean of the sum of monthly values of total runoff, direct runoff and baseflow on the BP catchment from 1960 to 2020.

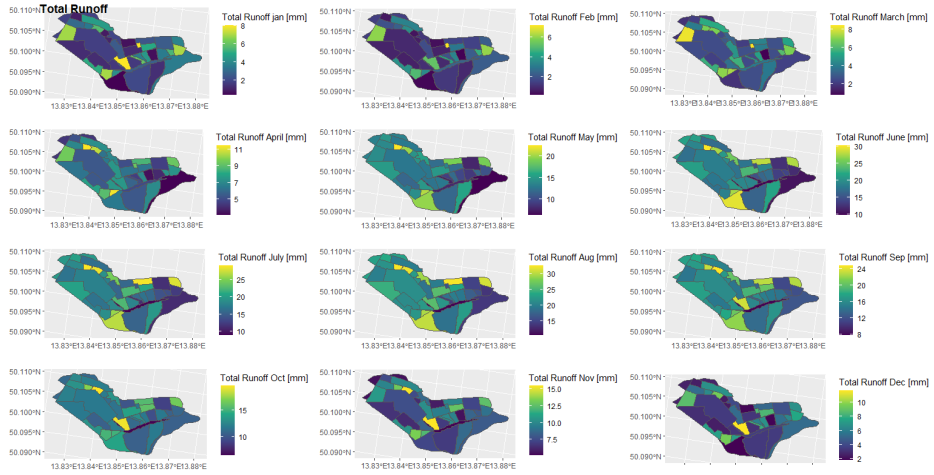


Fig. 3.1: Total runoff in BP\_D\_FG catchment

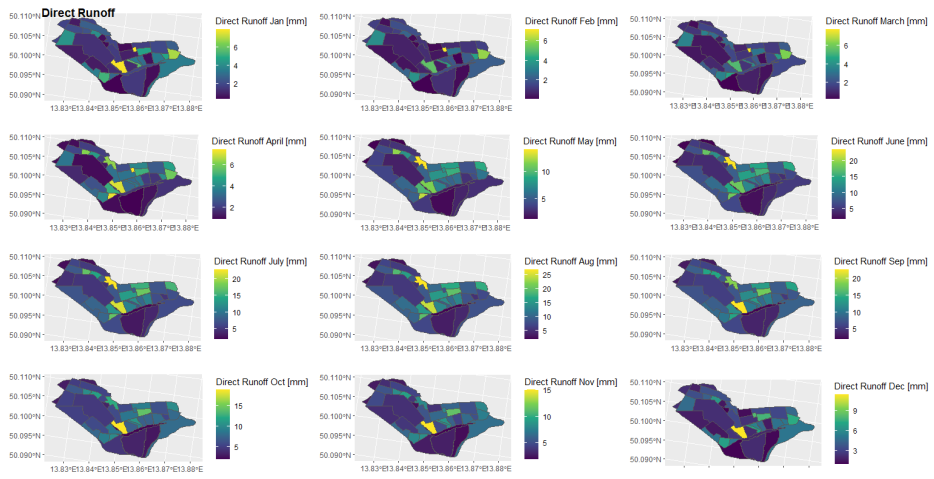


Fig. 3.2: Direct runoff in BP\_D\_FG catchment

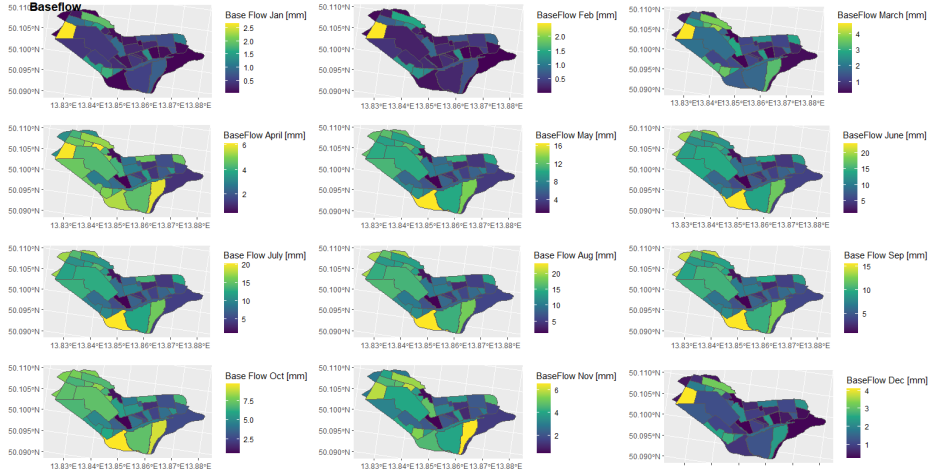


Fig. 3.3: Direct runoff in BP\_D\_FG catchment

As it can be seen in the figure 3.1, there are no specific patterns in the values of the total runoff between arable land and forest areas during a year; however, it shows that the value of total runoff increases significantly between May and September. On the other hand, the direct runoff in arable lands and building areas is higher than in forested regions, figure, 3.2. Also, figure 3.3 illustrates the high values of baseflow in the forested areas and areas with low slope.

The monthly mean values of interception, canopy and stem storage for the whole period of 1960-2020 are shown in figures 3.4, 3.5 and 3.6.

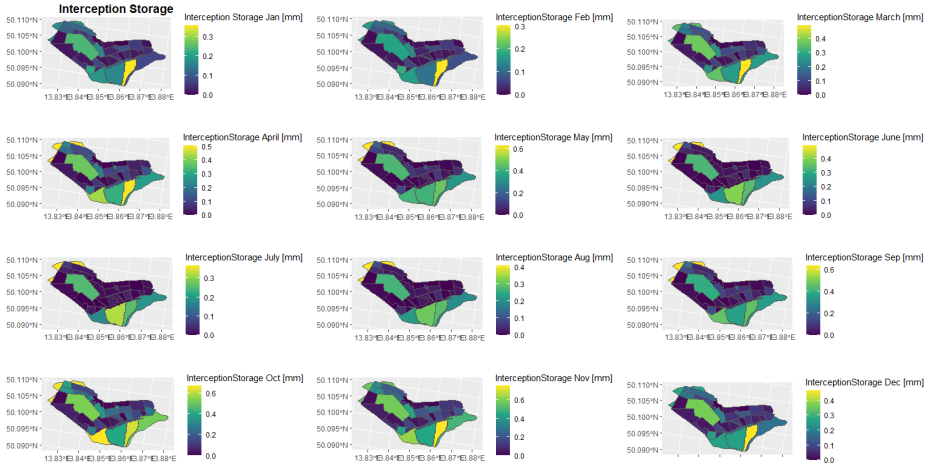


Fig. 3.4: Interception storage in BP\_D\_FG catchment

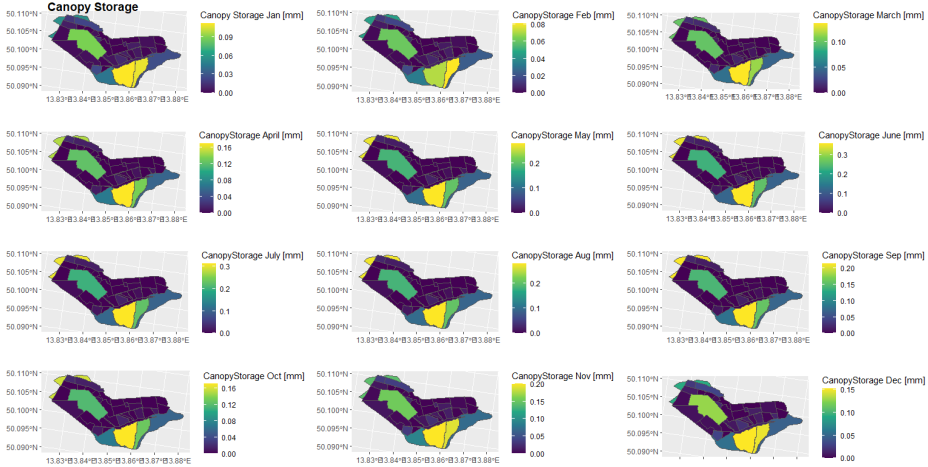


Fig. 3.5: Canopy storage in BP\_D\_FG catchment

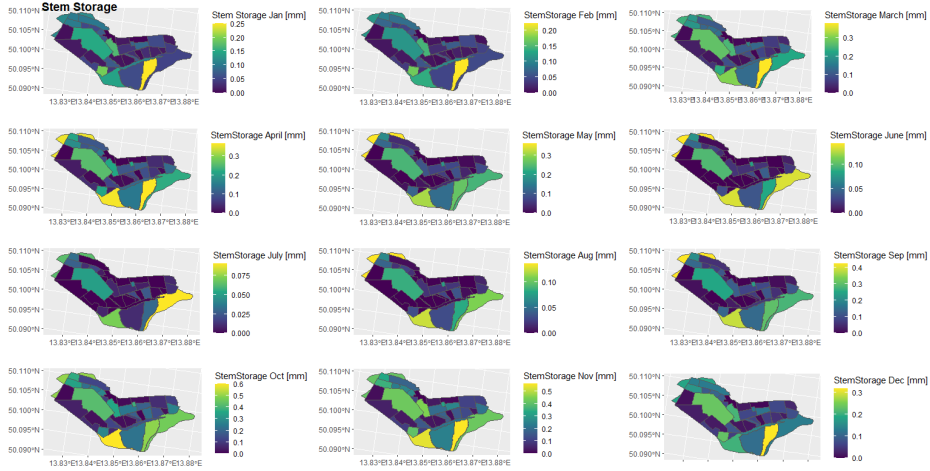


Fig. 3.6: Stem Storage in BP\_D\_FG catchment

According to the figures, the interception, canopy and stem storages are significantly higher in forested areas than in arable lands.

Although the obtained values of fluxes in the BP basin are visually sensible, there is no observation data to compare the obtained results of the calibration. The only available metric is FDC for the whole BP basin.

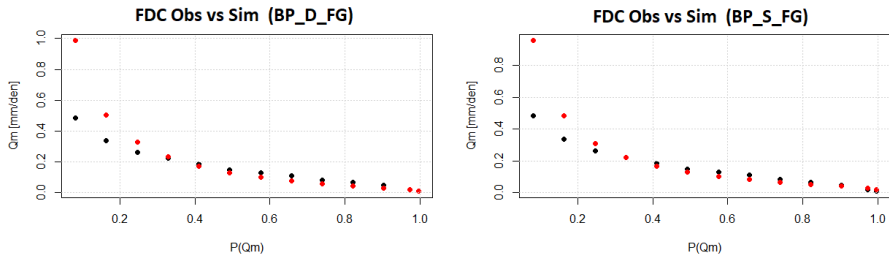


Fig. 3.7: FDCs of BP catchment (red curve= simulation and black curve= measurement)

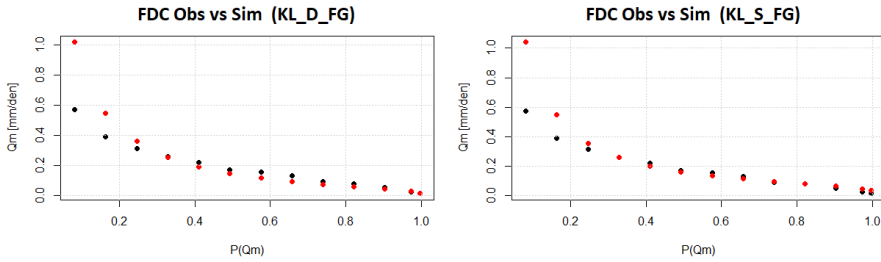


Fig. 3.8: FDCs of KL catchment (red curve= simulation and black curve= measurement)

### 3.3 Adding Soil moisture and Groundwater data to the Calibration Procedure

In this section, the GW and SM data are added to the calibration procedure. There are multiple GW and SM sensors in the HRUs which are shown by filled polygons in figures 3.9 and 3.10. One year before each calibration period is considered as the warm-up period to decrease the effects of the uncertain initial storages on model performance (Jahanshahi et al., 2021). The new measured data are incorporated to calibration procedure as follow:

1. Calculating the mean time series of sensors located in each HRU.
2. Running dHRUM as a lumped model for the HRUs with sensors and calibrating the soil storage and groundwater storage with respect to the measured time series using objective functions that are explained in section 2.4.1.
3. Running dHRUM for the whole BP or KL catchments as a semi-distributed model with the fixed parameter for HRUs with sensors, and constrained parameters for other HRUs according to the tables 2.7, 2.8, 2.9 and 2.10.

Figures 3.9 and 3.10 illustrate the coverage of GW and SM sensors in BP and KL catchments. According to the figures most sensors are installed in the frosted areas of BP and KL catchments.

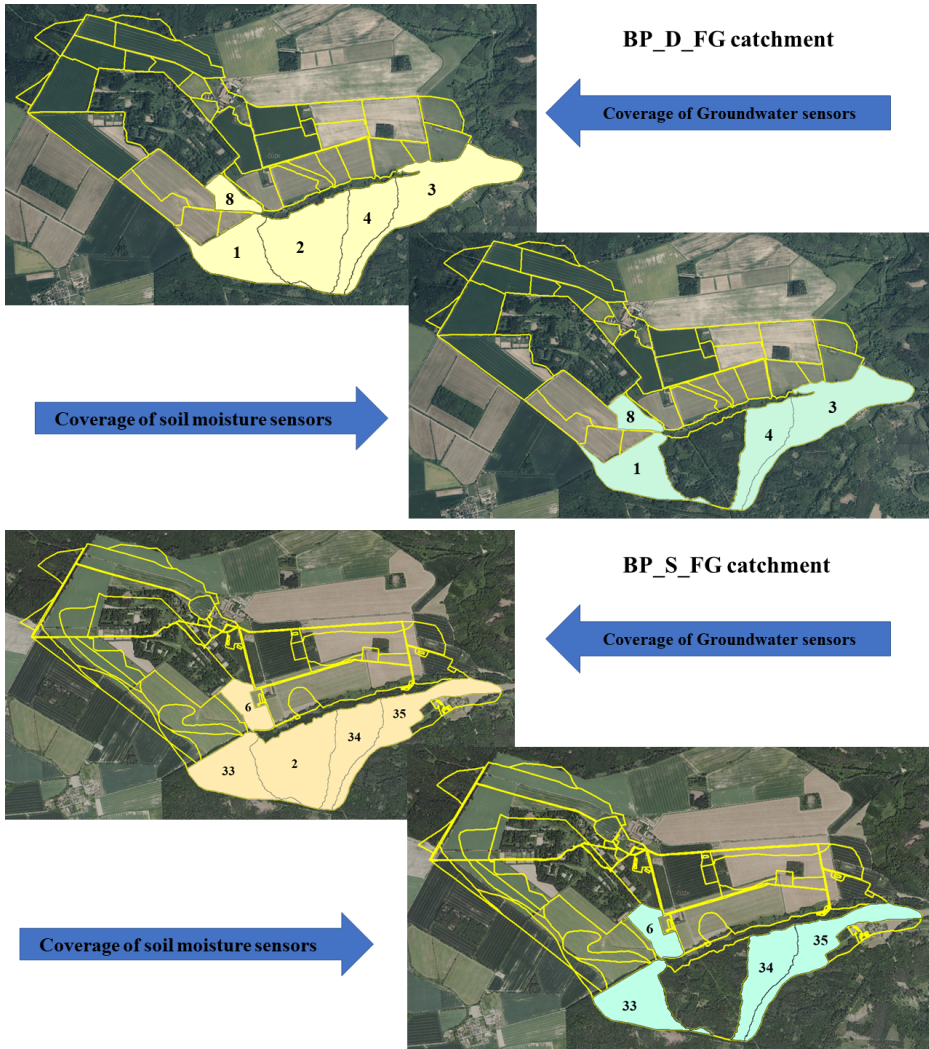


Fig. 3.9: Sensor coverage in BP\_D\_FG (UP) and BP\_S\_FG (down) catchment, the numbers on the polygons are HRU IDs

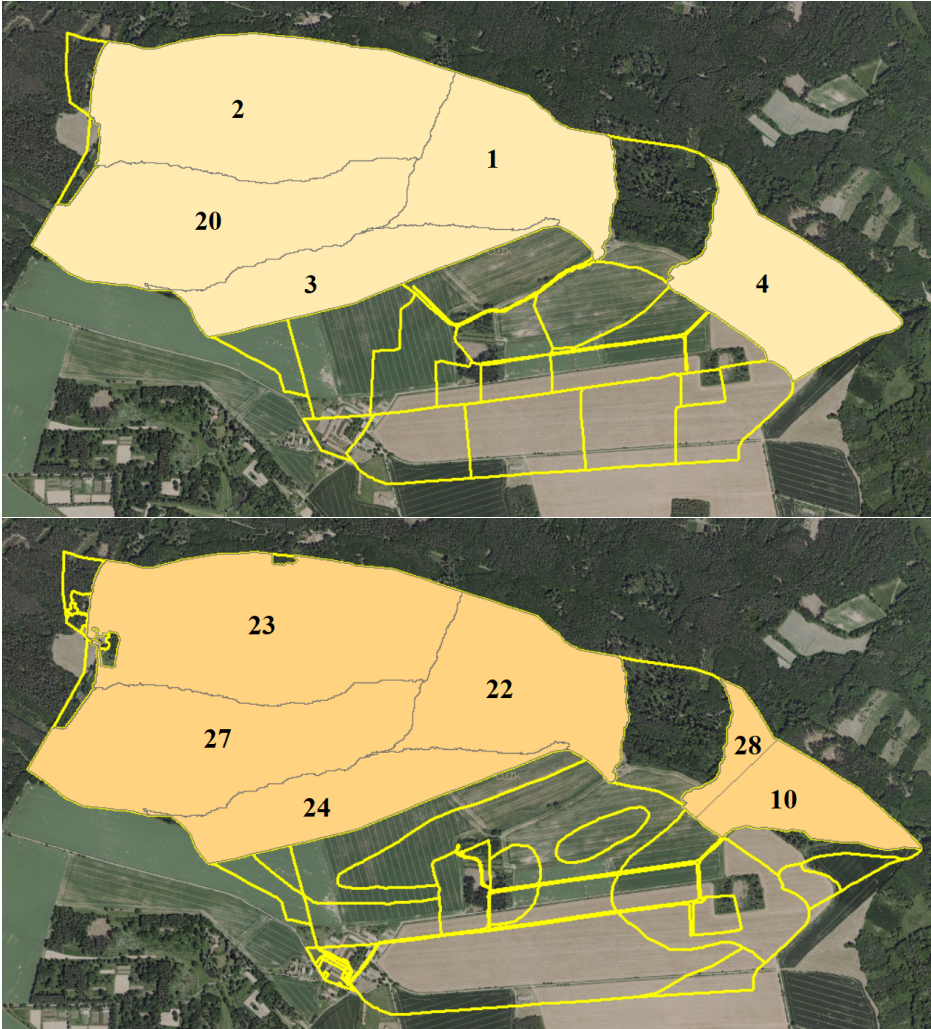


Fig. 3.10: Sensor coverage in KL\_D\_FG (UP) and KL\_S\_FG (down) catchment, the numbers on the polygons are HRU IDs

### 3.3.1 Calibration Using Groundwater Information

In this section, GW data is added to the procedure explained in section 3.4. Some of the obtained results of the simulation for each descritization are

represented in figures 3.11, 3.12, 3.13 and 3.14. They show the variations of GW level in HRUs number 8, 2, 1 and 27 in BP\_D\_FG, BP\_S\_FG, KL\_D\_FG and KL\_S\_FG catchments, respectively. The results for the rest of HRUs are shown in appendix 5.

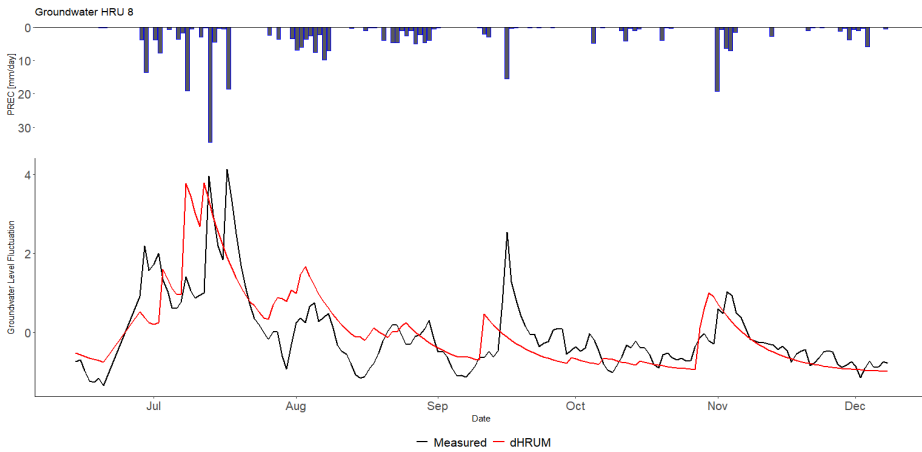


Fig. 3.11: Variations of GW level in HRU number 8 in BP\_D\_FG catchment; the blue bar graph shows the daily precipitation intensity

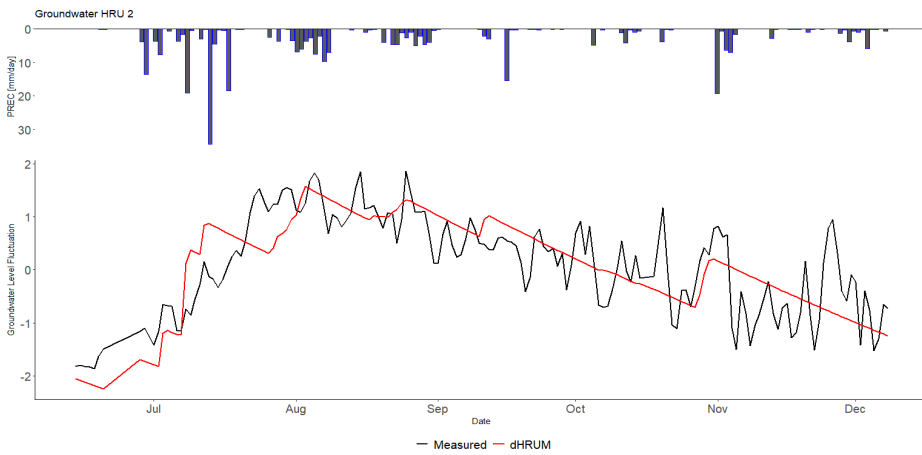


Fig. 3.12: Variations of GW level in HRU number 2 in BP\_S\_FG catchment; the blue bar graph shows the daily precipitation intensity

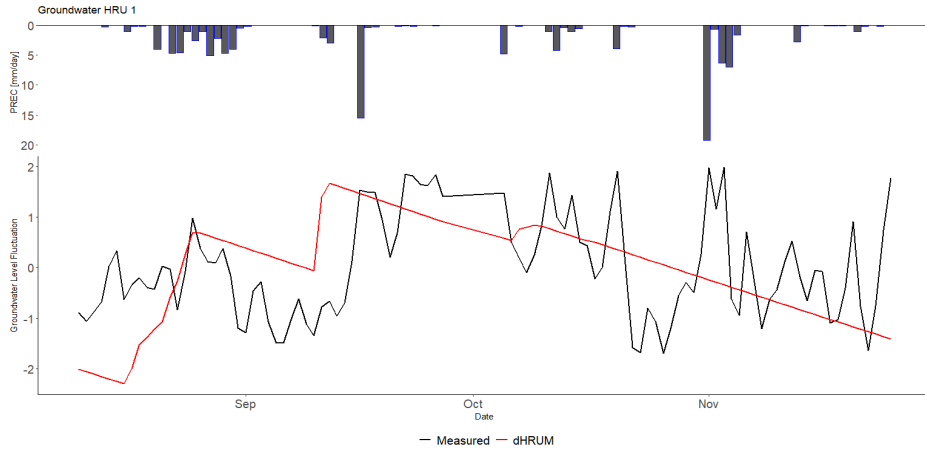


Fig. 3.13: Variations of GW level in HRU number 1 in KL\_D\_FG catchment; the blue bar graph shows the daily precipitation intensity

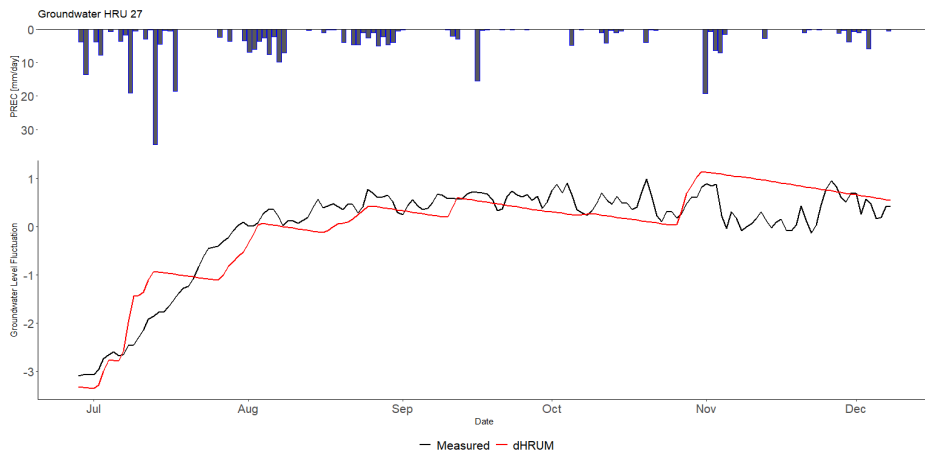


Fig. 3.14: Variations of GW level in HRU number 27 in KL\_S\_FG catchment; the blue bar graph shows the daily precipitation intensity

According to the figure 3.11, the variation of GW level is properly captured by dHRUM, however, there is a lag between simulated and measured peaks. The simulated time series reaches the peak values earlier

than measured ones. The same time series are shown for other HRUs and catchments. Figures 3.12, 3.13 and 3.14 show that the modeled and measured time series follow the same pattern, but dHRUM could not capture all the GW level fluctuations.

Tables 3.1 and 3.2 show the correlation coefficients between standardized GW storage and measured GW level in the BP and KL catchments, respectively.

Tab. 3.1: Correlation coefficients between standardized GW storage and measured GW level in BP

BP_D_FG		BP_S_FG	
HRU ID	Cor(stGW <sup>1</sup> , stGROS <sup>2</sup> )	HRU ID	Cor(stGW, stGROS)
1	0.91	2	0.83
2	0.82	6	0.68
3	0.85	33	0.90
4	0.83	34	0.57
8	0.67	35	0.85

<sup>1</sup> standardized value of measured GW level.

<sup>2</sup> standardized value of simulated GW storage.

Tab. 3.2: Correlation coefficients between standardized GW storage and measured GW level in KL

KL_D_FG		KL_S_FG	
HRU ID	Cor(stGW, stGROS)	HRU ID	Cor(stGW, stGROS)
1	0.32	10	0.69
2	0.85	22	0.27
3	0.83	23	0.87
4	0.72	24	0.84
20	0.92	27	0.89
-	-	28	0.80

According to the tables 3.1 and 3.2, the simulated time series by dHRUM

show good correlations with the measured data in almost most HRUs. Also, the relationships between simulated and measured values of GW are shown in figures 3.15 and 3.16 for BP and KL catchments, respectively.

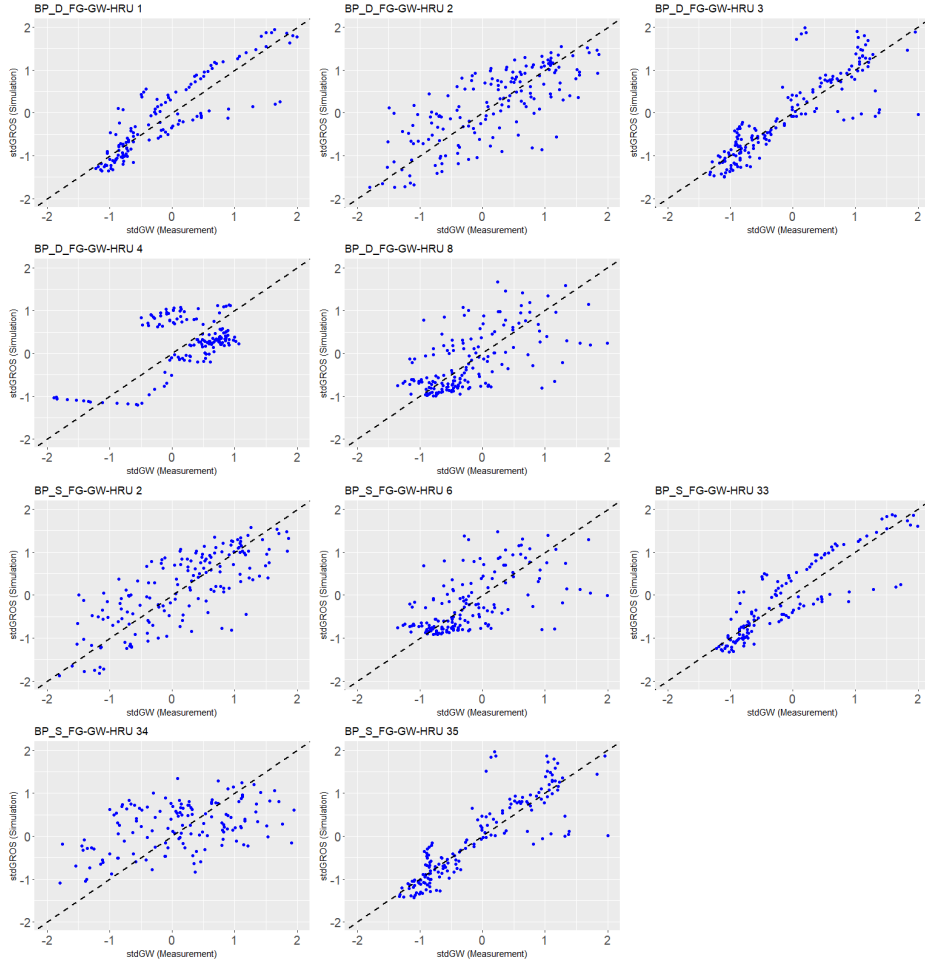


Fig. 3.15: Scatter plots of measured GW level versus simulated values in BP catchment

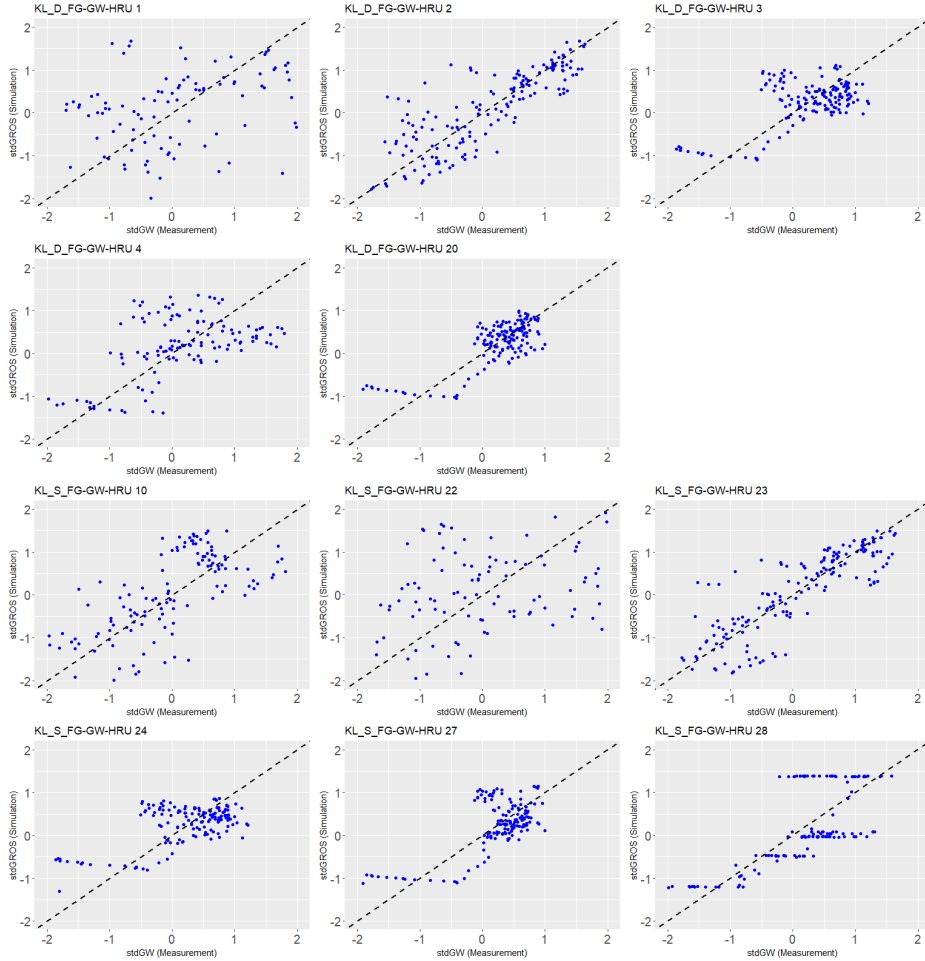


Fig. 3.16: Scatter plots of measured GW versus simulated values in KL catchment

According to the tables 3.2 and 3.2, the lowest value of correlation coefficient belong to the HRU number 22 in KL\_S\_FG catchment and HRU number 1 in KL\_D\_FG catchment which are 0.27 and 0.32. This low dependency can also be seen in figure 3.16 for their respective HRUs.

The semi-distributed version of dHRUM is applied to the whole BP and KL catchments to simulated the total runoff at the catchment outlet. The

parameters are constrained according to tables 2.7, 2.8, 2.9 and 2.10. The parameters for HRUs with the GW information are constrained according to the calculated values plus  $\pm 0.1parameter$ . The FDC curves for the BP and KL catchments are shown in figures 3.17 and 3.18.

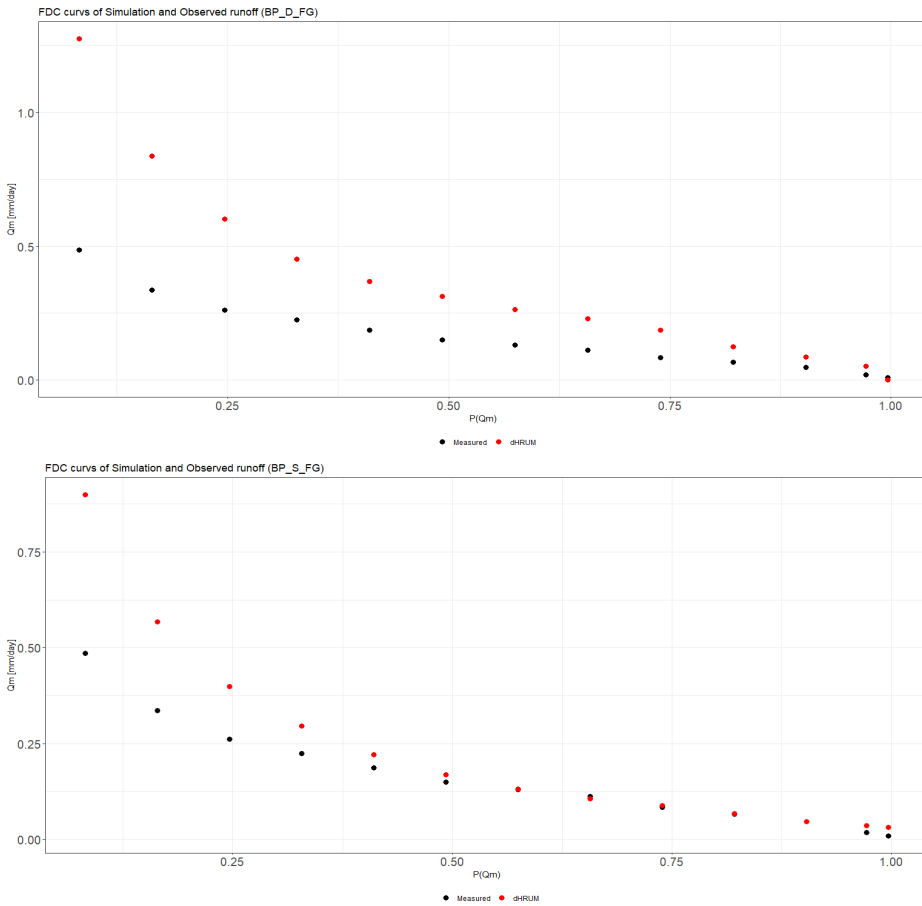


Fig. 3.17: FDCs curves of BP catchment derived from calibration using GW information

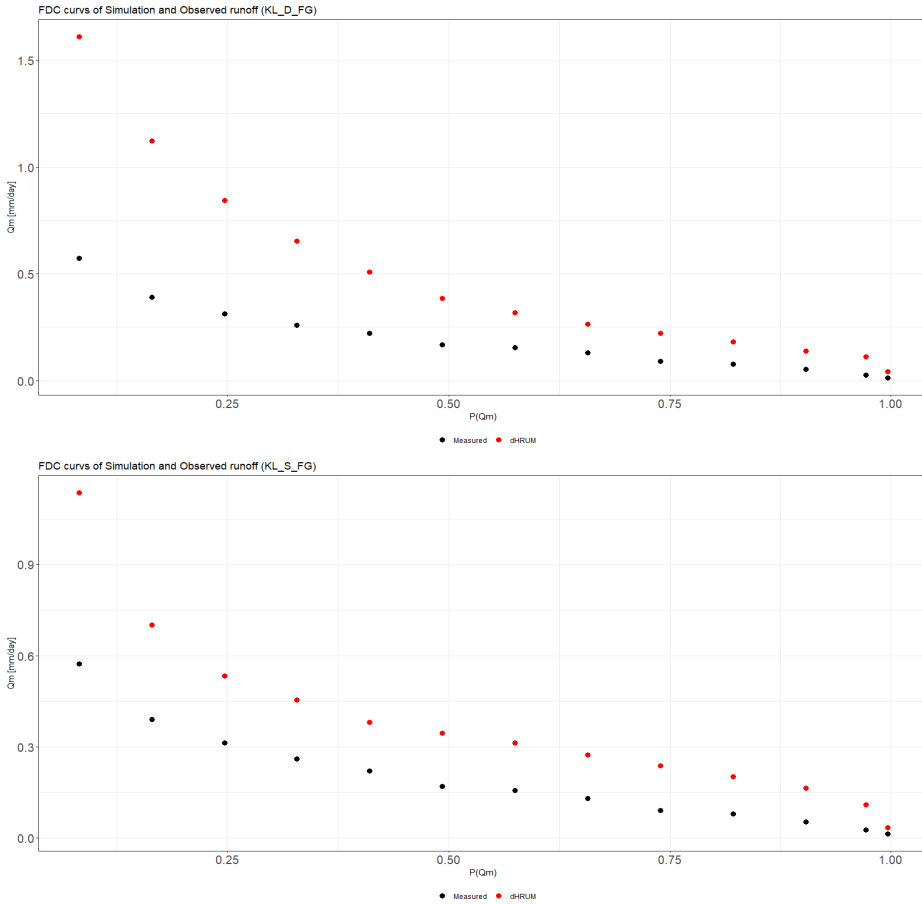


Fig. 3.18: FDCs curves of KL catchment derived from calibration using GW information

The obtained FDC curves show the runoff values are overestimated in all four catchments, especially in KL. The value of KS in HRUs with GW information is very small which leads to a very high groundwater storage and consequently higher baseflow and total runoff. The overestimation of runoff in KL catchments is more significant compared to the BP ones because GW sensors cover a larger area of the KL catchments than BP.

### 3.3.2 Calibration Using Soil Moisture Information

In this section, only SM data are used for the model calibration. The calibration procedure is explained in the section 3.4. Some of the obtained results for each discretization are represented in figures 3.19, 3.20, 3.21 and 3.22 which show the variations of SM storage in HRUs 4, 6, 20 and 10 in the their respective catchments. The results for the rest of HRUs are shown in appendix 5.

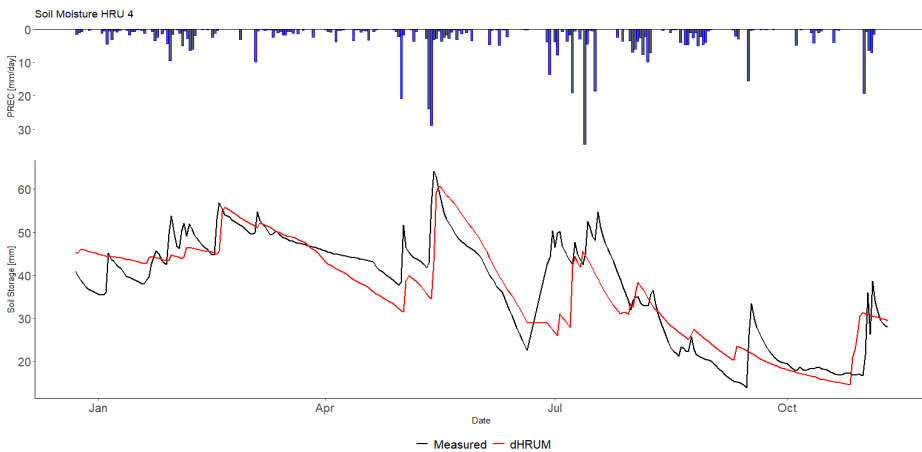


Fig. 3.19: SM versus soil storage in HRU number 4 in BP\_D\_FG catchment; the blue bar graph shows the daily precipitation intensity

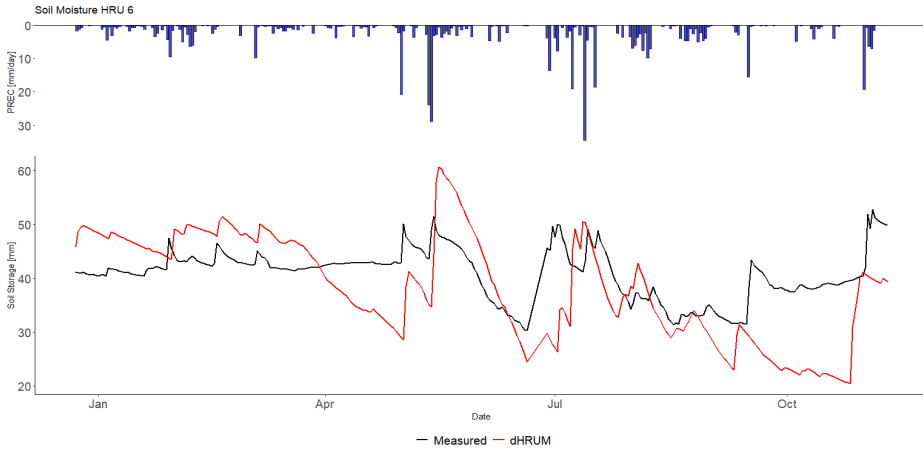


Fig. 3.20: SM versus soil storage in HRU number 6 in BP\_S\_FG catchment; the blue bar graph shows the daily precipitation intensity

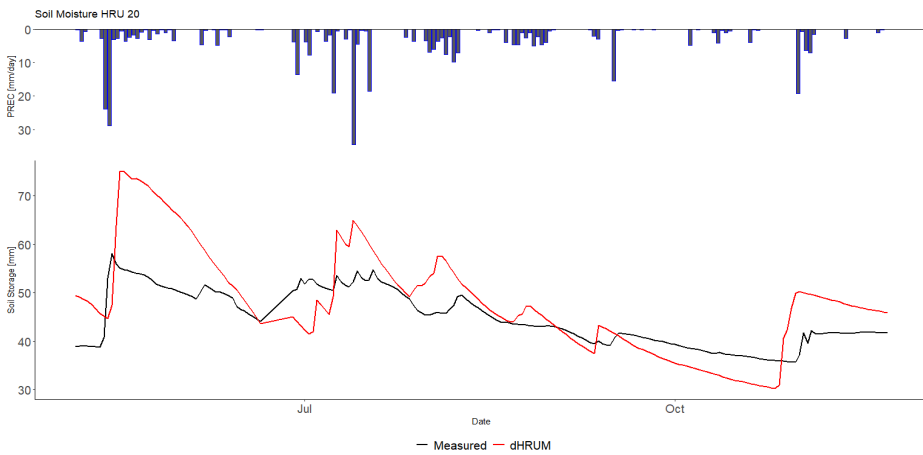


Fig. 3.21: SM versus soil storage in HRU number 20 in KL\_D\_FG catchment; the blue bar graph shows the daily precipitation intensity

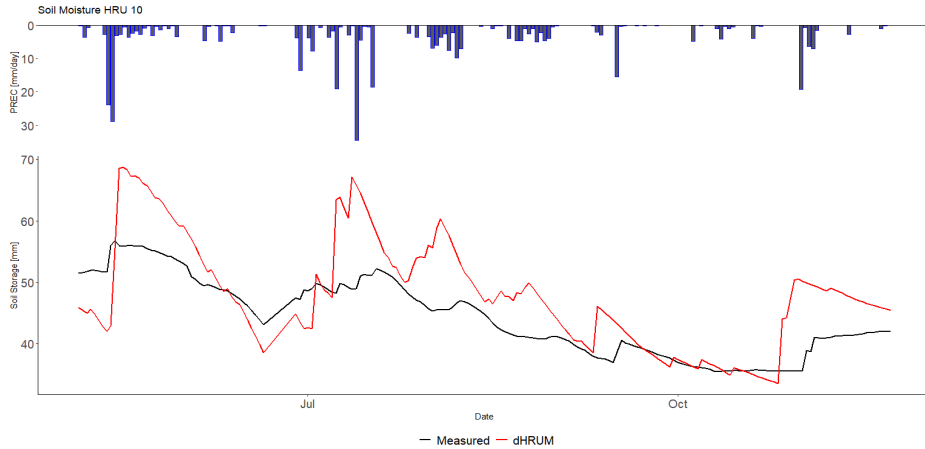


Fig. 3.22: SM versus soil storage in HRU number 10 in KL\_D\_FG catchment; the blue bar graph shows the daily precipitation intensity

Figure 3.19 shows that the SM storage simulated adequately in BP\_D\_FG catchment. However, in BP\_S\_FG, figure 3.20, although the simulated SM storage shows the same fluctuations as the measured data, the results are not as accurate as those of BP\_D\_FG catchment. In contrast, the SM storage fluctuation in KL catchment is not as large as that of BP. In this case, the model could properly simulate the the shape of measured data. But, according to the figures 3.21 and 3.22, dHRUM exaggerates all the fluctuation.

Tables 3.3 and 3.4 show the correlation coefficients between simulated soil storage and measured SM in BP and KL catchments.

Tab. 3.3: correlation coefficients between simulated soil storage and measured SM in BP

BP_D_FG		BP_S_FG	
HRU ID	Cor(SM <sup>1</sup> , SOIS <sup>2</sup> )	HRU ID	Cor(SM, SOIS)
1	0.68	6	0.50
3	0.28	33	0.65
4	0.85	34	0.83
8	0.35	35	0.23

<sup>1</sup> measured SM.<sup>2</sup> simulated soil storage.

Tab. 3.4: Correlation coefficients between simulated soil storage and measured SM in KL

KL_D_FG		KL_S_FG	
HRU ID	Cor(SM, SOIS)	HRU ID	Cor(SM, SOIS)
1	0.81	10	0.77
2	0.71	22	0.83
3	0.62	23	0.78
4	0.83	24	0.82
20	0.77	27	0.79

The values in tables 3.1 and 3.4 show high correlations between measured and simulated data for most HRUs and consequently an acceptable performance of dHRUM in simulating the variations of soil storage. Also, the relationships between simulated and measured values of soil storage and SM are shown in figures 3.23 and 3.24 for BP and KL catchments, respectively.

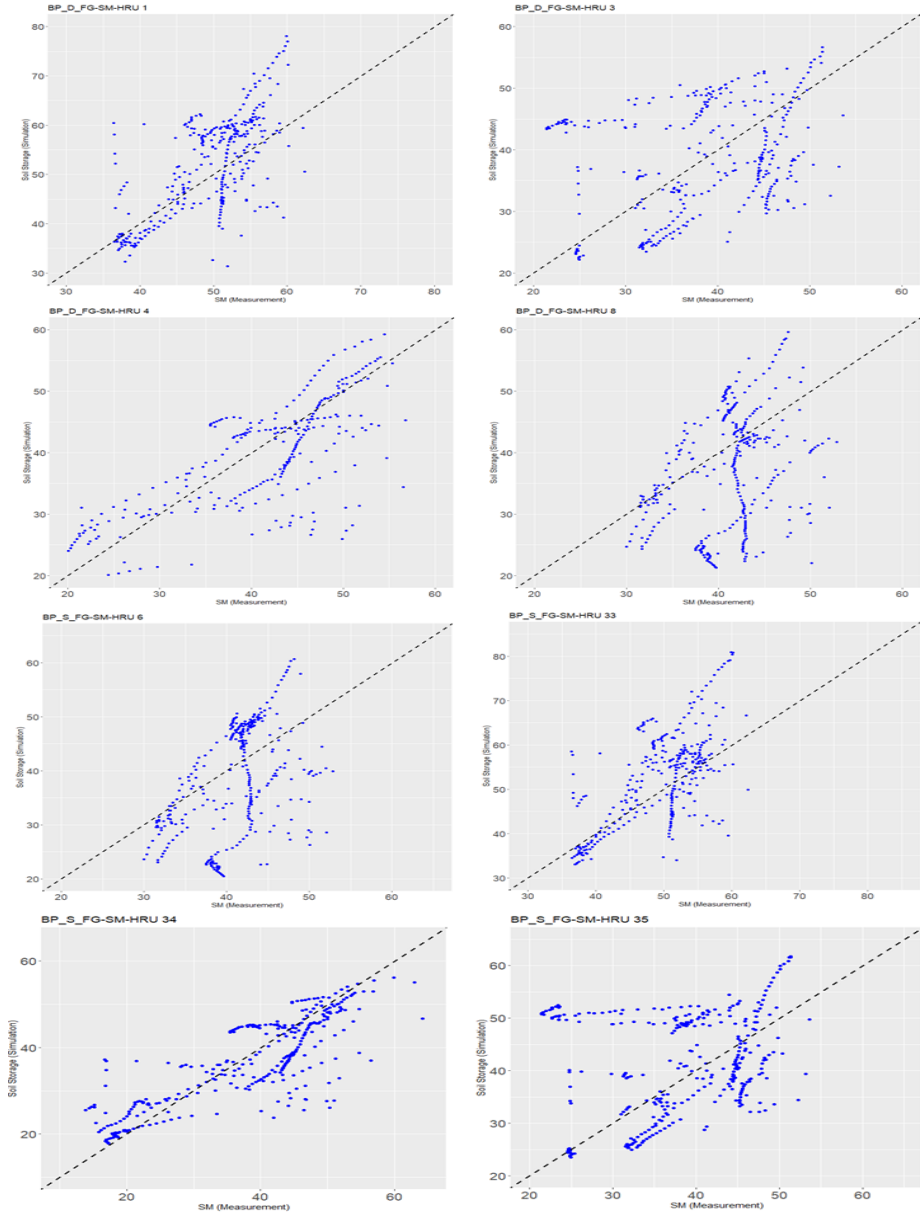


Fig. 3.23: Scatter plots of measured SM versus simulated values in BP catchment

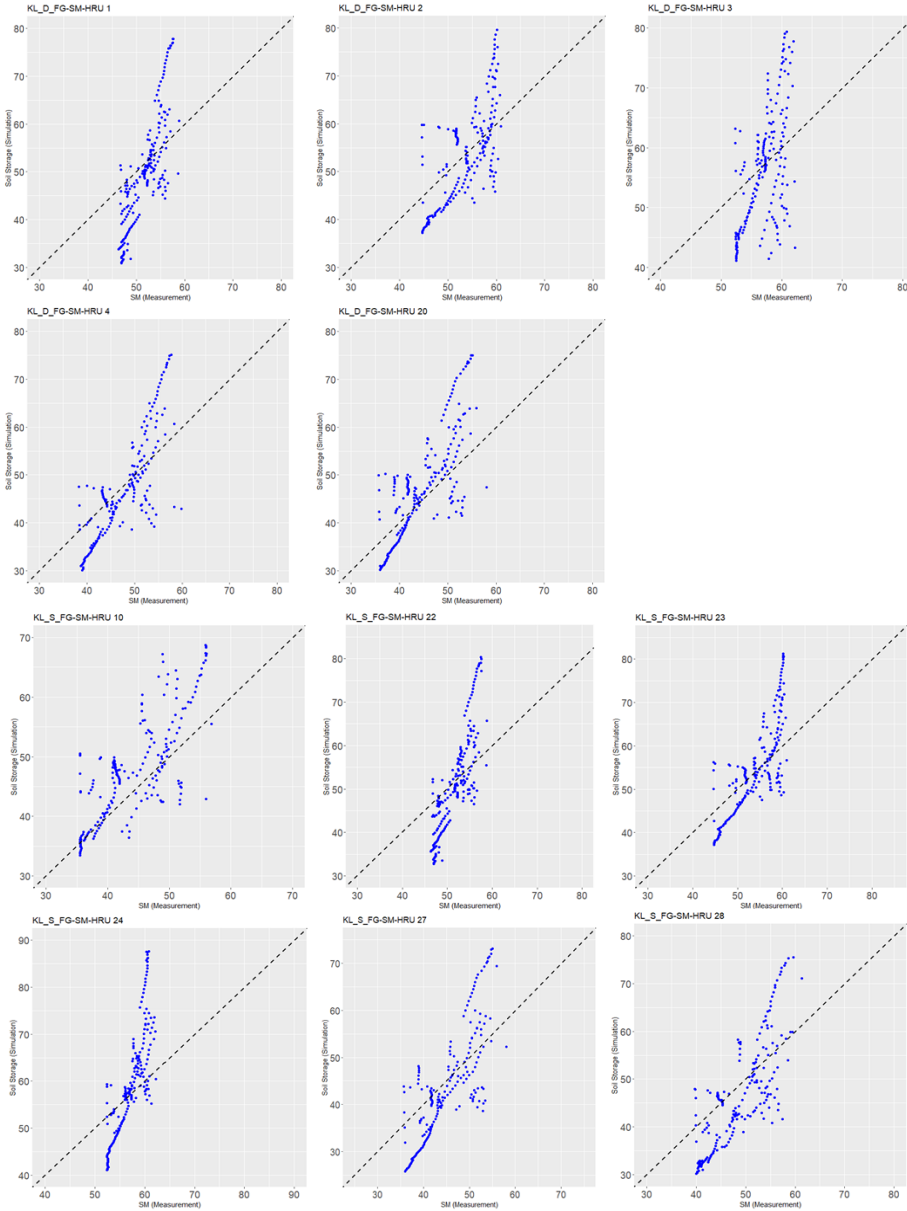


Fig. 3.24: Scatter plots of measured SM versus simulated values in KL catchment

Tables 3.3 and 3.4 show that the lowest values of correlation coefficient belong to the HRU number 35 in BP\_S\_FG catchment and HRU number 8 in BP\_D\_FG catchment which are 0.23 and 0.35. This low dependency can also be seen in figure 3.23 for their respective HRUs.

In all HRUs in KL catchment, figure 3.24, the trends of the scattered points are larger than 1. Therefore, it can be concluded that the model overestimates the high values of soil storage which also can be seen in figures 3.19, 3.20, 3.21 and 3.22.

The same as the previous the section, the semi-distributed version of dHRUM is applied to the whole BP and KL catchments to simulated the runoff at catchments outlet. The parameters are constrained according to tables 2.7, 2.8, 2.9 and 2.10. The parameters for HRUs with the SM information are constrained according to the calculated values plus  $\pm 0.1parameter$ . The FDC curves for the BP and KL catchments are shown in figures 3.25 and 3.26.

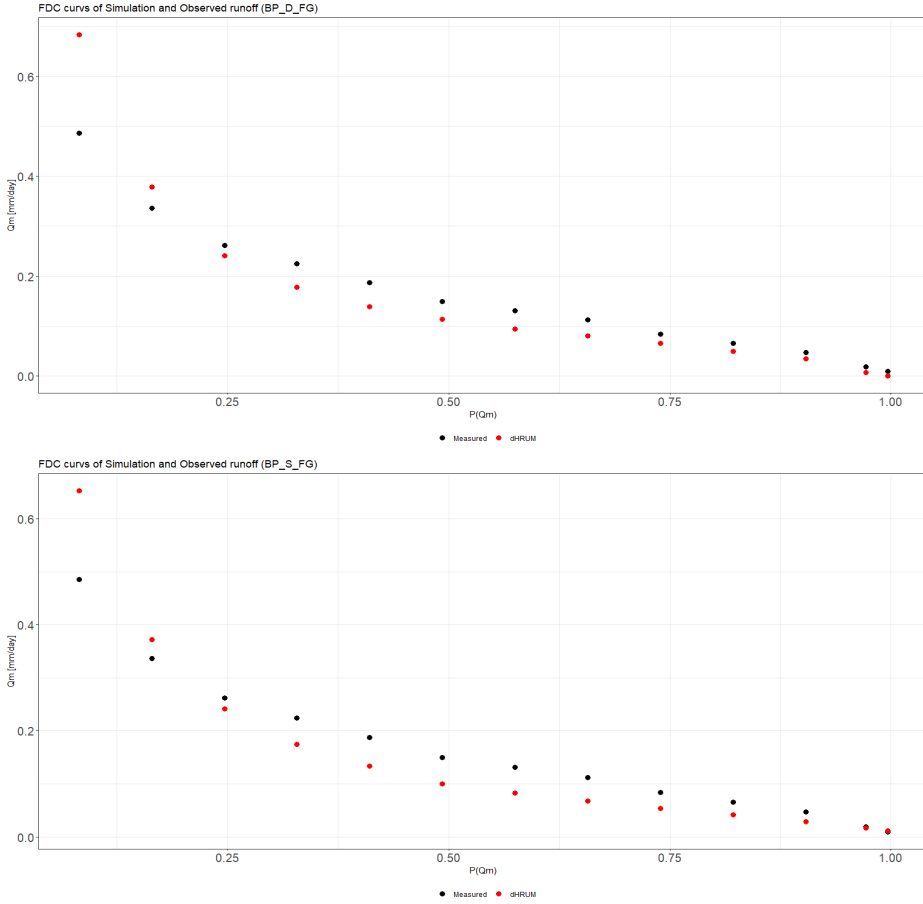


Fig. 3.25: FDCs curves of BP catchment derived from calibration using SM information

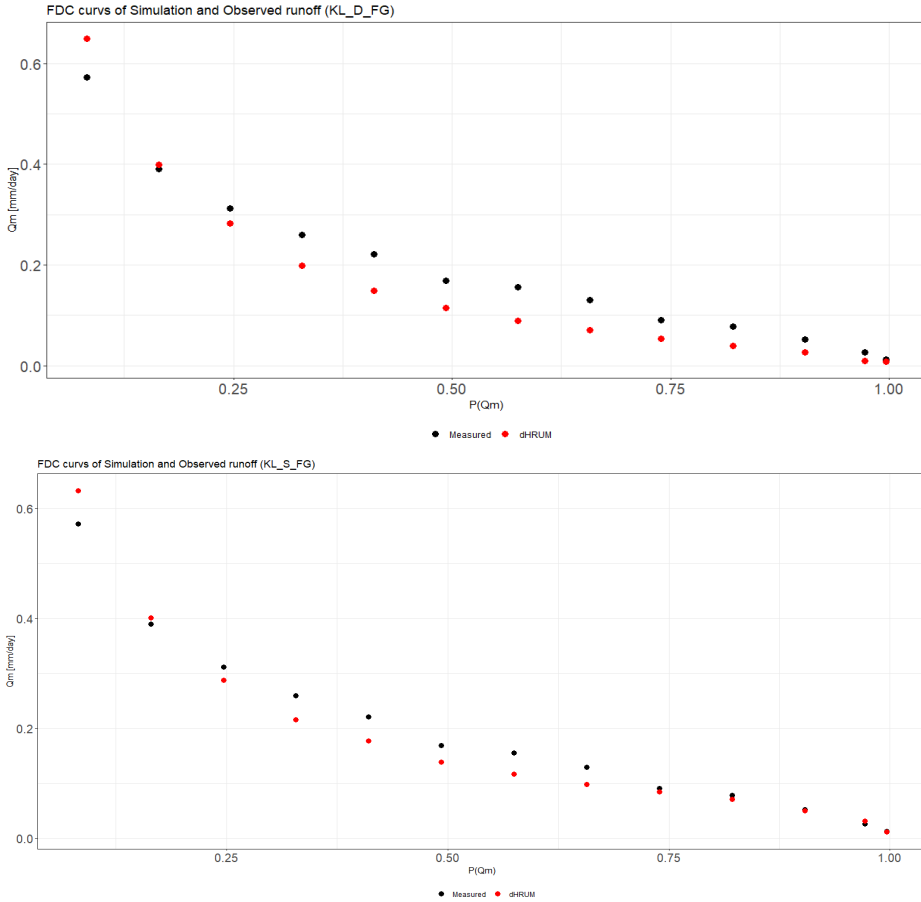


Fig. 3.26: FDCs curves of BP catchment derived from calibration using SM information

Figures 3.25 and 3.26 show a better fit for FDC compared to the case of GW calibration. According to the figures, the values of low and mid flows are underestimated, but the high flows are overestimated. In this case, the values of the parameter KS are significantly higher than the GW case. Therefore, the GW storage is lower and the baseflows and total runoff are lower.

### 3.3.3 Calibration Using Both Groundwater Level and Soil Moisture Information

In this section, both GW level and SM information are used for the model calibration. The calibration procedure has some extra steps compared to the section 3.4 which are as follows

1. Calibrating the model using GW data the same as section 3.4.1.
2. Constraining the calculated parameters from the previous step plus  $\pm 0.2 \text{parameter}$ .
3. Using the constrained parameters for calibrating the model with respect to SM data. The objective function  $OF$  in this step is

$$OF = 0.1 (1 - \text{cor}(\text{stdGW}, \text{stdGROS})) + 0.9 \text{MAE}(\text{SM}, \text{SOIS}), \quad (3.1)$$

where  $\text{cor}(\text{stdGW}, \text{GROS})$  is the correlation coefficient between standardized groundwater level,  $\text{stdGW}$ , and standardized simulated groundwater storage,  $\text{GROS}$  and  $\text{MAE}(\text{SM}, \text{SOIS})$  is mean absolute error between measured soil moisture –  $\text{SM}$ , and simulated soil storage –  $\text{SOIS}$ .

4. Running dHRUM for the whole BP or KL catchment as a semi-distributed model with the fixed parameter for HRUs with sensors, and constrained parameters for other HRUs.

Some of the obtained results for each discretization are represented in figures 3.27, 3.28, 3.29 and 3.30. They show the variations of SM storage in HRUs 4, 6, 20 and 10 in their respective catchments. The results for the rest of HRUs are shown in appendix 5.

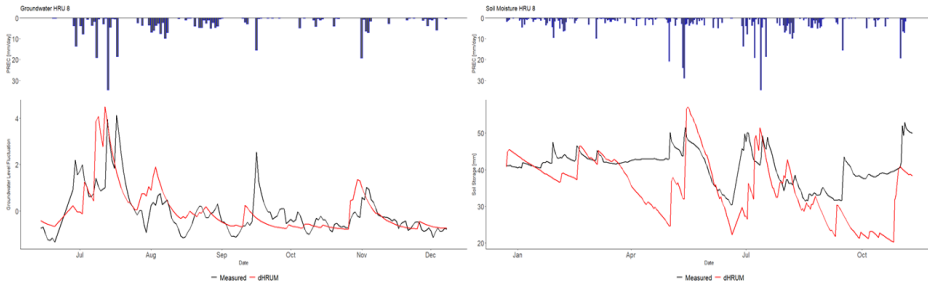


Fig. 3.27: GW and SM variations in HRU number 8 in BP\_D\_FG catchment; the blue bar graph shows the daily precipitation intensity

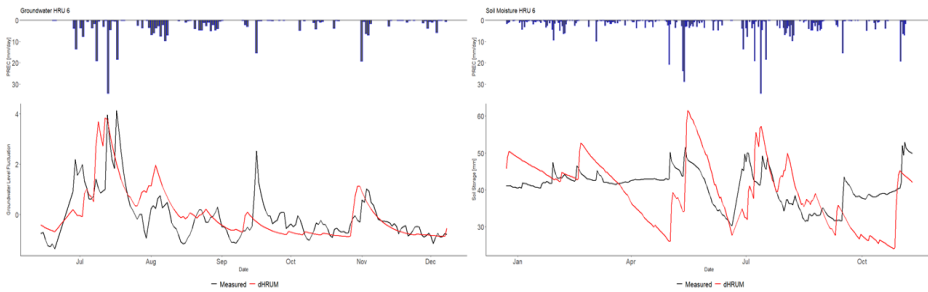


Fig. 3.28: GW and SM variations in HRU number 6 in BP\_S\_FG catchment; the blue bar graph shows the daily precipitation intensity

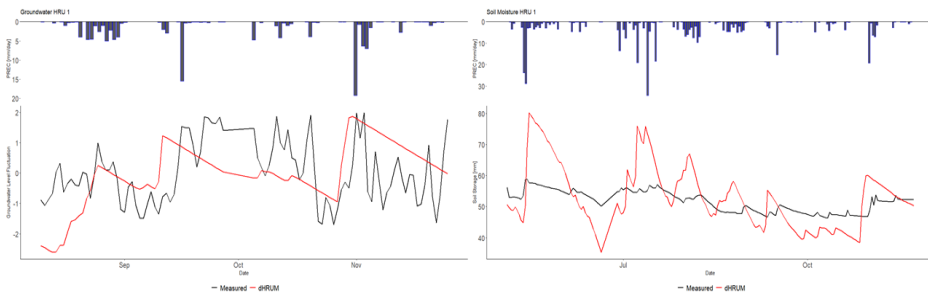


Fig. 3.29: GW and SM variations in HRU number 1 in KL\_D\_FG catchment; the blue bar graph shows the daily precipitation intensity

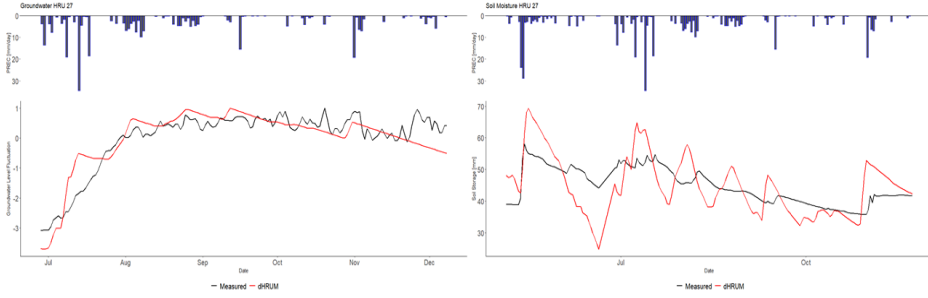


Fig. 3.30: GW and SM variations in HRU number 27 in KL\_S\_FG catchment; the blue bar graph shows the daily precipitation intensity

According to the figures above, the dHRUM shows an acceptable performance in terms of modelling of standardized GW level and SM storage simultaneously. However, the model lacks the ability to capture all the fluctuations properly. The model shows minor fluctuations in GW simulation but wide fluctuations in SM simulation.

Tables 3.5 and 3.6 show the correlation coefficients between standardized GW storage and measured GW level and between simulated soil storage and measured SM in BP and KL catchments.

Tab. 3.5: Correlation coefficients derived from calibration using both GW and SM data in BP catchment

BP_D_FG		
HRU ID	Cor(stGW <sup>1</sup> , stGROS <sup>2</sup> )	Cor(SM <sup>3</sup> , SOIS <sup>4</sup> )
1	0.91	0.76
2	0.84	-
3	0.85	0.12
4	0.81	0.72
8	0.61	0.45
BP_S_FG		
2	0.83	-
6	0.68	0.36
33	0.90	0.73
34	0.57	0.86
35	0.85	0.25

<sup>1</sup> standardized value of measured GW level.

<sup>2</sup> standardized value of simulated GW storage.

<sup>3</sup> measured SM.

<sup>4</sup> simulated soil storage.

Tab. 3.6: Correlation coefficients derived from calibration using both GW and SM data in KL catchment

KL_D_FG		
HRU ID	Cor(stGW, stGROS)	Cor(SM, SOIS)
1	0.25	0.65
2	0.88	0.53
3	0.88	0.66
4	0.72	0.66
20	0.89	0.50
KL_S_FG		
10	0.49	0.66
22	0.10	0.60
23	0.85	0.66
24	0.89	0.66
27	0.89	0.56
28	0.89	0.66

The values in tables 3.5 and 3.6 show high correlations between measured and simulated GW and SM data for most HRUs and consequently an acceptable performance of dHRUM in simulating the variations of GW level and soil storage. Also, the relationships between simulated and measured values of GW and SM are shown in figures 3.31, 3.32, 3.34 and 3.34, for BP and KL catchments, respectively.

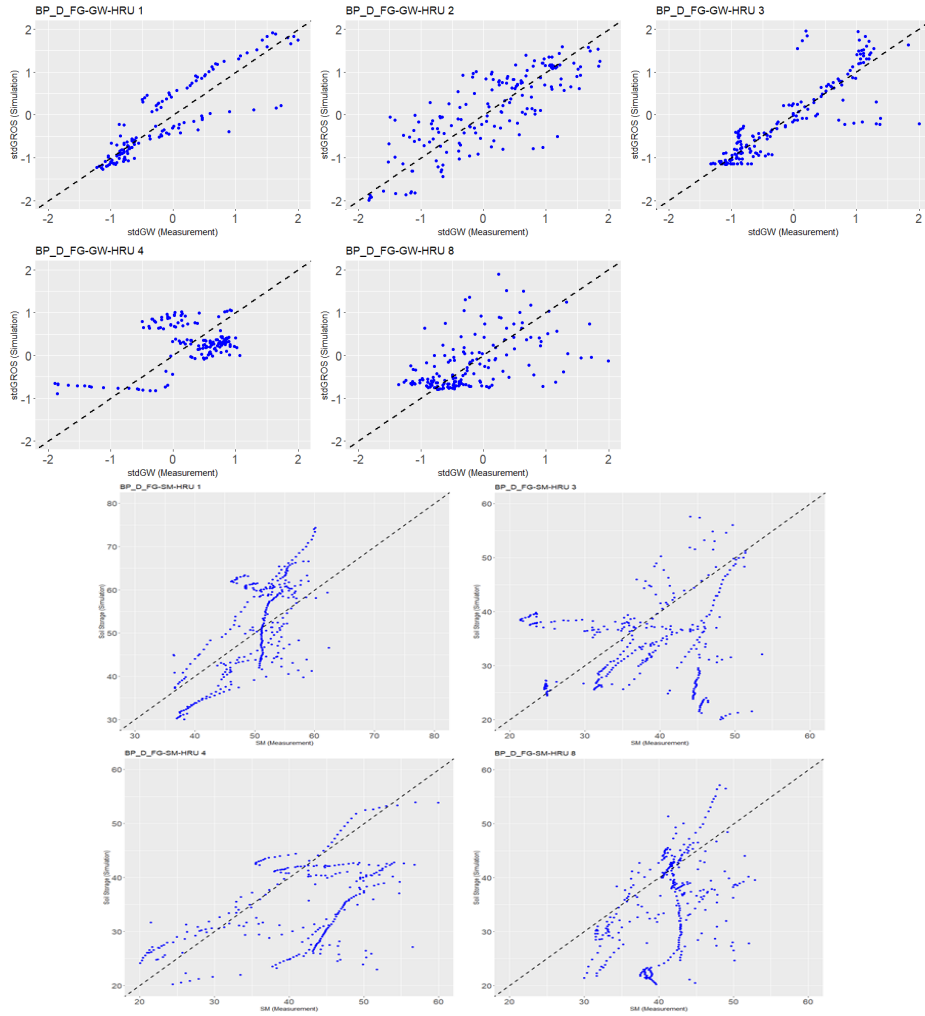


Fig. 3.31: Scatter plots of measured GW and SM versus simulated values in BP\_D\_FG catchment

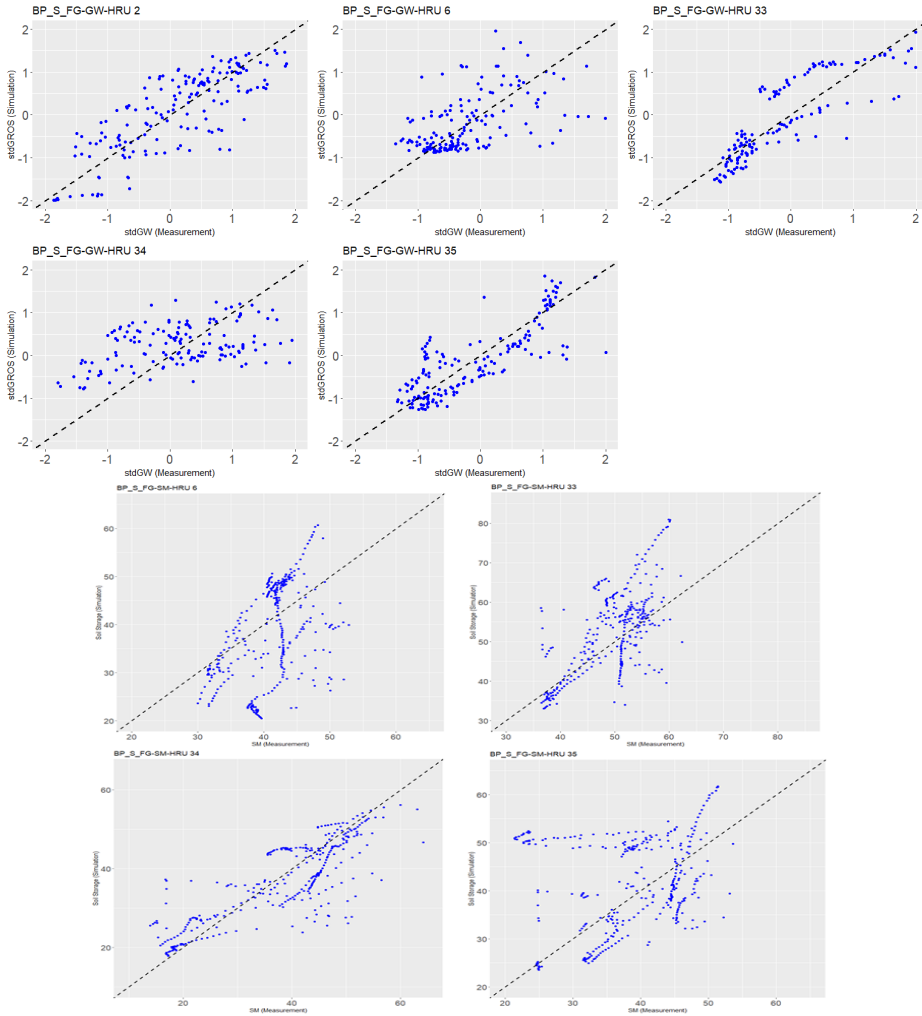


Fig. 3.32: Scatter plots of measured GW and SM versus simulated values in BP\_S\_FG catchment

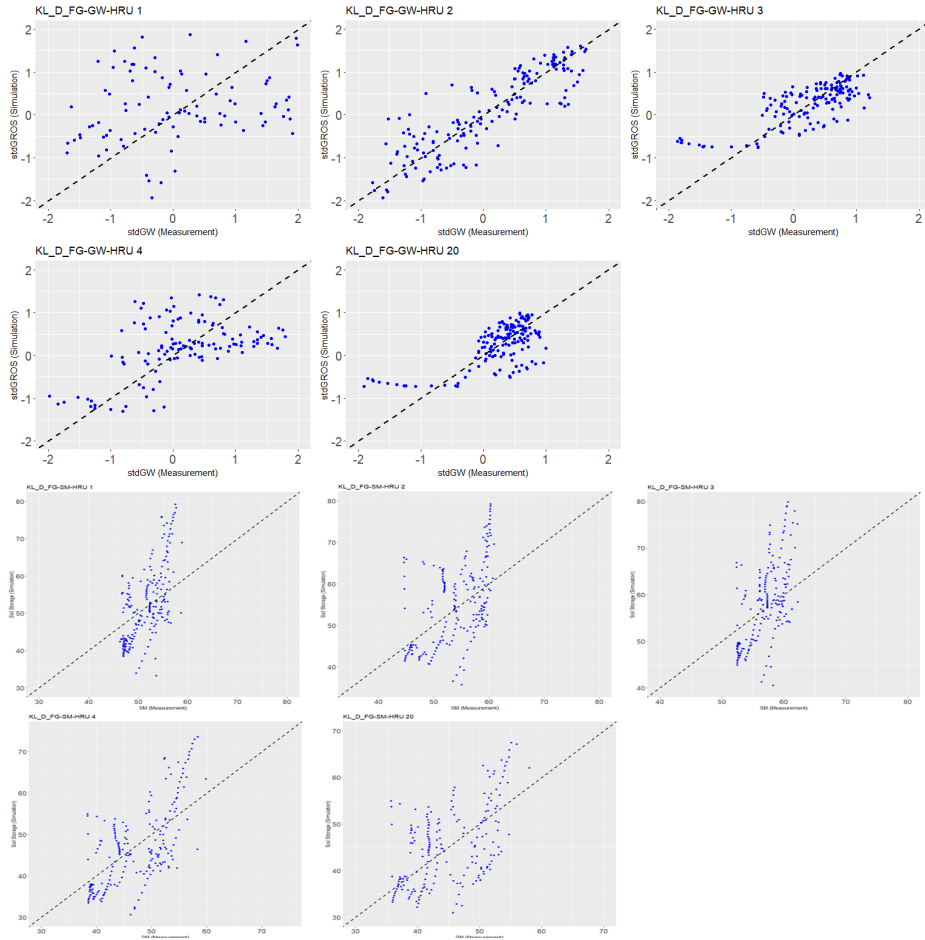


Fig. 3.33: Scatter plots of measured GW and SM versus simulated values in KL\_D\_FG catchment

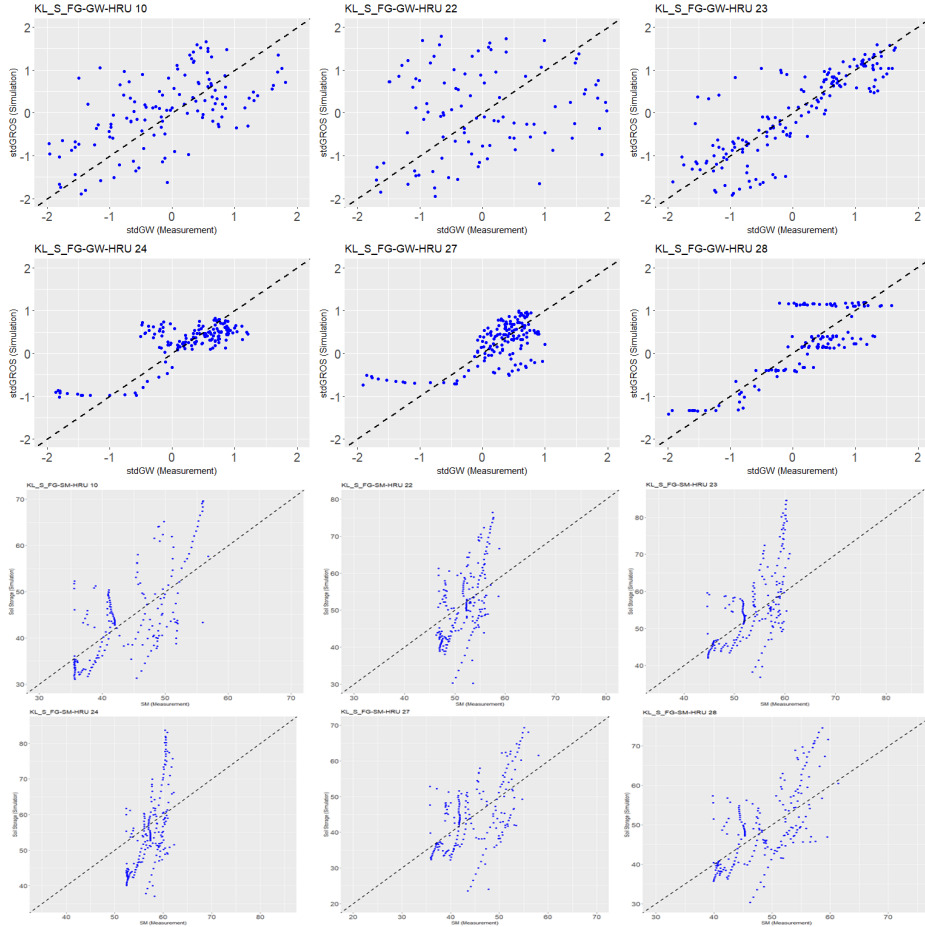


Fig. 3.34: Scatter plots of measured GW and SM versus simulated values in KL\_S\_FG catchment

According to the tables 3.5 and 3.6, the lowest values of correlation coefficient belong to the HRU number 22 in KL\_S\_FG catchment and HRU number 1 in KL\_D\_FG catchments which are 0.10 and 0.25. This low dependency can also be seen in figures 3.23 and 3.33 for their respective HRUs.

The same as the previous section, in all HRUs in KL catchment which

is shown in figure 3.34, the trends of the scattered points are larger than 1 and the model overestimates the high values of soil storage, figures 3.27, 3.28, 3.29 and 3.30.

The figures 3.35 and 3.36 show the FDC curves derived from running the semi-distributed version of dHRUM for the whole BP and KL catchments at the outlet points.

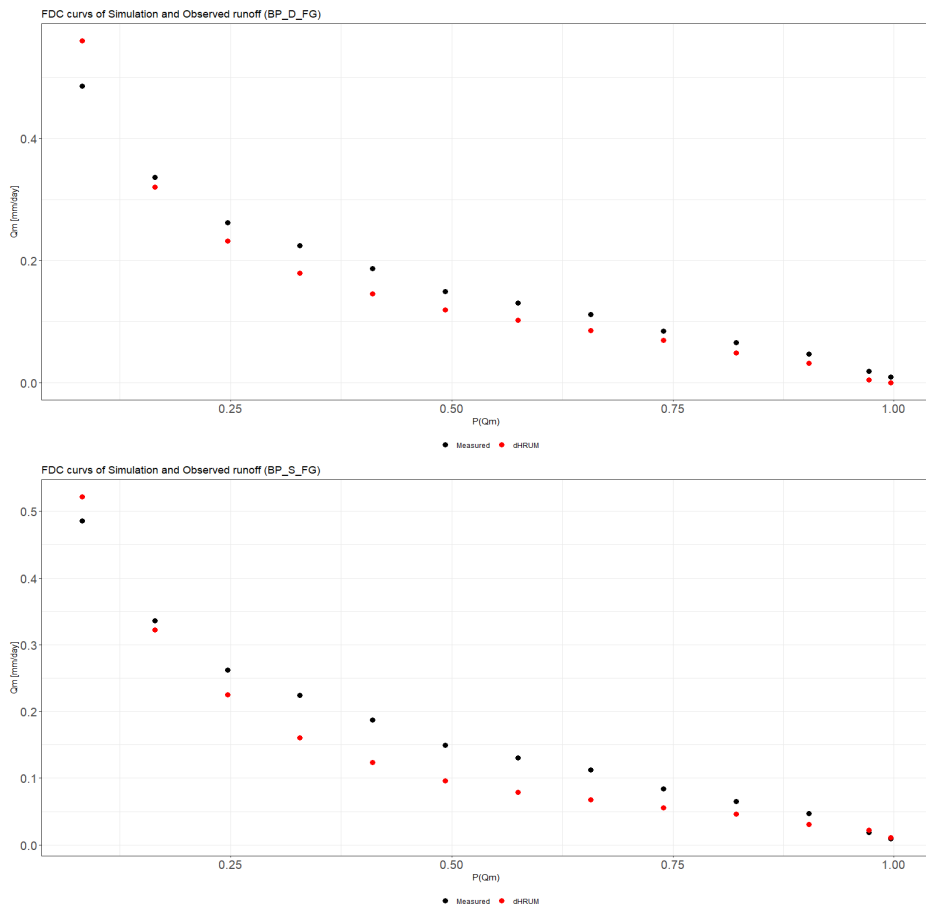


Fig. 3.35: FDCs curves of BP catchment using GW and SM information

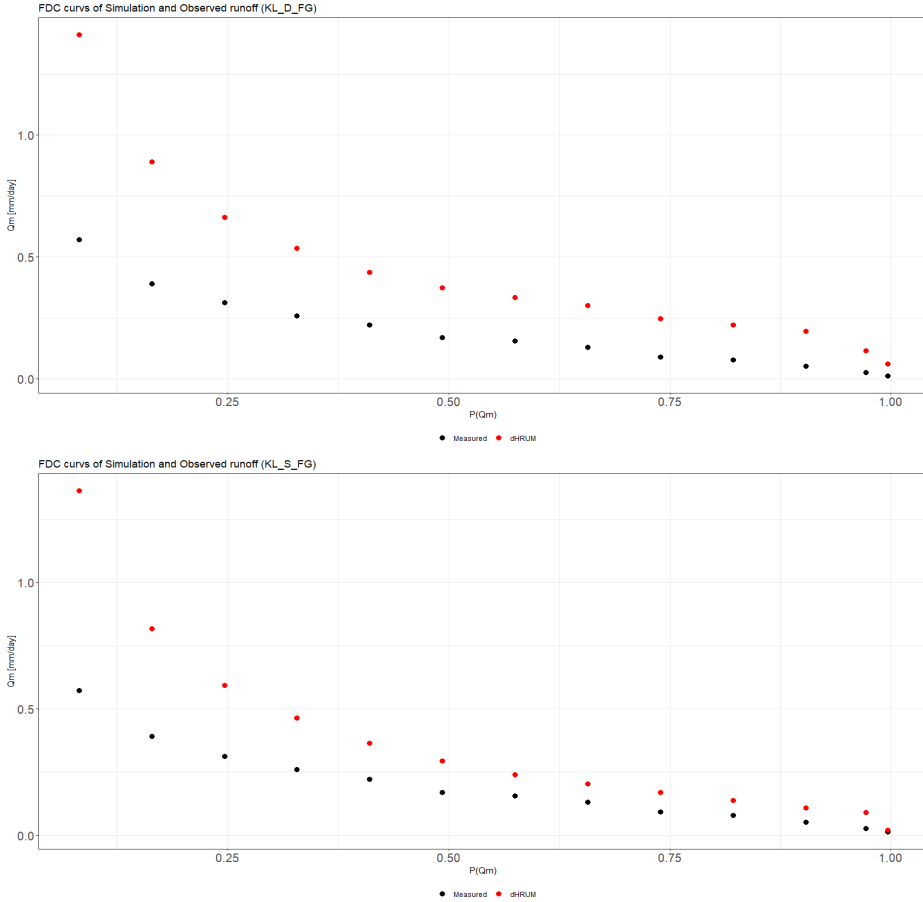


Fig. 3.36: FDCs curves of KL catchment using GW and SM information

According to the figure 3.35 considering both GW and SM information in BP catchment increases the model performance especially in BP\_D\_FG catchment. The 3.36. However, the in KL catchments this combination, GW and SM, exacerbates the model’s performance and leads to overestimation of total runoff.

## 3.4 The Effects of Catchment Discretization on Water Balance

This section explains the effects of the four types of discretizations on the water balance in the study area. To do so, first, the state variables, table 2.2, fluxes 2.3 and storage, 2.4 should be investigated for each catchment discretization. All of these variables, fluxes and storages are explained in sections 3.4.1, 3.4.2 and 3.4.3, respectively.

### 3.4.1 State Variables

The values of precipitation, temperature and potential evapotranspiration are almost the same in both BP and KL catchments. However, there are subtle differences between snow depth in BP and KL which can be seen in figure 3.37. The snow depths, especially high values, are larger in BP\_D\_FG catchment than BP\_S\_FG when using only expert knowledge, but in the rest calibration schemes, these values are almost the same.

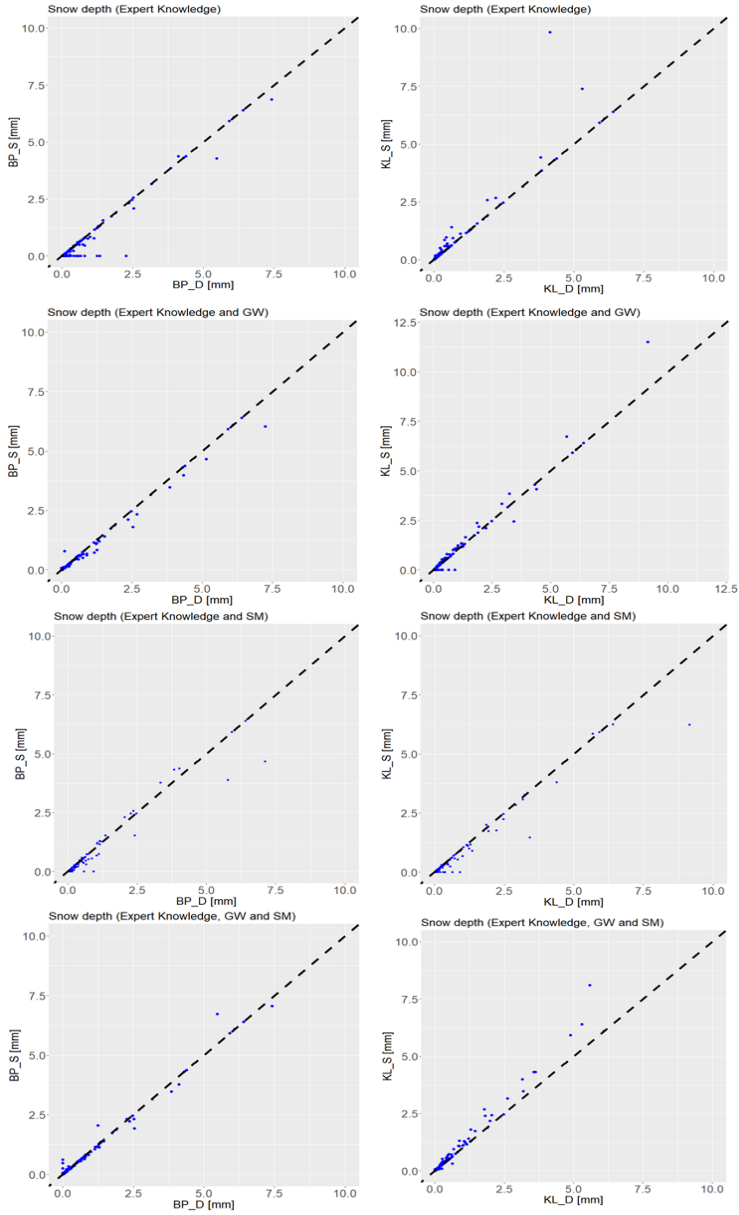


Fig. 3.37: The Scatted plots of snow depth in BP and KL catchments

### 3.4.2 Fluxes

This part explains the effects of catchment discretizations on the flux variables. These variables are baseflow, direct runoff, total runoff, percolation and melting.

Figures 3.38 and 3.39 show the scatter plots and the heat map of baseflow in BP and KL catchments for four different types of calibrations. According to the figures, the high baseflow values are more significant in the discretizations based on soil type than the drainage system when using GW and SM information in calibration. However, the the baseflow time series in all catchments are highly correlated, 3.39.

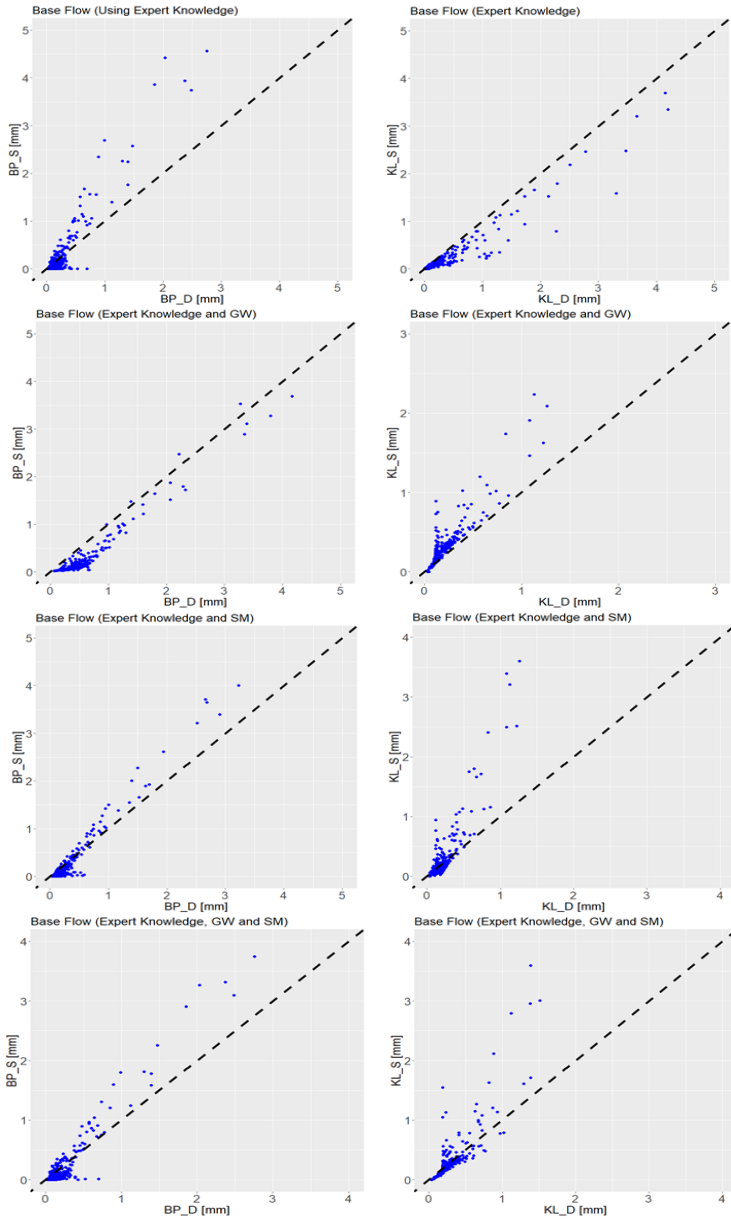


Fig. 3.38: The Scatted plots of baseflow in BP and KL catchments

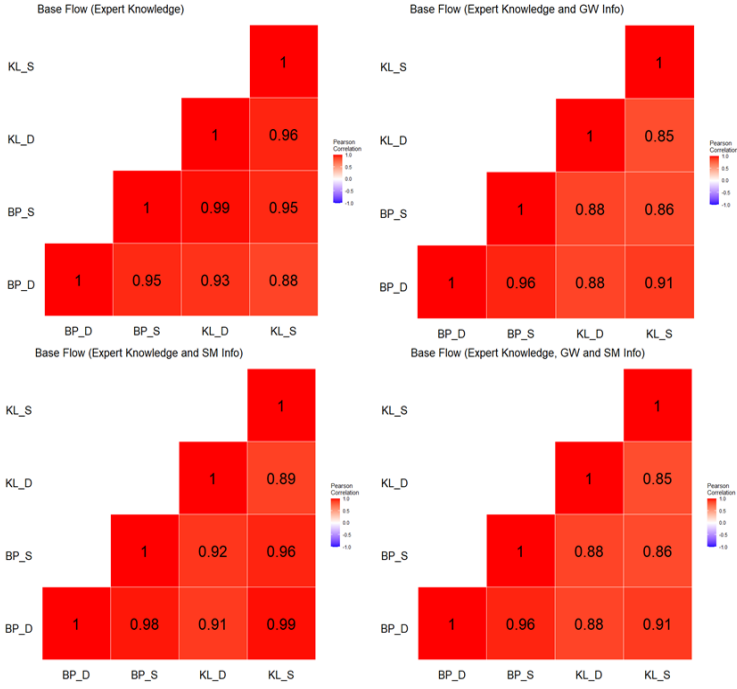


Fig. 3.39: The Heatmap of baseflow in BP and KL catchments

Figures 3.40 and 3.41 show the scatter plots and the heat map of direct runoff in BP and KL catchments for four different types of calibrations. The values of direct runoff in drainage-based discretizations are larger than soil-based ones. The heat map in figure 3.41 shows higher correlation between the direct runoff time series when using GW and/or SM information.

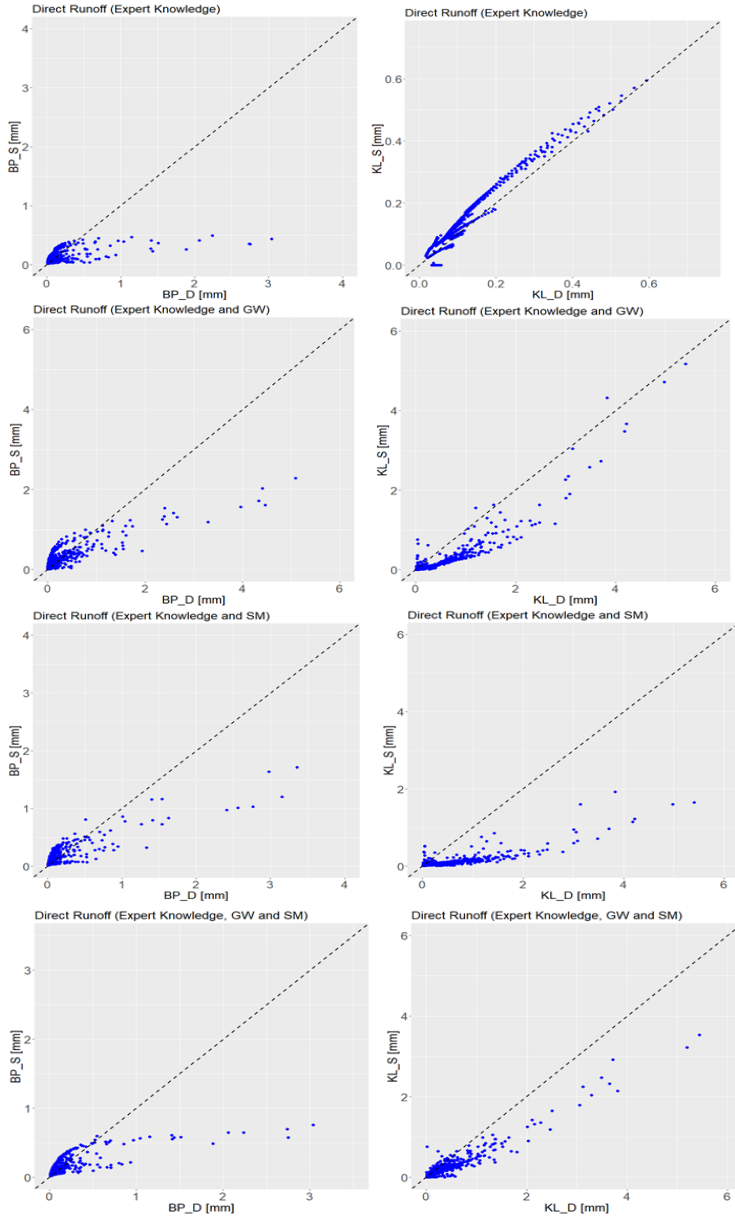


Fig. 3.40: The Scatted plots of direct runoff in BP and KL catchments

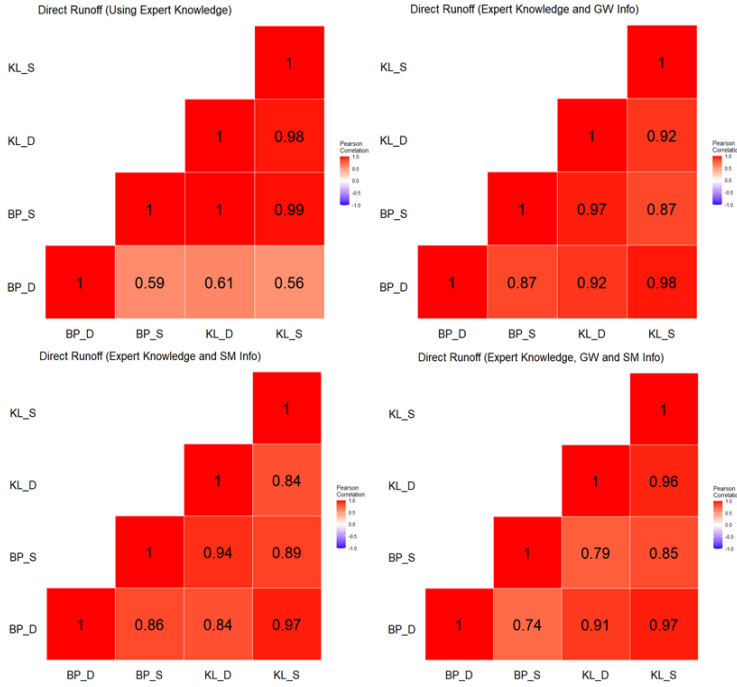


Fig. 3.41: The Heatmap of direct runoff in BP and KL catchments

Figures 3.42 and 3.43 show the scatter plots and the heat map of percolation in BP and KL catchments for four different types of calibrations. According to the figures this value is almost the same in all catchments except for KL\_D\_FG catchment when using SM data. In this case, the value of percolation in KL\_D\_FG catchment is larger than KL\_S\_FG. The heat map of percolation shows high correlation between the time series of percolation in all discretizations.

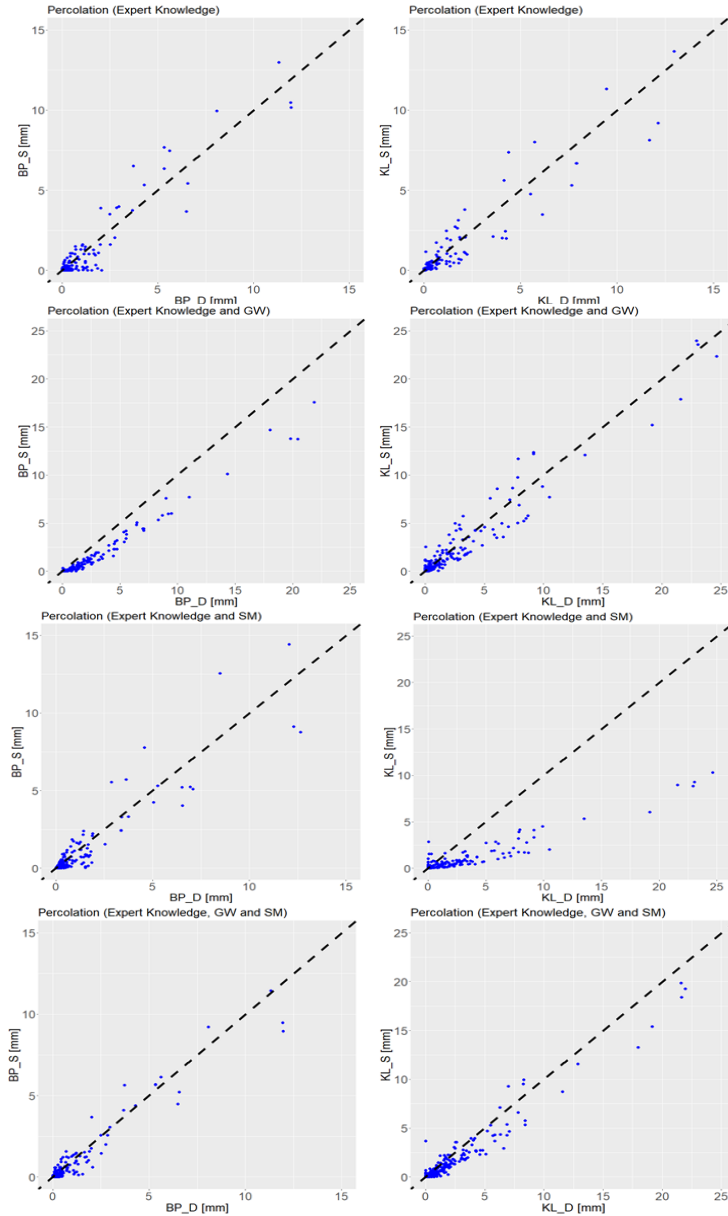


Fig. 3.42: The Scatted plots of percolation in BP and KL catchments

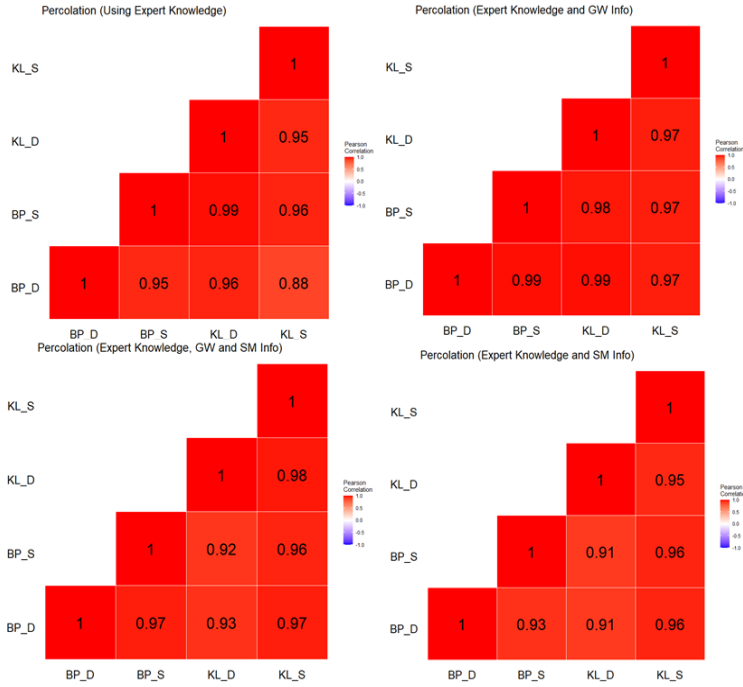


Fig. 3.43: The Heatmap of percolation in BP and KL catchments

Figures 3.45 and 3.44 show the scatter plots and the heat map of total runoff in BP and KL catchments for four different types of calibrations. According to the figures 3.45 total runoff in drainage-based discretizations have larger value of total runoff than soil-based discretizations. The heat map of total runoff also shows high correlations between total runoff values in all discretizations.

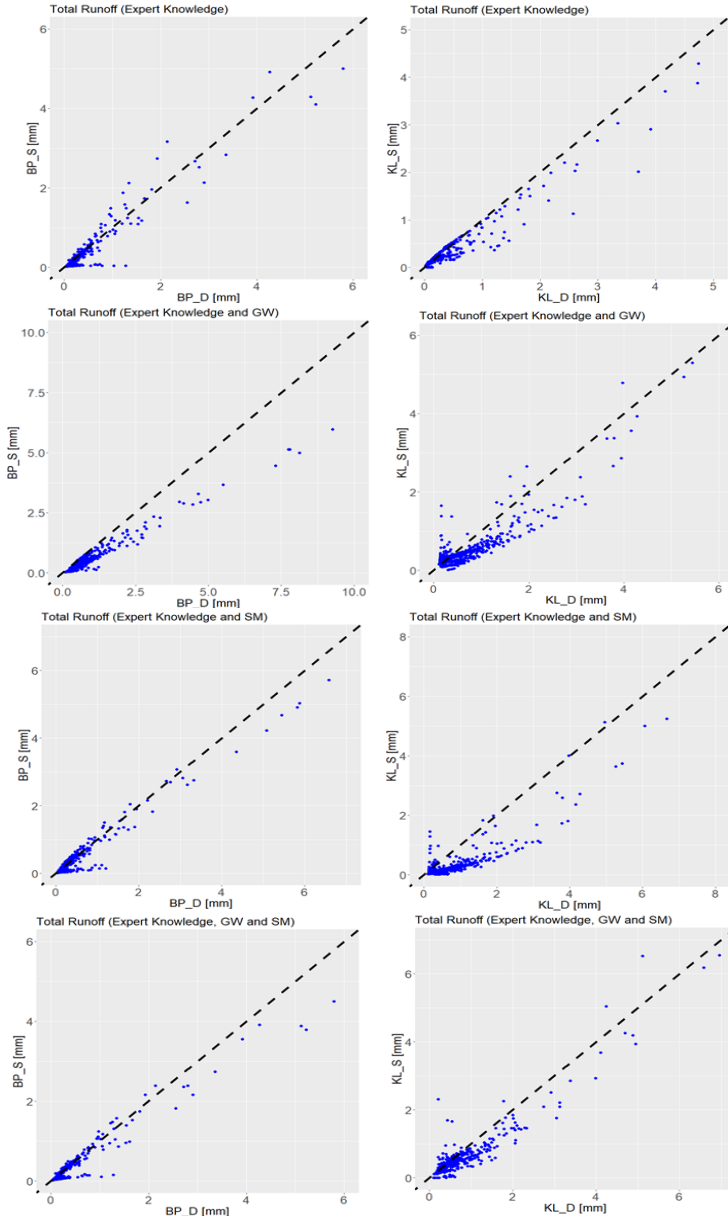


Fig. 3.44: The Scatted plots of total runoff in BP and KL catchments

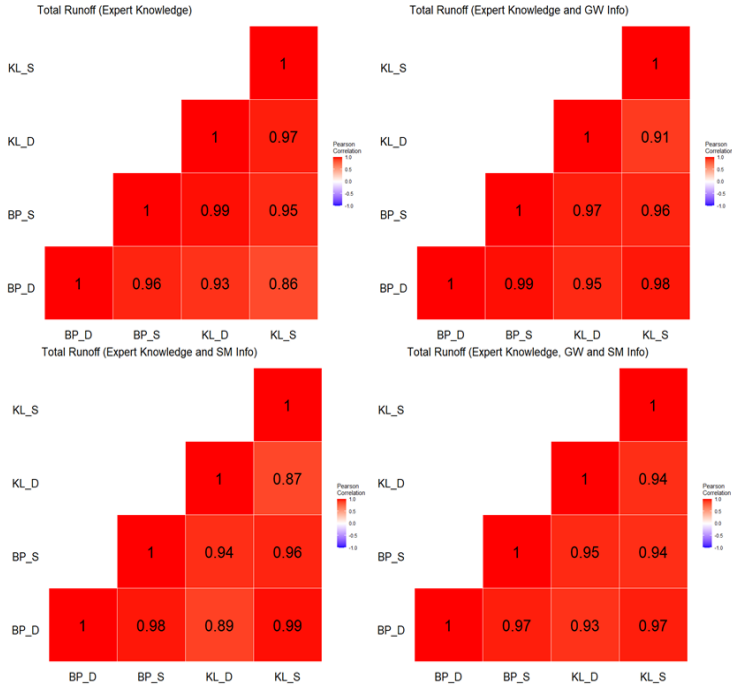


Fig. 3.45: The heatmap of total runoff in BP and KL catchments

Figures 3.46 and 3.39 show the scatter plots and the heat map of melting in BP and KL catchments for four different types of calibrations. According to the figures, the melting depth is higher in BP\_D\_FG catchment than BP\_S\_FG in the case of calibration using only expert knowledge. On the contrary, this value is higher in KL\_S\_FG catchment compared to KL\_D\_FG when adding GW and SM information. In addition, the heat map shows no correlation between BP\_D\_FG and BP\_S\_FG catchments when only expert knowledge is applied. The correlation value increases when the GW and SM information are added to the calibration procedure.

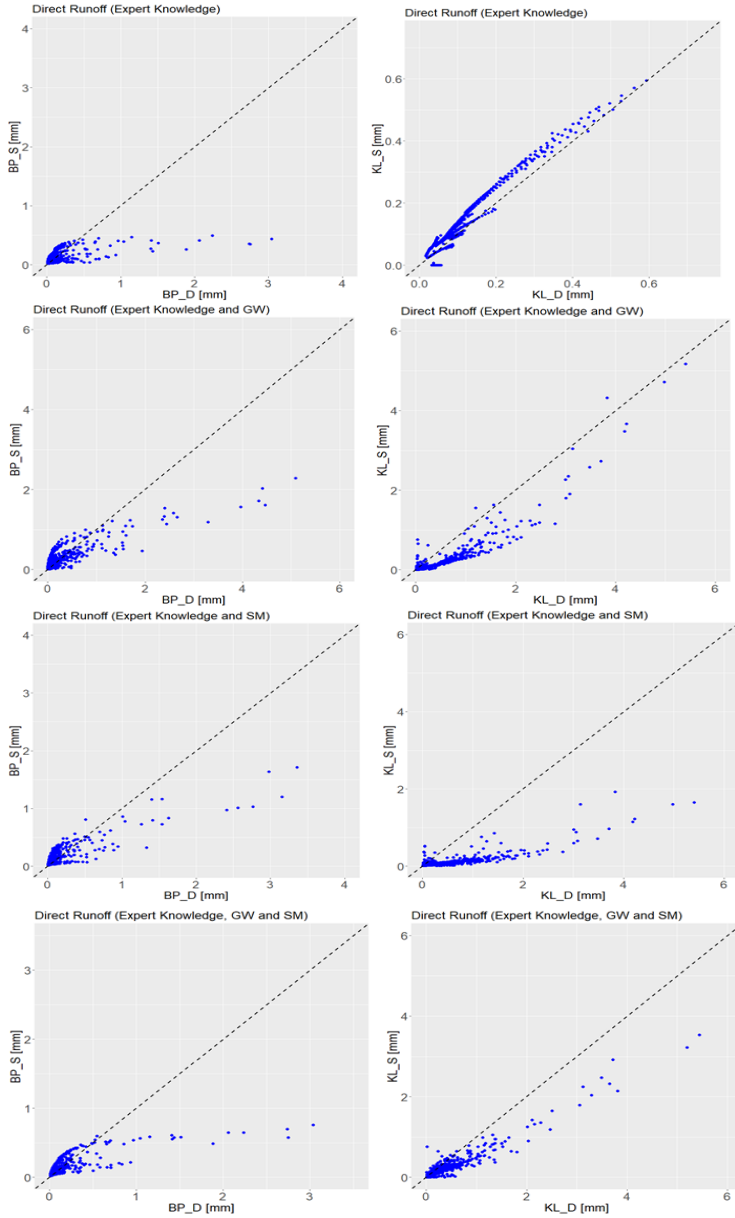


Fig. 3.46: The Scatted plots of melting in BP and KL catchments

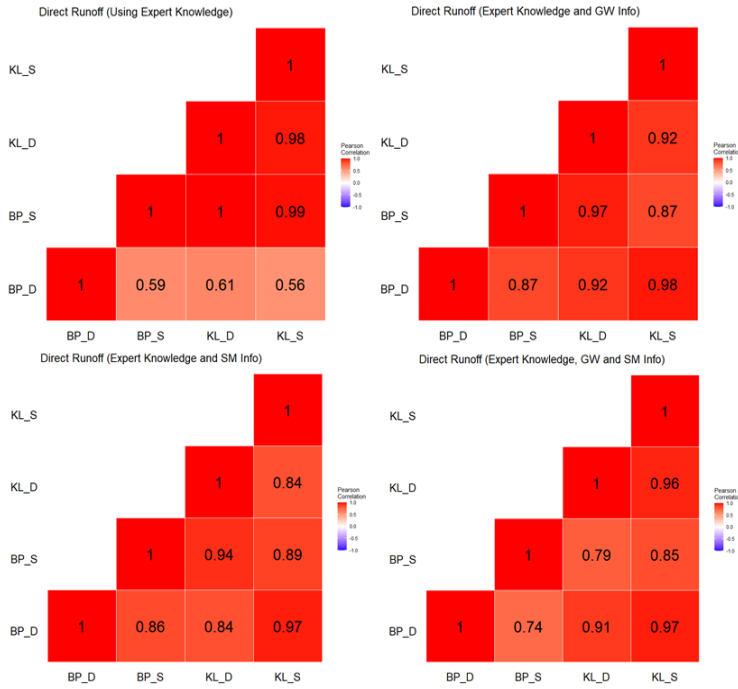


Fig. 3.47: The heatmap of melting in BP and KL catchments

The values of fluxes in four types of discretizations are compared and summarized in table 3.7. The table shows that the difference between fluxes are minimized when the GW and SM information have been added to the calibration procedure. In other words, the more information used in the calibration procedure, the less dependent are the fluxes on the discretization method.

Tab. 3.7: Comparison of fluxes in BP and KL catchments for four different types of calibrations

BP catchments				
Flux	Ex <sup>1</sup>	GW <sup>2</sup>	SM <sup>3</sup>	GW&SM <sup>4</sup>
BASF	D <sup>5</sup> > S <sup>6</sup>	D > S	D < S (High flows)	D < S (High flows)
DIRR	D > S	D > S	D > S (High flows)	D > S
TOTR	D ≈ S	D > S	D ≈ S	D ≈ S
PERC	D ≈ S	D > S	D ≈ S	D ≈ S
MELT	D > S	D > S	D > S	D > S
KL catchments				
BASF	D < S	D < S	D < S (High flows)	D < S (High flows)
DIRR	D ≈ S	D > S	D > S	D > S
TOTR	D > S	D > S	D > S	D ≈ S
PERC	D ≈ S	D ≈ S	D > S	D ≈ S
MELT	D ≈ S	D < S	D < S	D < S

<sup>1</sup> Calibration using Expert knowledge.

<sup>2</sup> Calibration using expert knowledge and GW information.

<sup>3</sup> Calibration using expert knowledge and SM information.

<sup>4</sup> Calibration using expert knowledge, GW and SM information.

<sup>5</sup> Drainage-based discretization.

<sup>6</sup> Soil-based discretization.

### 3.4.3 Storages

This part explains the effects of catchment discretizations on the storage variables. These variables are GW storage, soil storage, interception storage and surface retention.

Figures 3.48 and 3.49 show the scatter plots and the heat map of GW storage in BP and KL catchments for four different types of calibrations. According to the figures 3.45, GW storage in drainage-based discretizations is significantly larger than soil-based discretizations. The heat map of GW storage also shows the low correlations between GW storage values BP\_D\_FG and BP\_S\_FG when using expert knowledge in the calibration procedure, with the correlation coefficient of 0.47, and it increases when the GW information has been used in the calculations.

On the other hand, adding SM information to the calibration has led to a low correlation between KL\_D\_FG and KL\_S\_FG catchments, with the correlation coefficient of 0.39. This value increases in both in BP and KL catchments when GW and SM information have been applied to the calculation. The correlation coefficients are 0.68 and 1.0 for drainage- and soil-based discretizations, respectively.

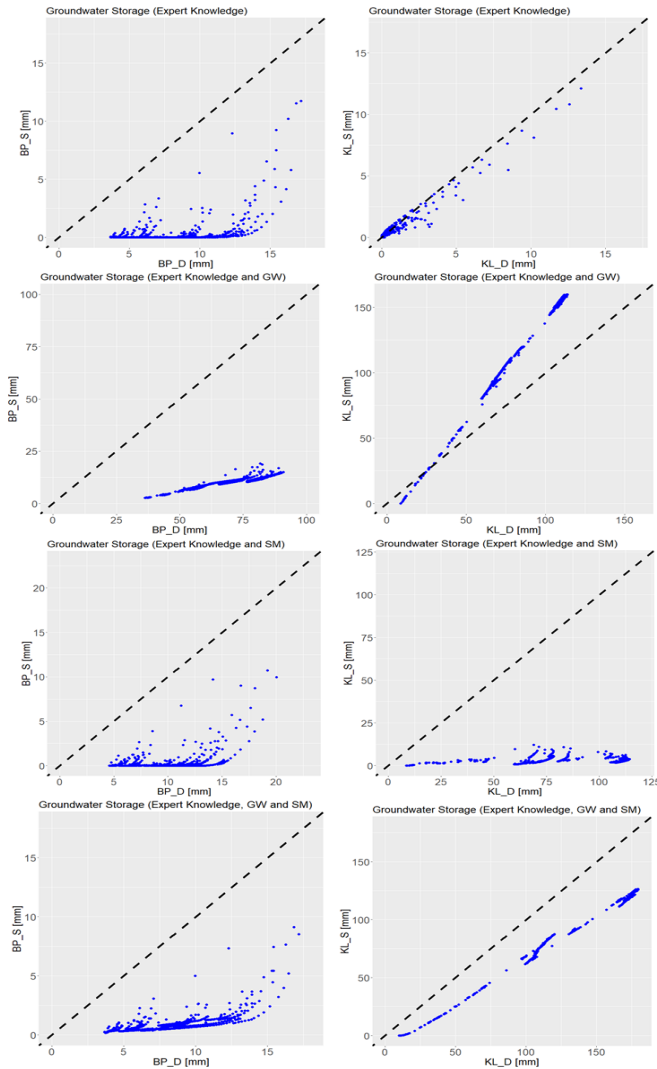


Fig. 3.48: The Scatted plots of GW storage in BP and KL catchments

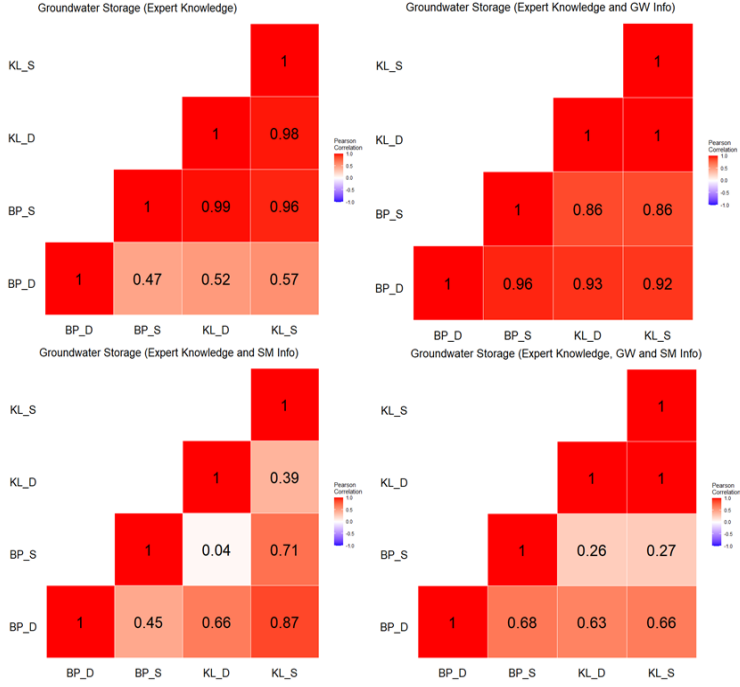


Fig. 3.49: The Heatmap of GW storage in BP and KL catchments

Figures 3.50 and 3.51 show the scatter plots and the heat map of interception in BP and KL catchments for four different types of calibrations. The figures show that using only expert knowledge in calibration lead to large values of interception storage in drainage-based discretizations compared to the soil-based ones. The obtained results show the GW and SM information lead to higher value of interception in soil-based discretization. The heat map of percolation shows high correlation between the time series of percolation in all discretizations.

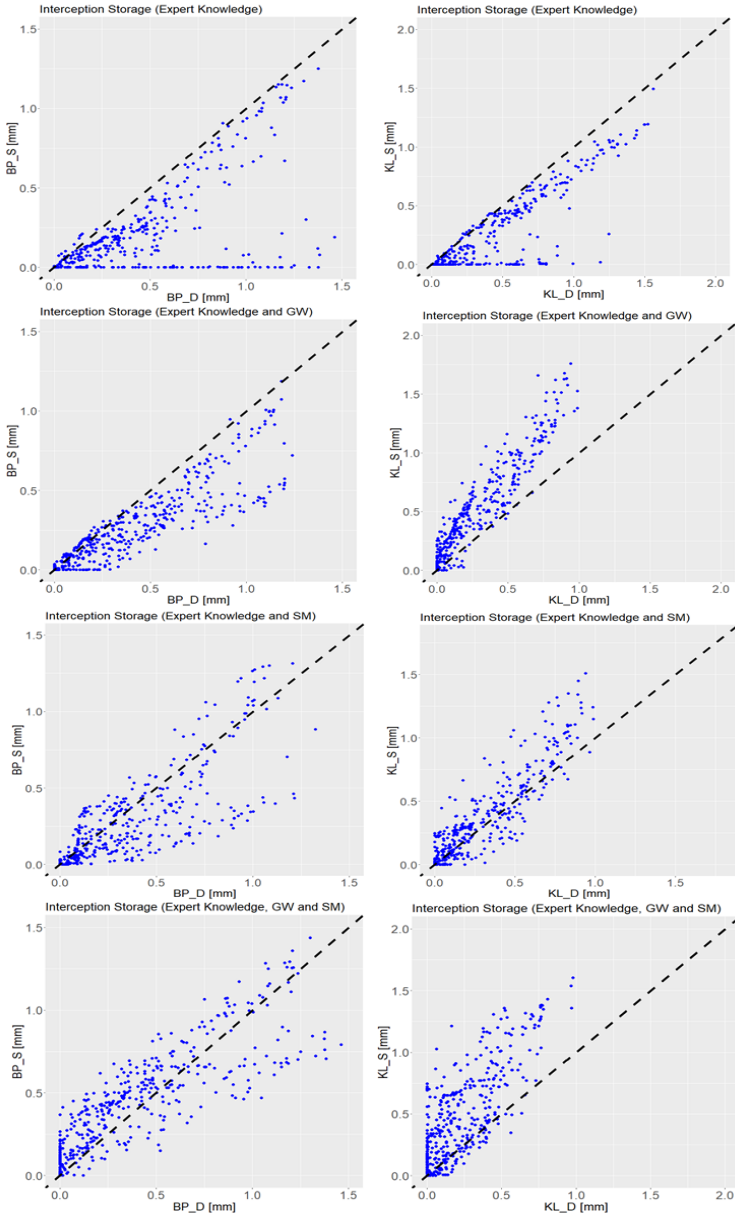


Fig. 3.50: The Scatted plots of interception storage in BP and KL catchments

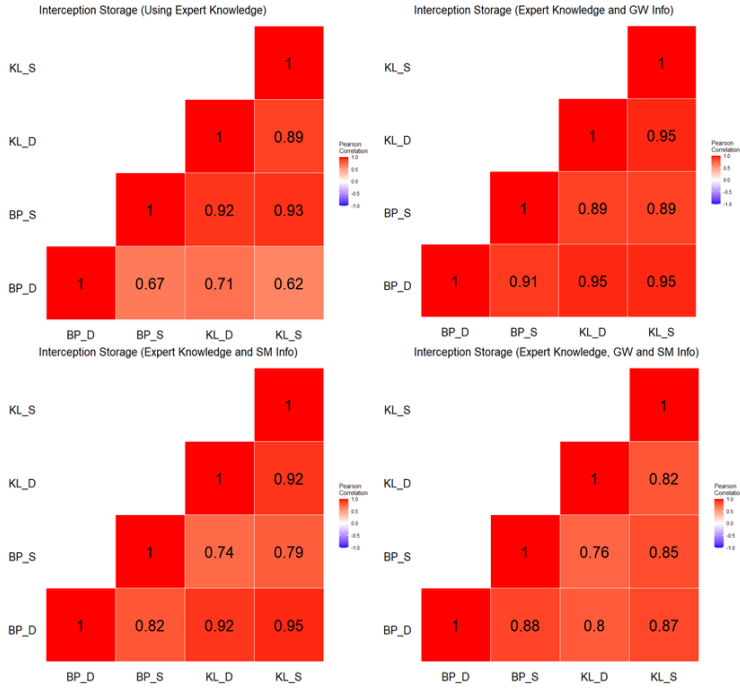


Fig. 3.51: The Heatmap of interception storage in BP and KL catchments

Figures 3.52 and 3.53 show the scatter plots and the heat map of soil storage in BP and KL catchments for four different types of calibrations. According to the figure 3.52, there are significant differences between drainage-based and soil-based discretizations when using only expert knowledge or GW information. However, adding the SM data to the calculation decreases the differences between different types of discretizations. Based on the heat map which is shown in figure 3.53, the correlation between drainage-based and soil-based discretizations increase significantly where the SM data is added to the calibration procedure.

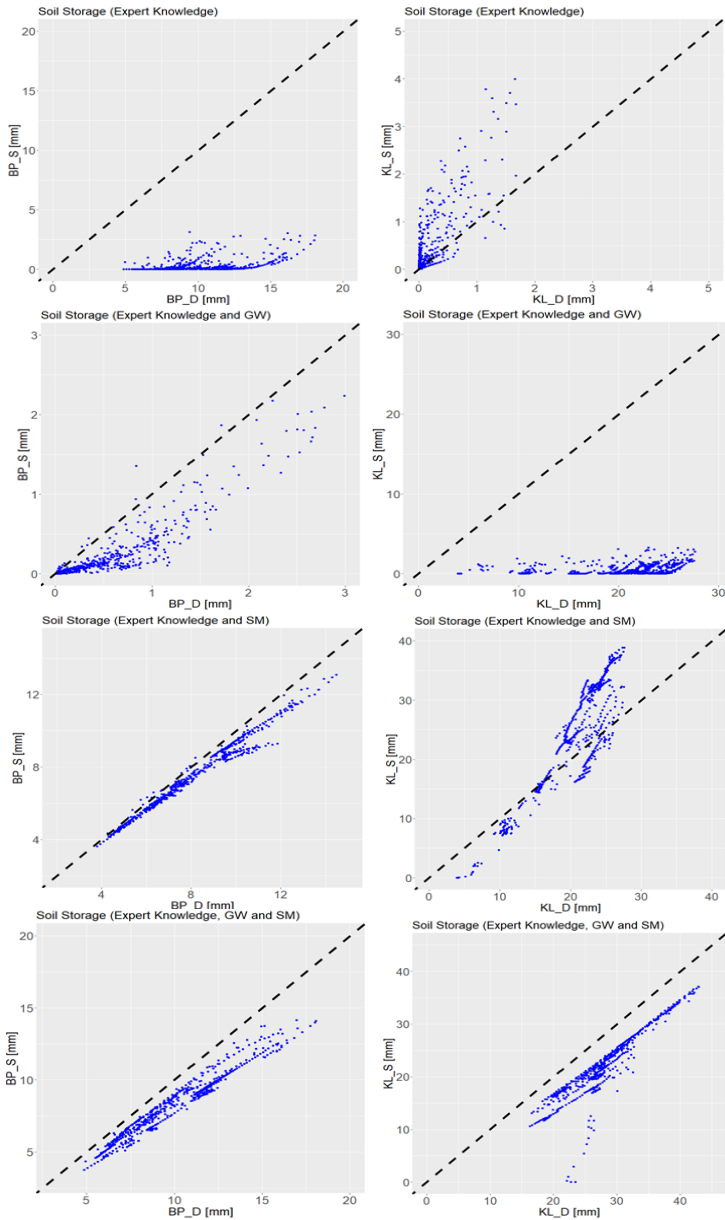


Fig. 3.52: The Scatted plots of soil storage in BP and KL catchments

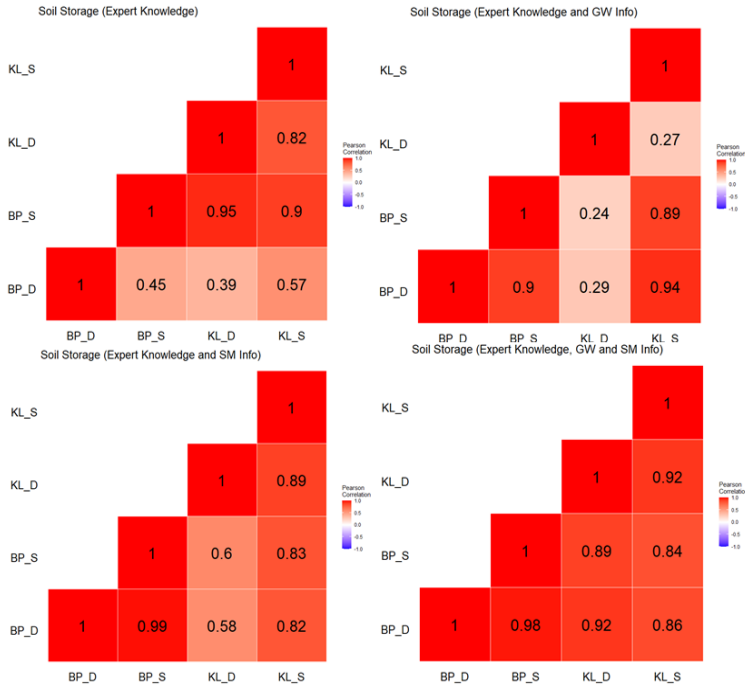


Fig. 3.53: The Heatmap of soil storage in BP and KL catchments

Figures 3.54 and 3.55 show the scatter plots and the heat map of surface retention in BP and KL catchments for four different types of calibrations. The values of surface retention are highly correlated when using expert knowledge.

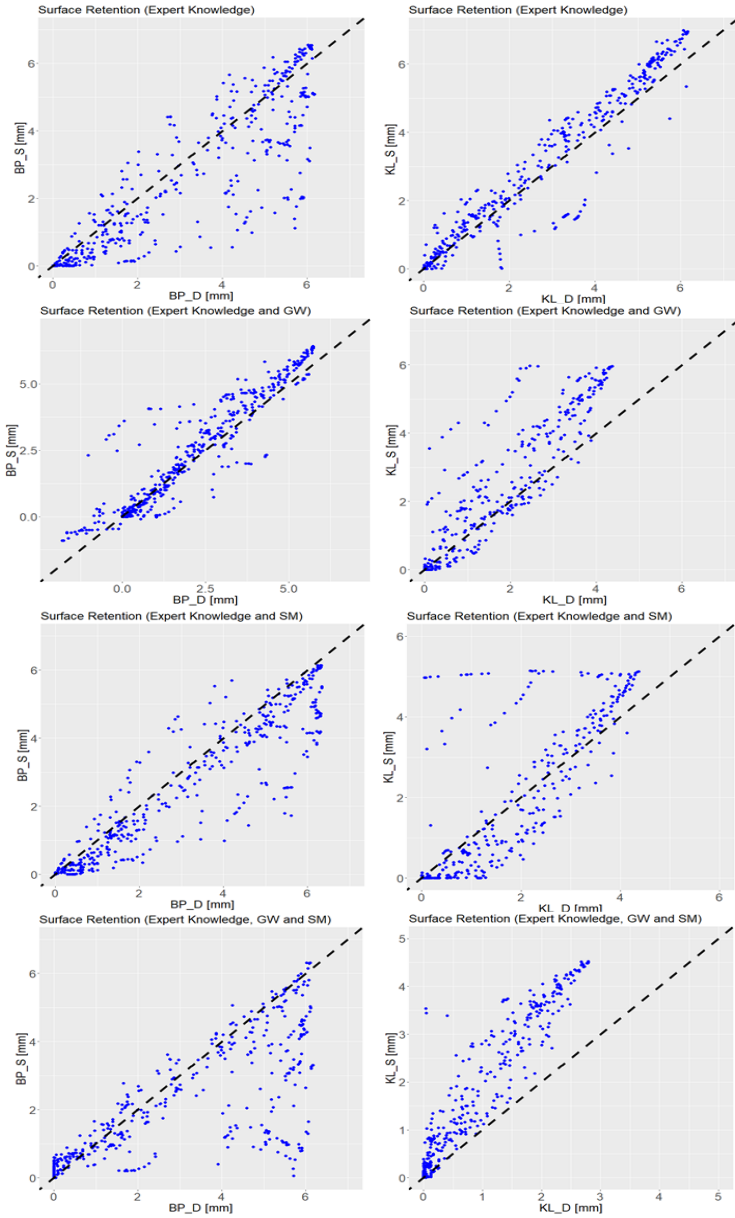


Fig. 3.54: The Scatted plots of surface retention in BP and KL catchments

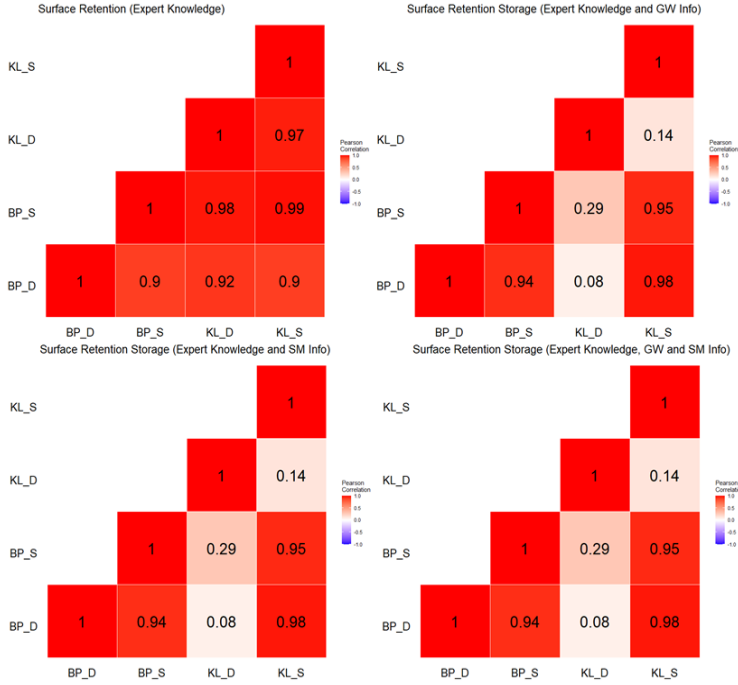


Fig. 3.55: The Heatmap of surface retention in BP and KL catchments

The values of storages in four types of discretizations are compared and summarized in table 3.8. In this case, the difference between soil- and drainage-based discretizations are minimized when we use SM data in the calibration procedures. All storage variables are highly sensitive to SM values. Therefore, using SM information reduce the dependencies storages on the catchment discretization.

Tab. 3.8: Comparison of storages in BP and KL catchments for four different types of calibrations

BP catchments				
Storage	Ex <sup>1</sup>	GW <sup>2</sup>	SM <sup>3</sup>	GW&SM <sup>4</sup>
GROS	D <sup>5</sup> > S <sup>6</sup>	D > S	D > S	D > S
INTS	D > S	D > S	D ≈ S	D ≈ S
SOIS	D > S	D < S	D ≈ S	D ≈ S
SURS	D > S	D ≈ S	D ≈ S	D < S
KL catchments				
GROS	D > S (High flows)	D < S	D > S	D > S
INTS	D > S	D < S	D ≈ S	D < S
SOIS	D < S	D > S	D ≈ S	D ≈ S
SURS	D ≈ S	D < S	D ≈ S	D < S

<sup>1</sup> Calibration using Expert knowledge.

<sup>2</sup> Calibration using expert knowledge and GW information.

<sup>3</sup> Calibration using expert knowledge and SM information.

<sup>4</sup> Calibration using expert knowledge, GW and SM information.

<sup>5</sup> Drainage-based discretization.

<sup>6</sup> Soil-based discretization.

# CHAPTER 4

## Discussion

In this chapter, the obtained results from the simulation are discussed. In the modelling procedure, first, the expert knowledge was used to constrained the parameters of the hydrological model. Constraining the solution space has led to obtain more conceptually realistic parameters, fluxes and storage variables. The obtained results of using expert knowledge in the modelling procedure are comparable to the results of the study of Gharari et al. (2014b) in which they constrained their model parameters to simulate fluxes in ungauged basins that there is no streamflow observation available.

Table 4.1 shows the mean absolute errors derived from comparing simulated and measured FDCs for all four discretizations.

Tab. 4.1: Mean absolute error of FDCs derived from simulations

Num	discretization	calibration using GW	calibration using SM	calibration using GW & SM
1	BP_D_FG	0.25	0.04	0.03
2	BP_S_FG	0.07	0.04	0.03
3	KL_D_FG	0.30	0.04	0.26
4	KL_S_FG	0.18	0.02	0.17

According to the table 4.1, the produced FDCs by dHRUM have the smallest value of MAE when both GW and SM are used together in BP catchments. On the other hand, in KL catchments, applying SM data has led to the best calibration results and the errors are 0.04 and 0.02 for KL\_D\_FG and KL\_S\_FG, respectively. It shows that the simulated total runoff is significantly sensitive to SM variations. This result is comparable to the work of Wang-Erlandsson et al. (2014) in which they concluded that in the wet catchments where the soil is close to the saturation state, any changes in precipitation can highly affect the runoff.

The worst fit belongs to KL when GW and SM are used simultaneously in calibration process. However, the simulated FDC can be modified by multiplying some coefficients to TETR, CDIV, C\_MAX, CMIN, RETCAP, KF, KS and ADIV parameters according to table 4.2.

Tab. 4.2: Parameters and their applied coefficients for producing more accurate FDCs in KL\_D\_FG catchment

Parameter	Coefficients 1	Coefficients 2
ADIV	1.5	0.5
C_MAX	1.15	-
CMIN	0.2	0.3
CDIV	0.15	-
KF	1.5	-
KS	0.4	0.4
RETCAP	0.2	-
TETR	1.2	2
FDCs' MAE <sup>1</sup> for each set of parameters		
MAE	0.03	0.01

<sup>1</sup> Mean Absolute Error derived from comparing simulated FDC with observation

Although the modified parameters resulted in creating more accurate FDCs, they violated the constraints that were defined in the previous chapters. There may be other sets of parameters that lead to the same or even more accurate FDCs. This situation is called equifinality. Equifinality is one of the major sources of uncertainties in hydrological modelling. Table

4.2 shows that the model reaches an acceptable accuracy using more than one different sets of parameters. The resulted FDCs derived from applying the coefficients 1 and 2 are shown in figures 4.1 and 4.2.

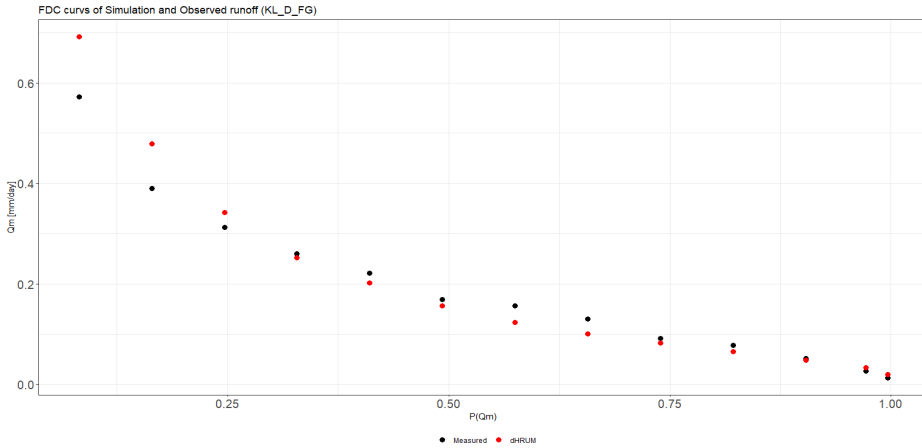


Fig. 4.1: Modified FDCs of KL\_D\_FG catchment using coefficient 1

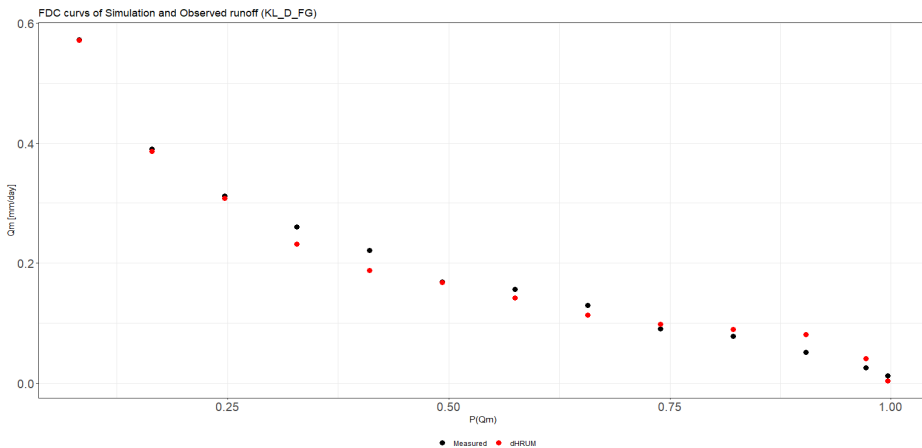


Fig. 4.2: Modified FDCs of KL\_D\_FG catchment using coefficient 2

According to the obtained results, it can be concluded that constraining the solution space of parameters using expert knowledge and available data can significantly reduce the effects of equifinality, decrease the parametric uncertainty, and obtain a single set of effective parameters which results in a more realistic behaviour of the catchment. This investigation confirms the obtained results from the study of Kelleher et al. (2017) in which they used regional data sets, expert knowledge and observations, namely GW level, to identify a set of effective parameters that reduces equifinality and simulate the spatial and temporal processes at the catchment scale more accurately.

Another important result that is worth discussing here is the strong response of the dHRUM to the precipitation when simulating groundwater or soil storage. This characteristic leads to overestimation and underestimation of high and low values, respectively, especially where the observation time series follows a smooth pattern without wide fluctuations, like SM time series in KL catchment, figure 3.33. Therefore, the fluctuations of the measured SM are not completely captured by dHRUM. This problem magnifies when simulating soil storage in KL catchments where the measured values have mild fluctuations but dHRUM shows wide fluctuations.

In addition, the results show that the catchment discretization can highly affect the water balance, storage and flux variables, in the study area. This effect is even higher when it comes to the high values of fluxes and storages. In other words, high flows are more sensitive to HRU configuration than low flows. Moreover, adding SM data to the calibration procedure leads to minimize the difference between flux and storage variables in drainage-based and soil-based discretizations and rise the accuracy of simulated processes in the catchment, the same as the results derived from study of Kumar et al. (2013).

## Conclusion

This study investigated the effects of expert knowledge, discretization of catchments and the application of different data types on predicting water balance in ungauged catchments. This information is used to define a realistic relationship between state variables, fluxes and storage variables in the hydrological model. The study area was divided into two main parts called BP and KL catchments, and each catchment was discretized based on soil type and drainage system. The hydrological model, dHRUM, was applied to both catchments and calibrated based on different information from the catchments.

First, the model parameters were constrained using only the obtained knowledge from the catchments, expert knowledge. Using this knowledge led to obtain a conceptually more realistic distribution of hydrological processes over the catchments. These processes are calculated according to the land cover, land slope and distance from the catchment outlet. However, these constraints resulted in overestimating high flows in all catchments.

In the second approach, the measured GW level information was used as a benchmark to simulate the fluctuation of groundwater storage in the

HRUs with available GW information. The lumped version of dHRUM was used to simulate GW level variations for a set of selected HRUs. The model showed a good performance in all catchments. Then the semi-distributed version of the model was used to simulate the total runoff, FDC, for both BP and KL catchments. The model significantly overestimated the total runoff.

The third step followed the procedure same as step two, but in this case, the SM data was used to calibrate the model. The obtained FDCs showed that the using SM data leads to underestimation of total runoff in BP catchment but acceptable results in KL catchment.

In the last step, both BP and SM information were used simultaneously to calibrate the model. In this case, the model showed a good performance in simulating FDCs in BP catchment. However, it overestimated the curves in acKL catchment.

Some of the key findings of this research are as follows:

- Expert knowledge can significantly help represent the processes in the catchment more realistically, when there is no available streamflow observation.
- Considering GW and SM data in calibration procedure can considerably increase the accuracy of the simulated FDC in BP catchment.
- Considering only SM information in calibration procedure results in an acceptable simulation of FDC in KL catchment. However, using both GW and SM data leads to overestimation of FDCs. This inaccuracy could be solved by decreasing the sizes of HRUs around the sensors. Because in the current discretizations, it is assumed that the sensors cover almost entire forested areas and around 60 percent of the whole KL basin. Therefore, as the recorded information from these sensors may not represent the GW and SM variation for the

whole area, other types of HRU configuration should be tested when using both GW and SM data in calibration procedure.

- Constraining the solution space using expert knowledge and available data when finding the effective parameters leads to decrease the parameter uncertainty and reduce the effects of equifinality. Consequently, it produces a single set time series of fluxes and storages that represents the processes in the catchment more realistically.
- Using the GW and SM information can lead to increase the accuracy of simulated fluxes in the catchments. This data reduces the dependency of fluxes on the HRUs configuration and decreases the difference between simulated fluxes in drainage-based and soil-based discretizations.
- Storage variables, namely surface retention, GW storage, interception storage and soil storage, are highly sensitive to SM variations. Applying SM data leads to higher accuracy of simulated storages and decrease the correlation between drainage-based and soil-based discretizations.
- The largest difference between fluxes and storages in drainage-based and soil-based discretizations belongs to the high values.

In conclusion, the quality, quantity and type of information about the study area and its processes can significantly reduce the uncertainty of the simulation output. Also, expert knowledge plays a crucial role in finding effective model parameters in ungauged basins with no time series of streamflow observation. This knowledge can be used to keep the parameters in a feasible range during the calibration process, which leads to a single set of outputs representing the hydrological processes more realistically. Also, the results showed that the model sensitivity to the catchment discretization was reduced when more information, like GW and

SM data, was added to the modelling and calibration procedure. However, still more investigation should be conducted to determine the effects of different HRU configurations on the water balance variables.

# Bibliography

- Mohamed A. M. Abd Elbasit, Majed M. Abu-Zreig, Chandra S. P. Ojha, Hiroshi Yasuda, and Liu Gang. Estimation of surface depression storage capacity from random roughness and slope. *Water SA*, 46(3):404–409, 2020. doi: {10.17159/wsa/2020.v46.i3.8650}.
- David Ardia, Kris Boudt, Peter Carl, Katharine M. Mullen, and Brian G. Peterson. Differential Evolution with DEoptim. *The R Journal*, 3(1): 27–34, 2011. doi: 10.32614/RJ-2011-005.
- JC Bathurst, J Ewen, G Parkin, PE O’Connell, and JD Cooper. Validation of catchment models for predicting land-use and climate change impacts. 3. Blind validation for internal and outlet responses. *J. Hydrol.*, 287(1-4): 74–94, 2004. doi: {10.1016/j.jhydrol.2003.09.021}.
- Sten Bergström. *Development and application of a conceptual runoff model for Scandinavian catchments*. Lund Institute of Technology, University of Lund, Lund, Sweden, 1976.
- Beven. How far can we go in distributed hydrological modelling? *Hydrol. Earth Syst. Sci.*, 5:1–12, 2001. doi: {10.5194/hess-5-1-2001}.
- K Beven. Towards a coherent philosophy for modelling the environment. *Proc. R. Soc. A: Math. Phys. Eng. Sci.*, 458(2026):2465–2484, OCT 8 2002. ISSN 1364-5021. doi: {10.1098/rspa.2002.0986}.

- Keith Beven. *Environmental Modelling An Uncertain Future?* Routledge, London, 2009.
- Keith Beven. *Rainfall-Runoff Modelling: The Primer, 2nd Edition.* John Wiley and Sons Ltd, 2012.
- Gunter Bloeschl, Marc F. P. Bierkens, and et. al. Twenty-three unsolved problems in hydrology (uph) - a community perspective. *Hydrol Sci J HYDROLOG SCI J*, 64(10):1141–1158, 2019. doi: 10.1080/02626667.2019.1620507.
- Gunter Bloeschl, Christian Reszler, and Jurgen Komma. A spatially distributed flash flood forecasting model. *Environ. Model. Softw.*, 23(4): 464–478, 2008. doi: {10.1016/j.envsoft.2007.06.010}.
- Martyn P. Clark, Dmitri Kavetski, and Fabrizio Fenicia. Pursuing the method of multiple working hypotheses for hydrological modeling. *Water Resour. Res.*, 47, 2011. doi: {10.1029/2010WR009827}.
- Martyn P. Clark, Bart Nijssen, Jessica D. Lundquist, Dmitri Kavetski, David E. Rupp, Ross A. Woods, Jim E. Freer, Ethan D. Gutmann, Andrew W. Wood, Levi D. Brekke, Jeffrey R. Arnold, David J. Gochis, and Roy M. Rasmussen. A unified approach for process-based hydrologic modeling: 1. Modeling concept. *Water Resour. Res.*, 51(4):2498–2514, 2015. doi: {10.1002/2015WR017198}.
- J Ewen and G Parkin. Validation of catchment models for predicting land-use and climate change impacts .1. Method. *J. Hydrol.*, 175(1-4): 583–594, 1996. doi: {10.1016/S0022-1694(96)80026-6}.
- Fabrizio Fenicia, Hubert H. G. Savenije, Patrick Matgen, and Laurent Pfister. Understanding catchment behavior through stepwise model concept improvement. *Water Resour. Res.*, 44(1), 2008. doi: {10.1029/2006WR005563}.

- S. Gharari, M. Hrachowitz, F. Fenicia, H. Gao, and H. H. G. Savenije. Using expert knowledge to increase realism in environmental system models can dramatically reduce the need for calibration. *Hydrol. Earth Syst. Sci. Discuss.*, 18(12):4839–4859, 2014a. doi: {10.5194/hess-18-4839-2014}.
- S. Gharari, M. Shafiei, M. Hrachowitz, R. Kumar, F. Fenicia, H. V. Gupta, and H. H. G. Savenije. A constraint-based search algorithm for parameter identification of environmental models. *Hydrol. Earth Syst. Sci. Discuss.*, 18(12):4861–4870, 2014b. doi: {10.5194/hess-18-4861-2014}.
- M. Hrachowitz, O. Fovet, L. Ruiz, T. Euser, S. Gharari, R. Nijzink, J. Freer, H. H. G. Savenije, and C. Gascuel-Oudou. Process consistency in models: The importance of system signatures, expert knowledge, and process complexity. *Water Resour. Res.*, 50(9):7445–7469, 2014. doi: {10.1002/2014WR015484}.
- Afshin Jahanshahi, Lieke A. Melsen, Sopan D. Patil, and Erfan Goharian. Comparing spatial and temporal scales of hydrologic model parameter transfer: A guide to four climates of iran. *J. Hydrol.*, 603(C), 2021. doi: {10.1016/j.jhydrol.2021.127099}.
- Simon Judd. *The MBR Book, Second Edition: Principles and Applications of Membrane Bioreactors for Water and Wastewater Treatment*. Butterworth-Heinemann, 2010.
- Christa Kelleher, Brian McGlynn, and Thorsten Wagener. Characterizing and reducing equifinality by constraining a distributed catchment model with regional signatures, local observations, and process understanding. *HYDROLOGY AND EARTH SYSTEM SCIENCES*, 21(7):3325–3352, JUL 5 2017. ISSN 1027-5606. doi: 10.5194/hess-21-3325-2017.
- J. W. Kirchner. Aggregation in environmental systems - Part 2: Catchment mean transit times and young water fractions under hydrologic

- nonstationarity. *Hydrol. Earth Syst. Sci. Discuss.*, 20(1):299–328, 2016. doi: {10.5194/hess-20-299-2016}.
- JW Kirchner. Getting the right answers for the right reasons: Linking measurements, analyses, and models to advance the science of hydrology. *Water Resour. Res.*, 42(3), 2006. doi: {10.1029/2005WR004362}.
- V Klemes. Operational Testing of Hydrological Simulation-models. *Hydrol Sci J HYDROLOG SCI J*, 31(1):13–24, 1986. doi: {10.1080/02626668609491024}.
- Wouter J. M. Knoben, Jim E. Freer, Keirnan J. A. Fowler, Murray C. Peel, and Ross A. Woods. Modular Assessment of Rainfall-Runoff Models Toolbox (MARRMoT) v1.2: an open-source, extendable framework providing implementations of 46 conceptual hydrologic models as continuous state-space formulations. *Geosci. Model Dev.*, 12(6):2463–2480, 2019. doi: {10.5194/gmd-12-2463-2019}.
- Rohini Kumar, Luis Samaniego, and Sabine Attinger. Implications of distributed hydrologic model parameterization on water fluxes at multiple scales and locations. *WATER RESOURCES RESEARCH*, 49(1):360–379, 2013. doi: 10.1029/2012WR012195.
- R. J. Moore. The PDM rainfall-runoff model. *Hydrol. Earth Syst. Sci. Discuss.*, 11(1, 3):483–499, 2007. doi: {10.5194/hess-11-483-2007}.
- R. C. Nijzink, S. Almeida, I. G. Pechlivanidis, R. Capell, D. Gustafssons, B. Arheimer, J. Parajka, J. Freer, D. Han, T. Wagener, R. R. P. van Nooijen, H. H. G. Savenije, and M. Hrachowitz. Constraining conceptual hydrological models with multiple information sources. *Water Resour. Res.*, 54(10):8332–8362, 2018. doi: {10.1029/2017WR021895}.
- Murray C. Peel and Guenter Bloeschl. Hydrological modelling in a changing world. *Prog Phys Geogr.*, 35(2):249–261, 2011. doi: {10.1177/0309133311402550}.

- Luis Samaniego, Rohini Kumar, and Sabine Attinger. Multiscale parameter regionalization of a grid-based hydrologic model at the mesoscale. *Water Resour. Res.*, 46, 2010. doi: {10.1029/2008WR007327}.
- Jan Seibert and H. J. (Ilja) van Meerveld. Hydrological change modeling: Challenges and opportunities. *Hydrol. Process.*, 30(26):4966–4971, 2016. doi: {10.1002/hyp.10999}.
- R Storn and K Price. Differential evolution - a simple and efficient heuristic for global optimization over continuous spaces. *J Glob Optim*, 11(4): 341–359, 1997. doi: {10.1023/A:1008202821328}.
- Stephan Thober, Matthias Cuntz, Matthias Kelbling, Rohini Kumar, Juliane Mai, and Luis Samaniego. The multiscale routing model mRM v1.0: simple river routing at resolutions from 1 to 50 km. *Geosci. Model Dev.*, 12(6):2501–2521, 2019. doi: {10.5194/gmd-12-2501-2019}.
- Hatice Turk. Modelling hydrological balance using lumped and semi-distributed hydrological model. Master’s thesis, Czech University of Life Sciences Prague, Czech Republic, 2020.
- Thorsten Wagener, Murugesu Sivapalan, Peter A. Troch, Brian L. McGlynn, Ciaran J. Harman, Hoshin V. Gupta, Praveen Kumar, P. Suresh C. Rao, Nandita B. Basu, and Jennifer S. Wilson. The future of hydrology: An evolving science for a changing world. *Water Resour. Res.*, 46, 2010. doi: {10.1029/2009WR008906}.
- L. Wang-Erlandsson, R. J. van der Ent, L. J. Gordon, and H. H. G. Savenije. Contrasting roles of interception and transpiration in the hydrological cycle - part 1: Temporal characteristics over land. *EARTH SYSTEM DYNAMICS*, 5(2):441–469, 2014. doi: 10.5194/esd-5-441-2014.

# Appendix A: Outputs from Expert Calibration

The model outputs for BP\_S\_FG catchment

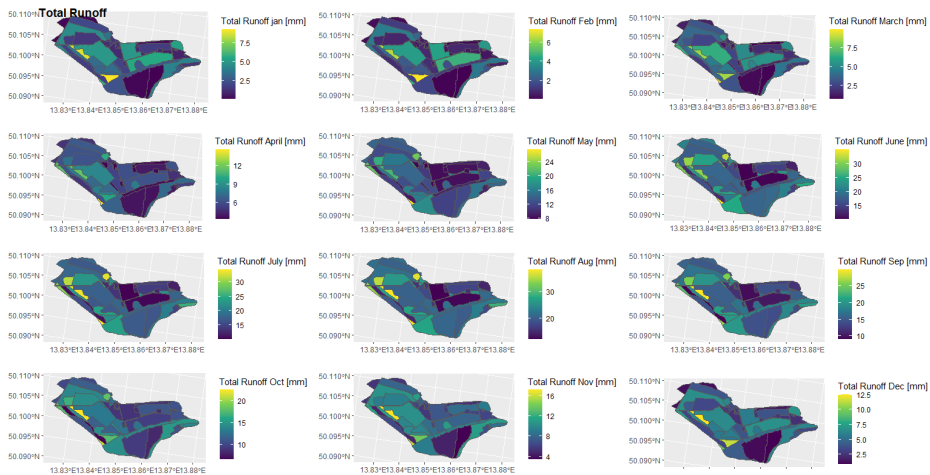


Fig. 1: Total runoff in BP\_S\_FG catchment

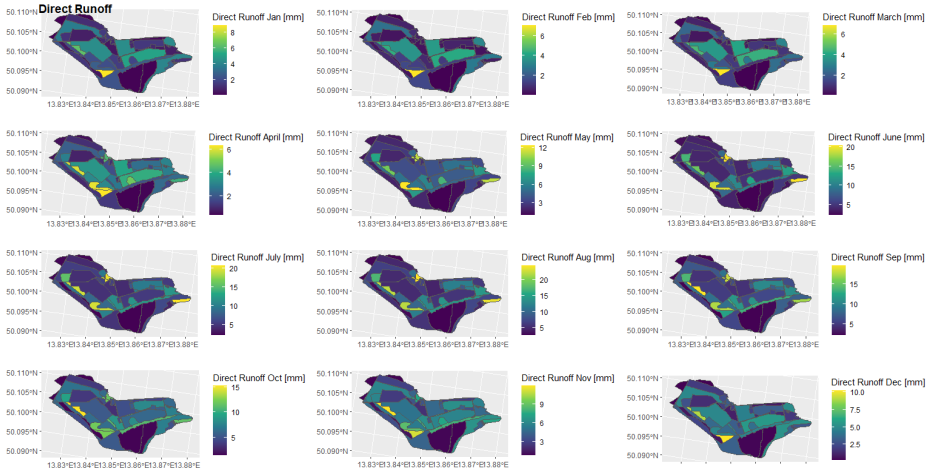


Fig. 2: Direct runoff in BP\_S\_FG catchment

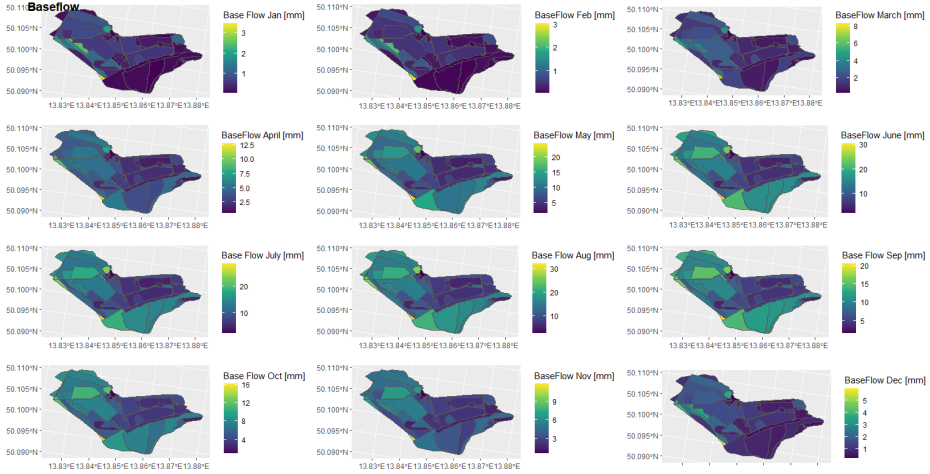


Fig. 3: Baseflow in BP\_S\_FG catchment

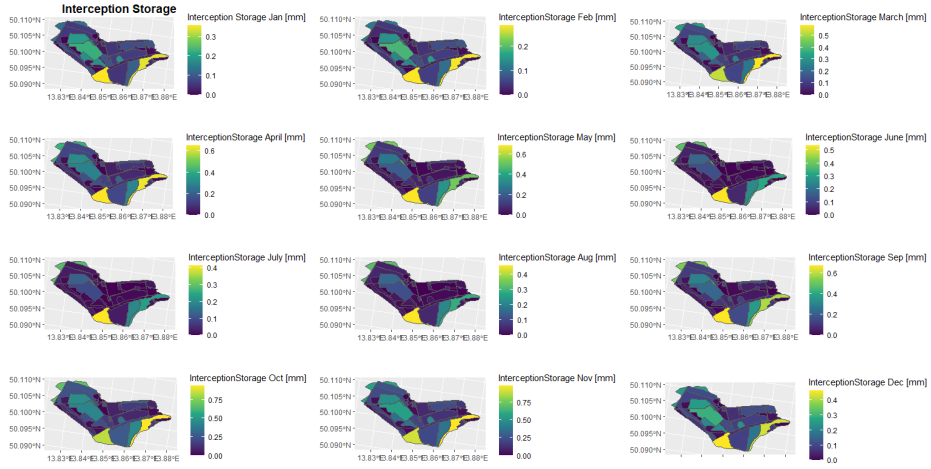


Fig. 4: Interception in BP\_S\_FG catchment

The model outputs for KL\_D\_FG catchment

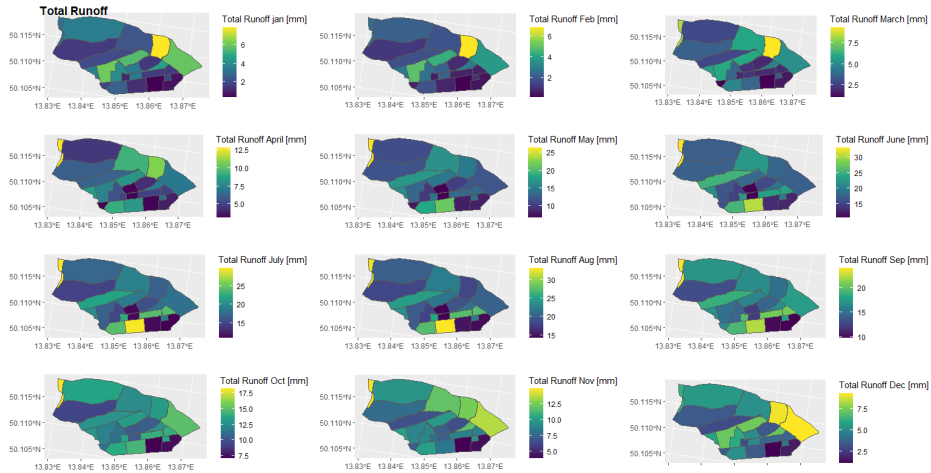


Fig. 5: Total runoff in KL\_D\_FG catchment

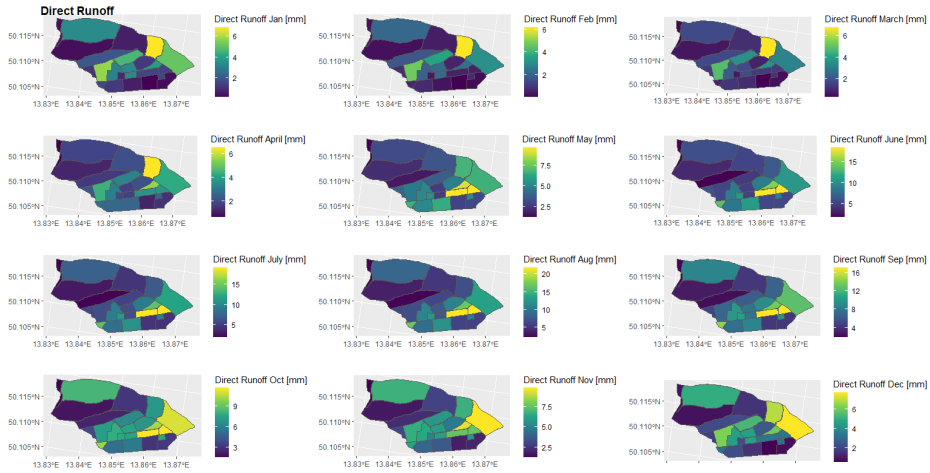


Fig. 6: Direct runoff in KL\_D\_FG catchment

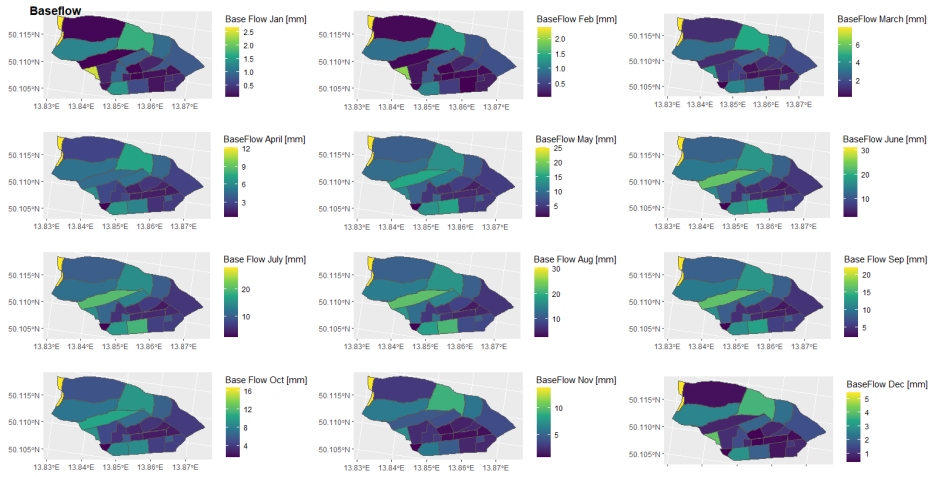


Fig. 7: Baseflow in KL\_D\_FG catchment

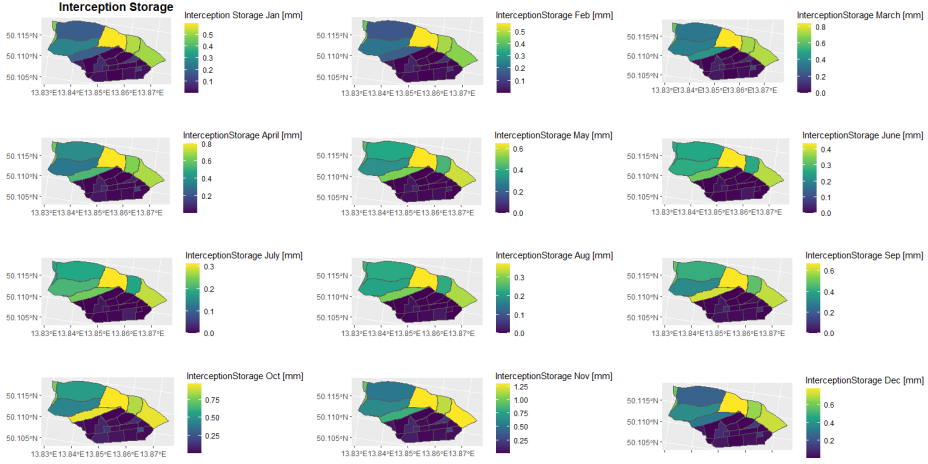


Fig. 8: Interception in KL\_D\_FG catchment

The model outputs for KL\_S\_FG catchment

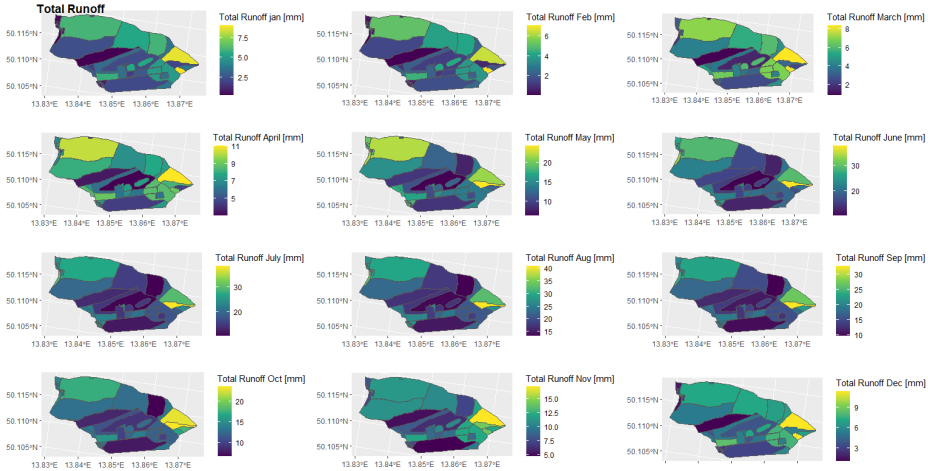


Fig. 9: Total runoff in KL\_S\_FG catchment

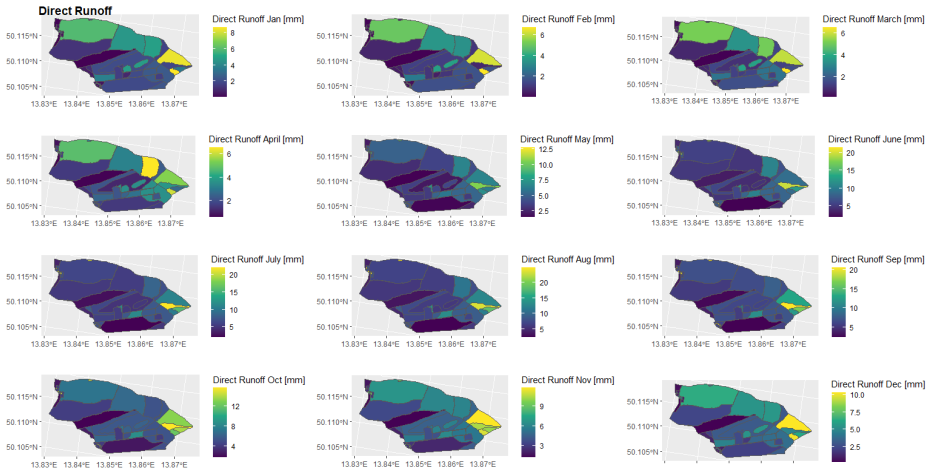


Fig. 10: Direct runoff in KL\_S\_FG catchment

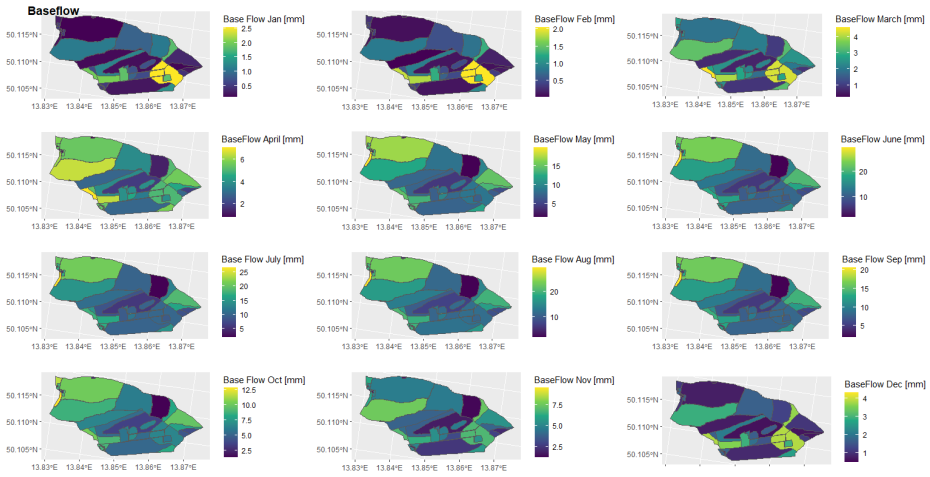


Fig. 11: Baseflow in KL\_S\_FG catchment

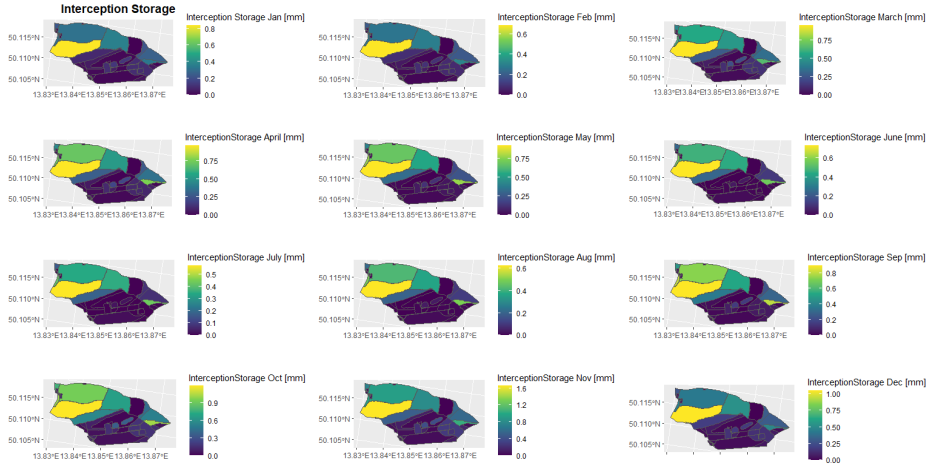


Fig. 12: Interception in KL\_S\_FG catchment

# Appendix B: Calibration Results Using SM and GW Information

BP\_D\_FG catchment

Calibration Results Using GW

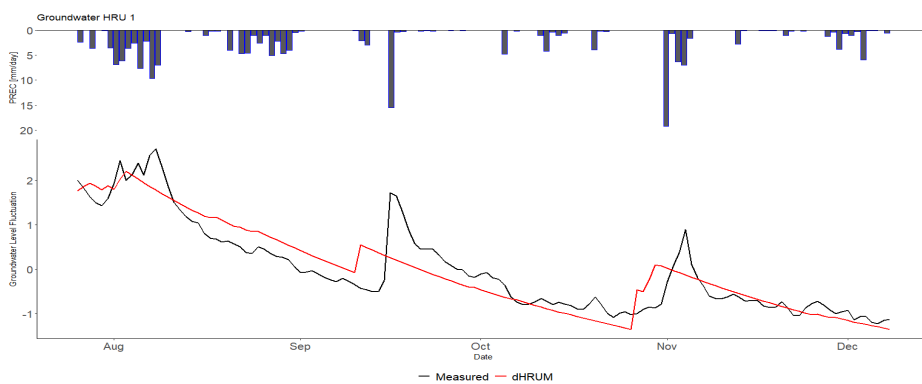


Fig. 13: Variations of GW level in HRU number 1 in BP\_D\_FG catchment

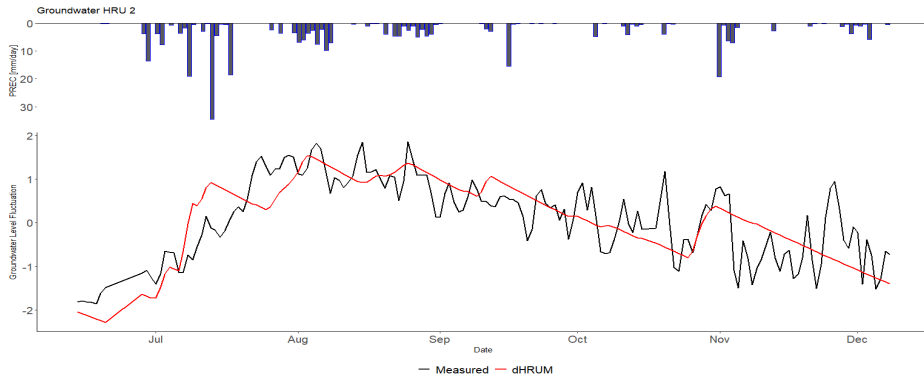


Fig. 14: Variations of GW level in HRU number 2 in BP\_D\_FG catchment

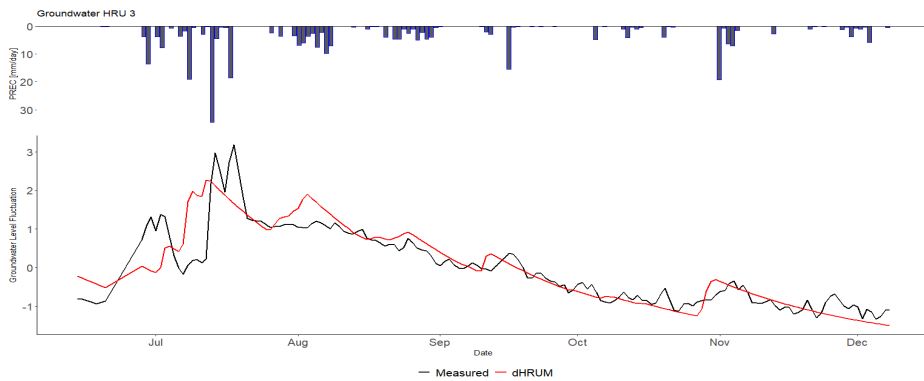


Fig. 15: Variations of GW level in HRU number 3 in BP\_D\_FG catchment

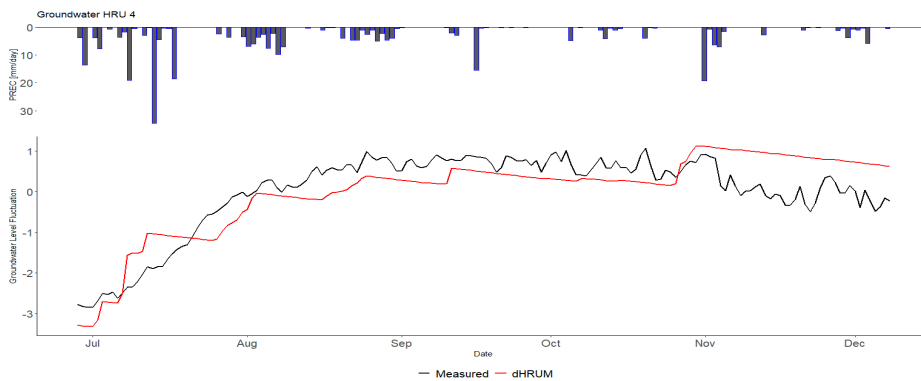


Fig. 16: Variations of GW level in HRU number 4 in BP\_D\_FG catchment

### Calibration Results Using SM

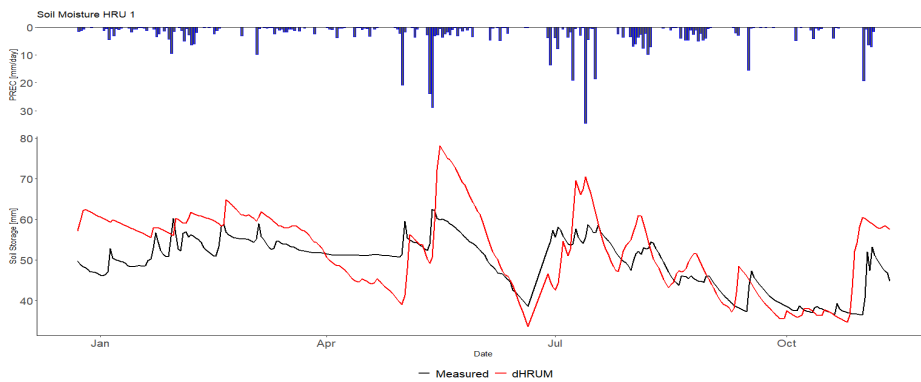


Fig. 17: Variations of SM storage in HRU number 1 in BP\_D\_FG catchment

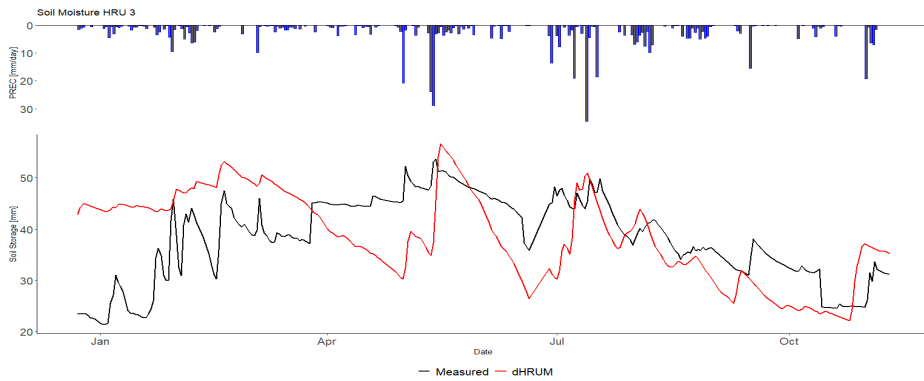


Fig. 18: Variations of SM storage in HRU number 3 in BP\_D\_FG catchment

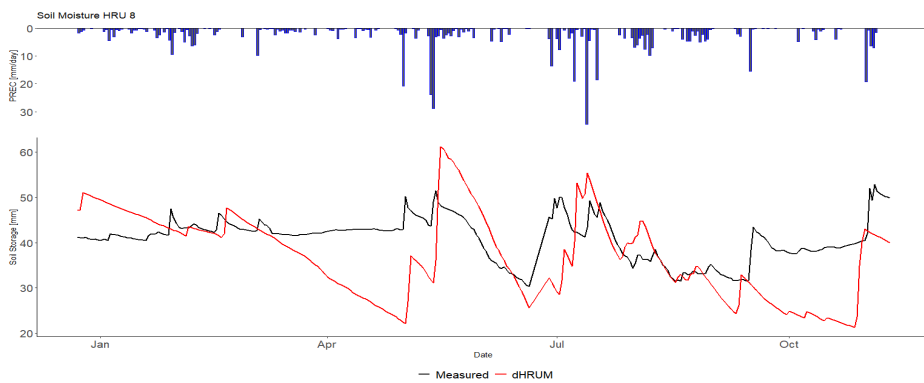


Fig. 19: Variations of SM storage in HRU number 8 in BP\_D\_FG catchment

### Calibration Results Using Both GW and SM

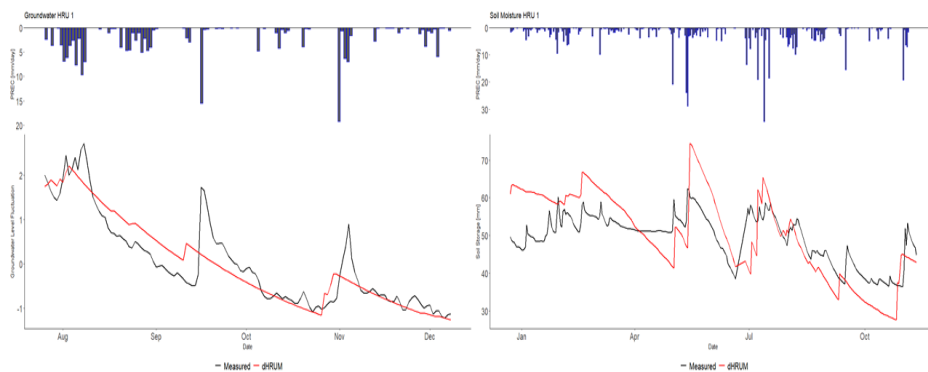


Fig. 20: Variations of GW and SM levels in HRU number 1 in BP\_D\_FG catchment

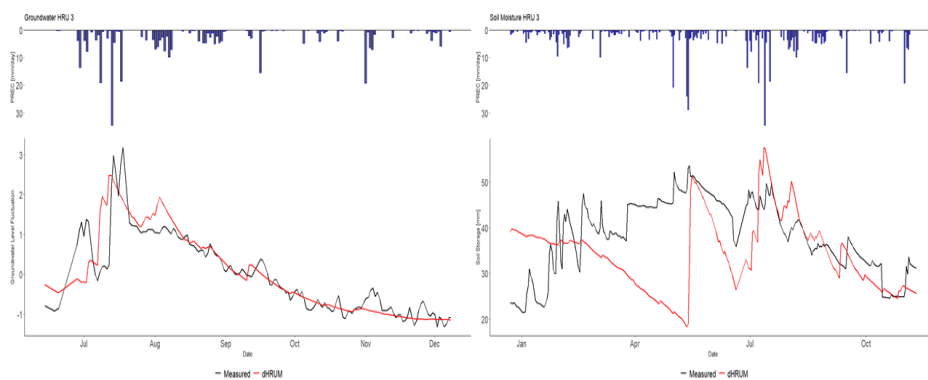


Fig. 21: Variations of GW and SM levels in HRU number 3 in BP\_D\_FG catchment

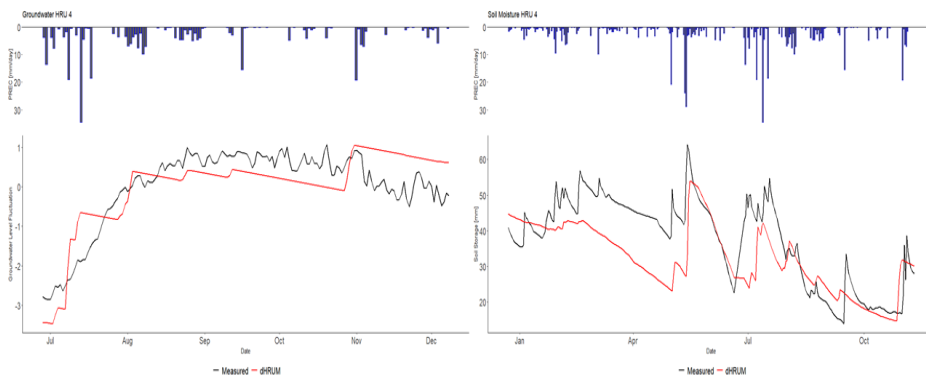


Fig. 22: Variations of GW and SM levels in HRU number 4 in BP\_D\_FG catchment

## BP\_S\_FG catchment

### Calibration Results Using GW

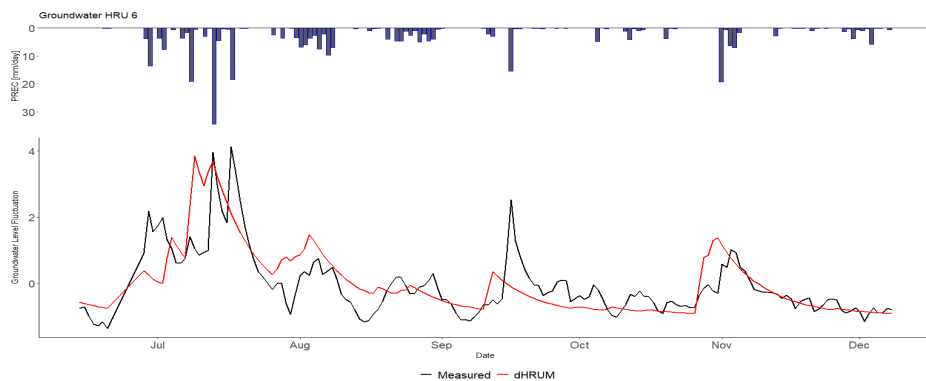


Fig. 23: Variations of GW level in HRU number 6 in BP\_S\_FG catchment

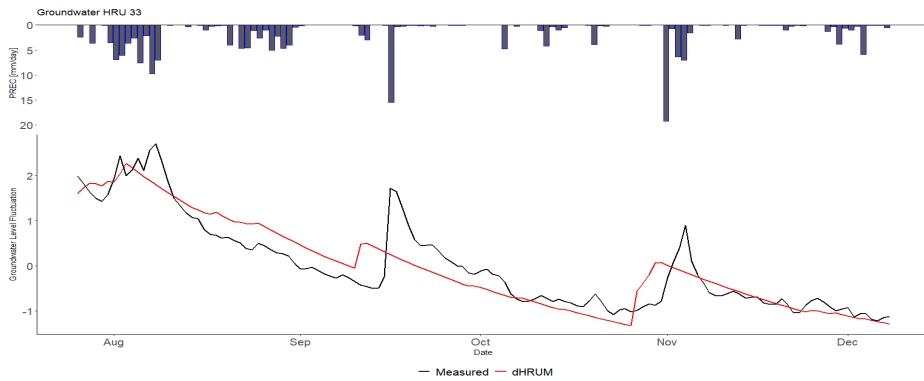


Fig. 24: Variations of GW level in HRU number 33 in BP\_S\_FG catchment

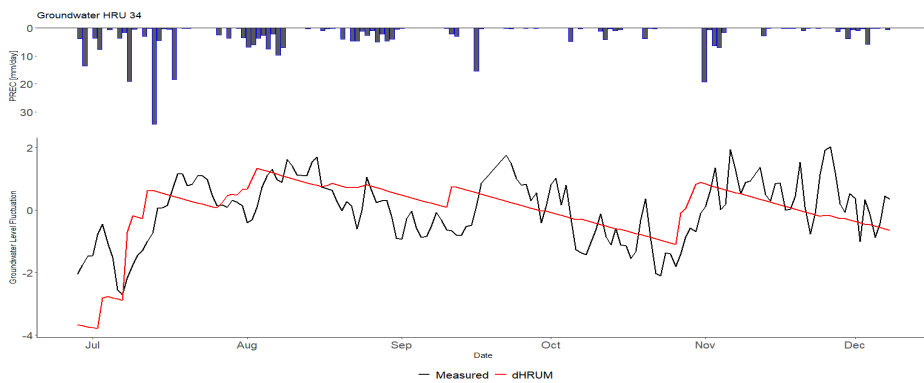


Fig. 25: Variations of GW level in HRU number 34 in BP\_S\_FG catchment

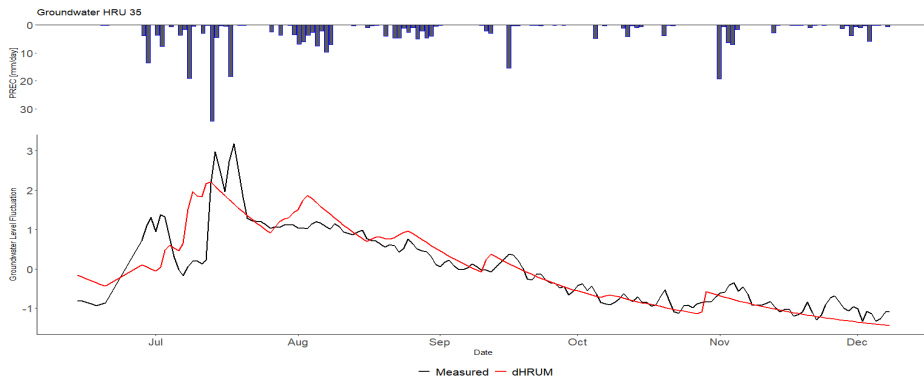


Fig. 26: Variations of GW level in HRU number 35 in BP\_S\_FG catchment

### Calibration Results Using SM

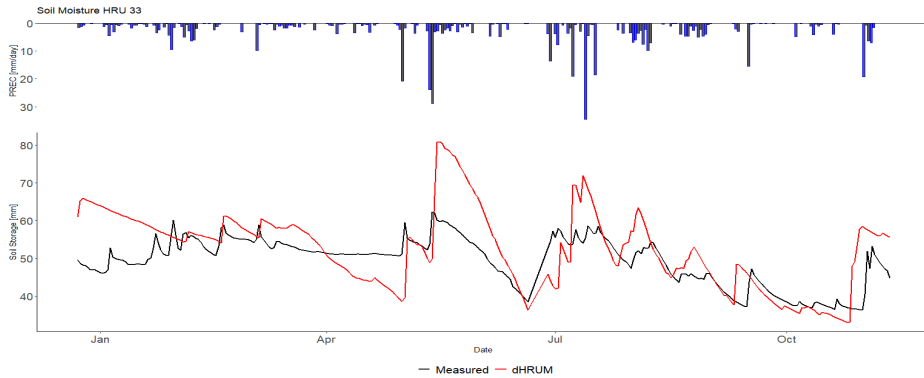


Fig. 27: Variations of SM storage in HRU number 33 in BP\_S\_FG catchment

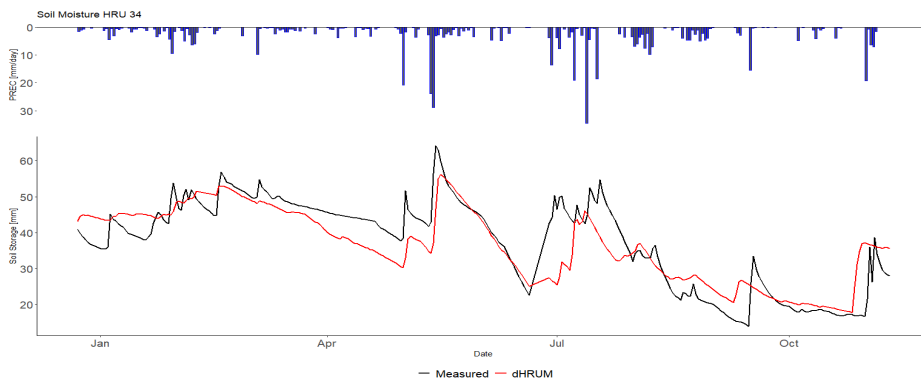


Fig. 28: Variations of SM storage in HRU number 34 in BP\_S\_FG catchment

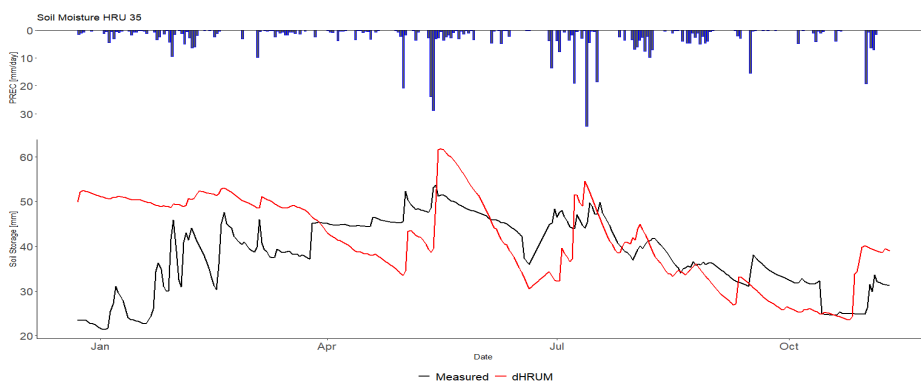


Fig. 29: Variations of SM storage in HRU number 35 in BP\_S\_FG catchment

### Calibration Results Using Both GW and SM

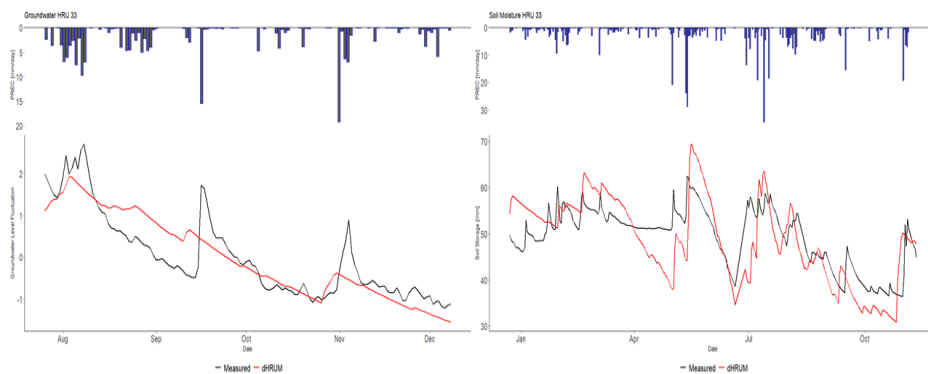


Fig. 30: Variations of GW and SM levels in HRU number 33 in BP\_S\_FG catchment

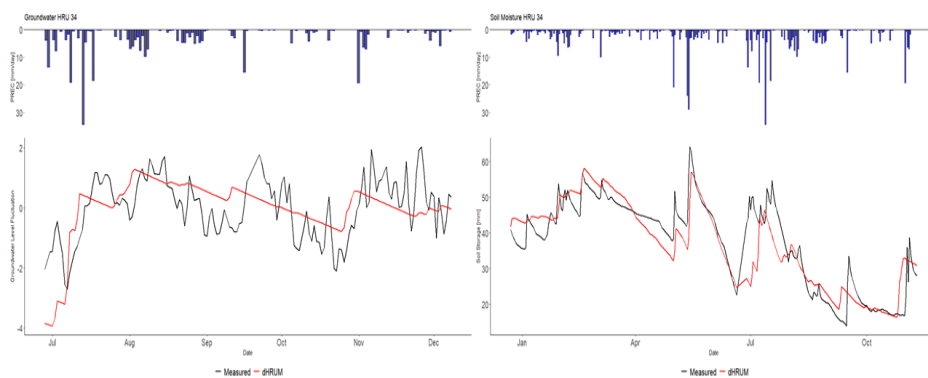


Fig. 31: Variations of GW and SM levels in HRU number 34 in BP\_S\_FG catchment

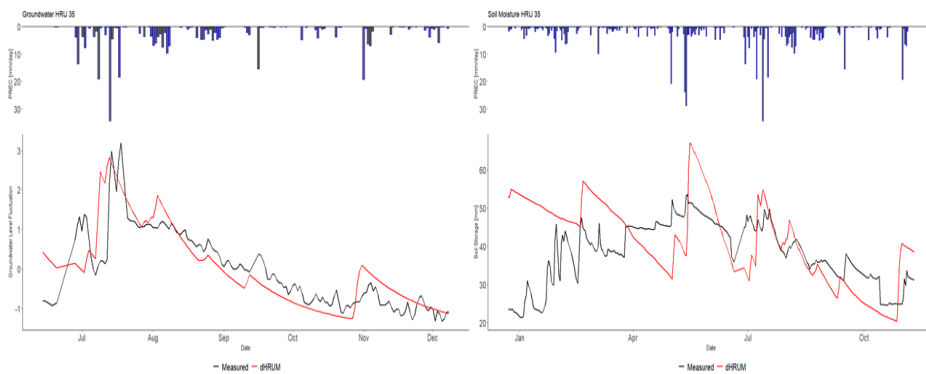


Fig. 32: Variations of GW and SM levels in HRU number 35 in BP\_S\_FG catchment

## KL\_D\_FG catchment

### Calibration Results Using GW

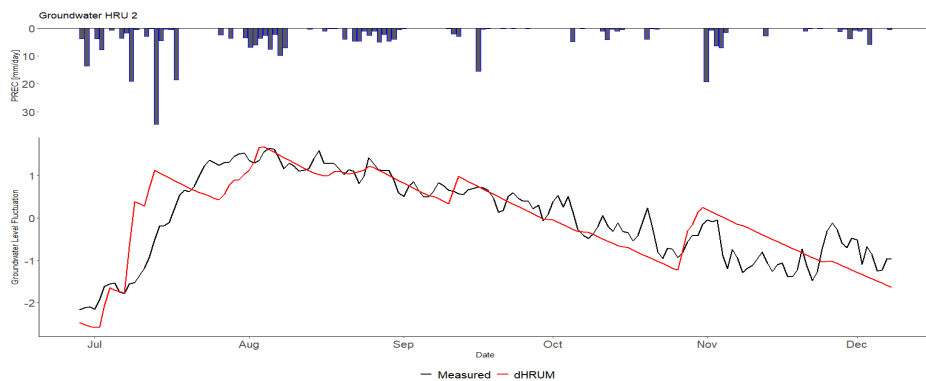


Fig. 33: Variations of GW level in HRU number 2 in KL\_D\_FG catchment

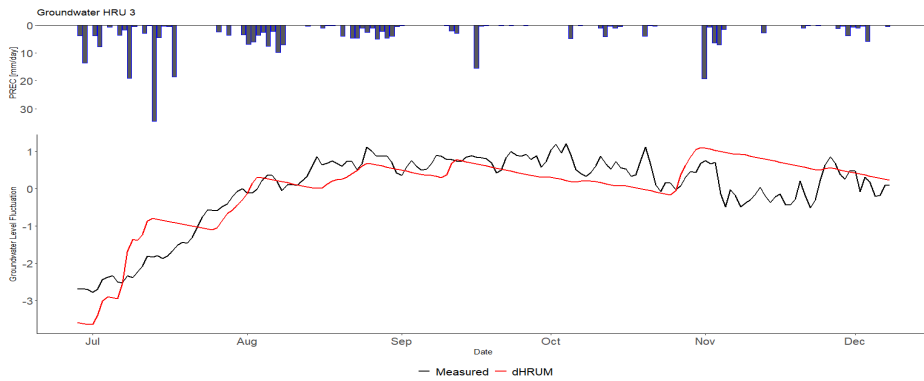


Fig. 34: Variations of GW level in HRU number 3 in KL\_D\_FG catchment

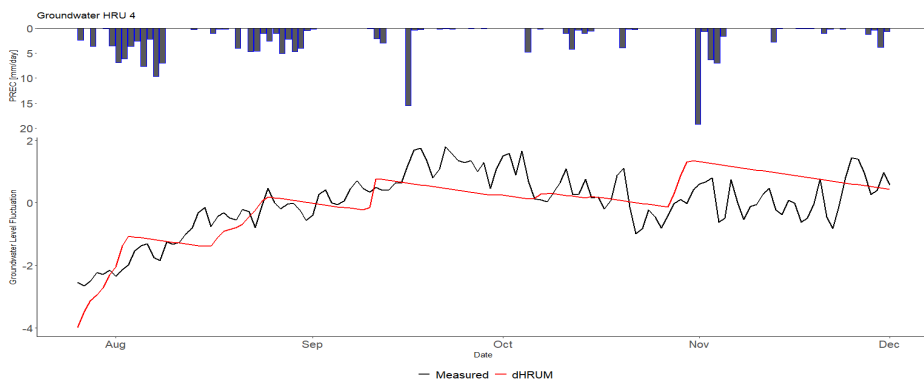


Fig. 35: Variations of GW level in HRU number 4 in KL\_D\_FG catchment

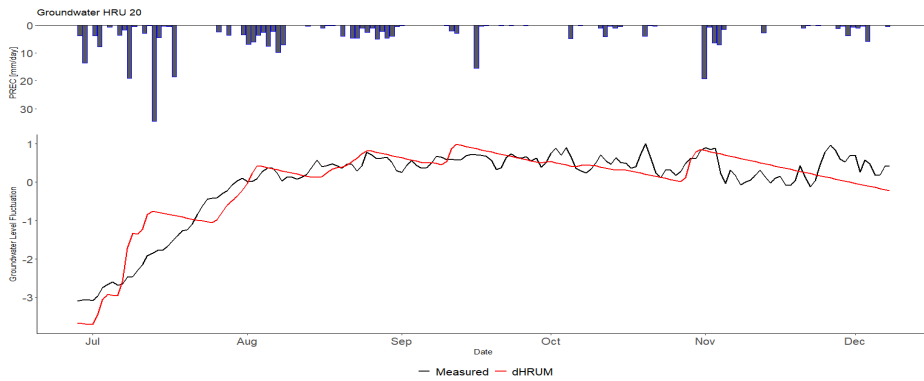


Fig. 36: Variations of GW level in HRU number 20 in KL\_D\_FG catchment

### Calibration Results Using SM

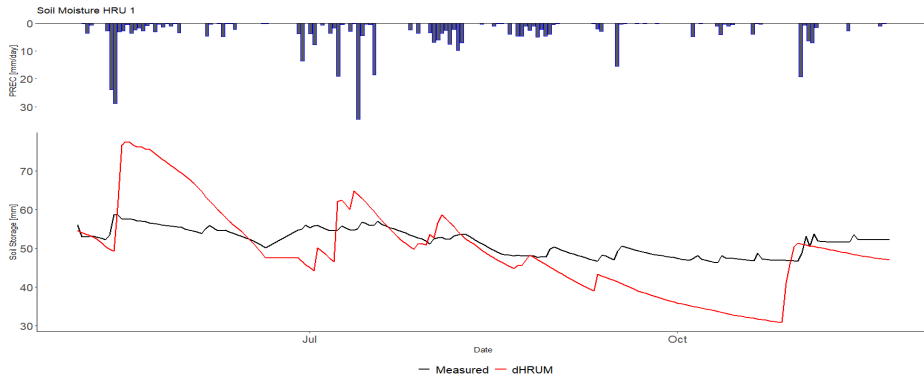


Fig. 37: Variations of SM storage in HRU number 1 in KL\_D\_FG catchment

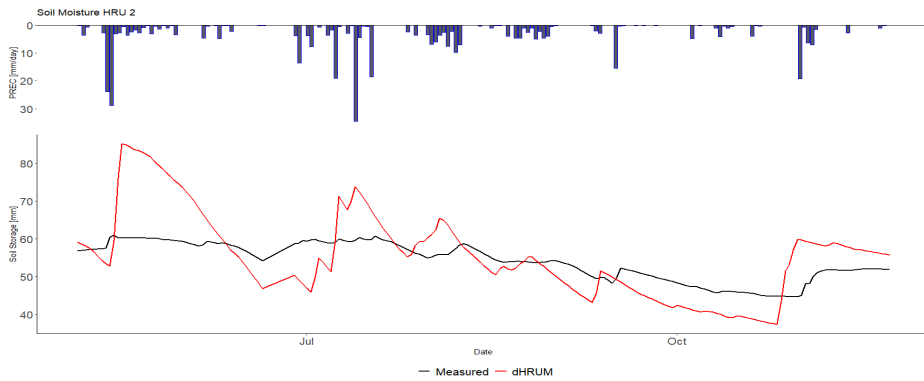


Fig. 38: Variations of SM Storage in HRU number 2 in BP\_S\_FG catchment

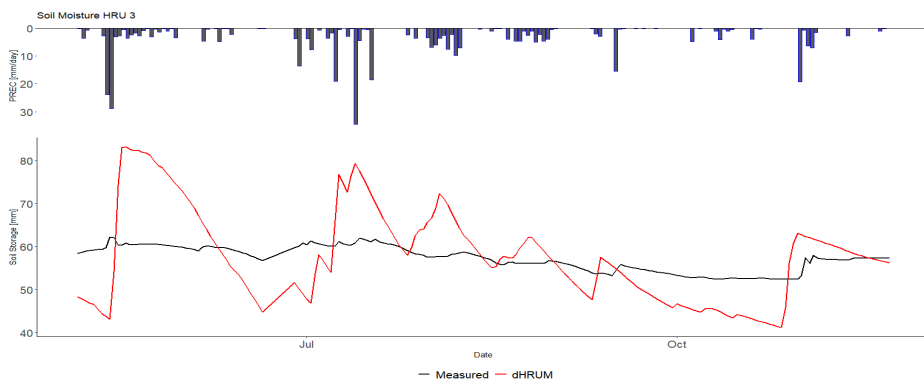


Fig. 39: Variations of SM Storage in HRU number 3 in KL\_D\_FG catchment

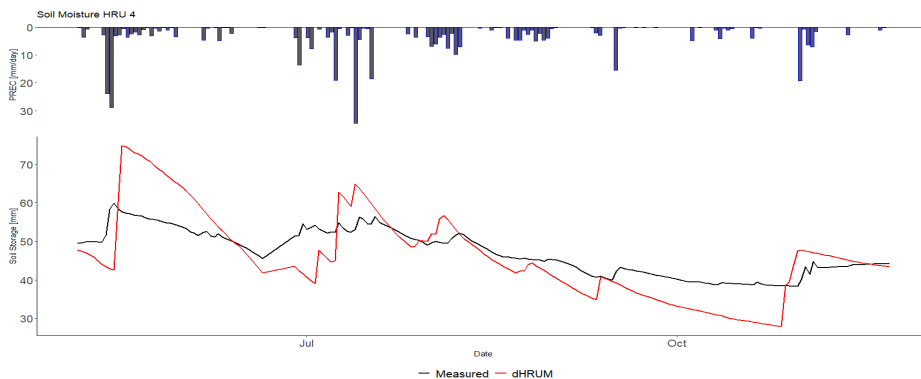


Fig. 40: Variations of SM Storage in HRU number 4 in KL\_D\_FG catchment

### Calibration Results Using Both GW and SM

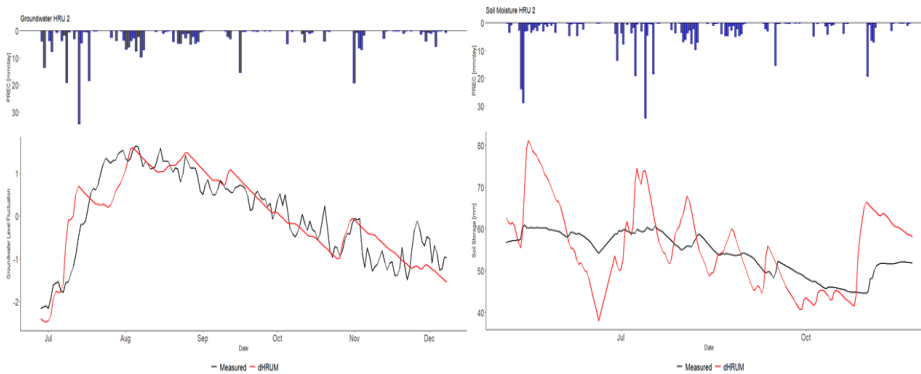


Fig. 41: Variations of GW and SM levels in HRU number 2 in KL\_D\_FG catchment

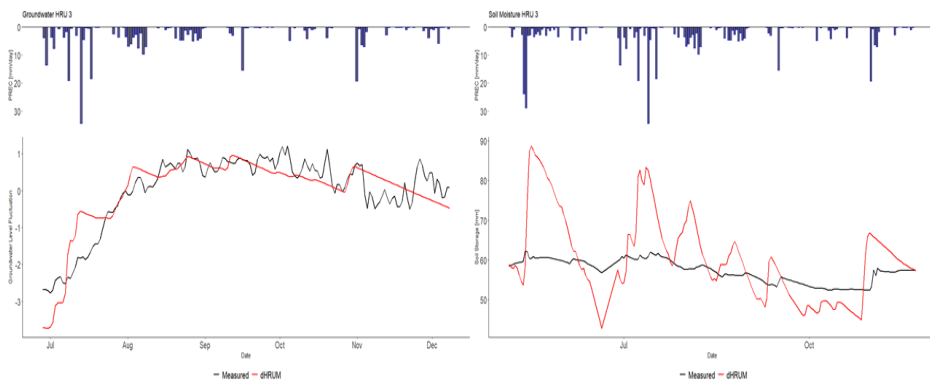


Fig. 42: Variations of GW and SM levels in HRU number 3 in KL\_D\_FG catchment

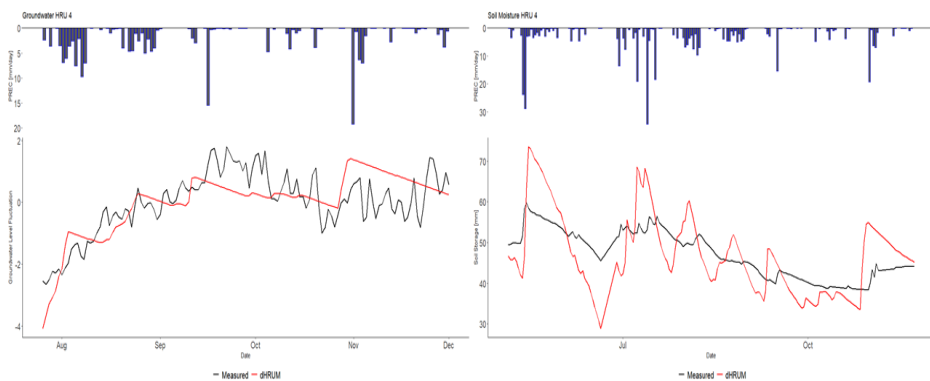


Fig. 43: Variations of GW and SM levels in HRU number 4 in KL\_D\_FG catchment

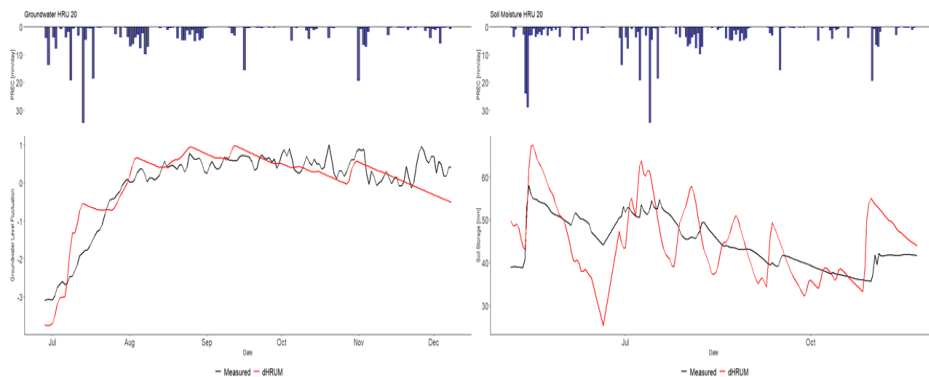


Fig. 44: Variations of GW and SM levels in HRU number 20 in KL\_D\_FG catchment

## KL\_S\_FG catchment

### Calibration Results Using GW

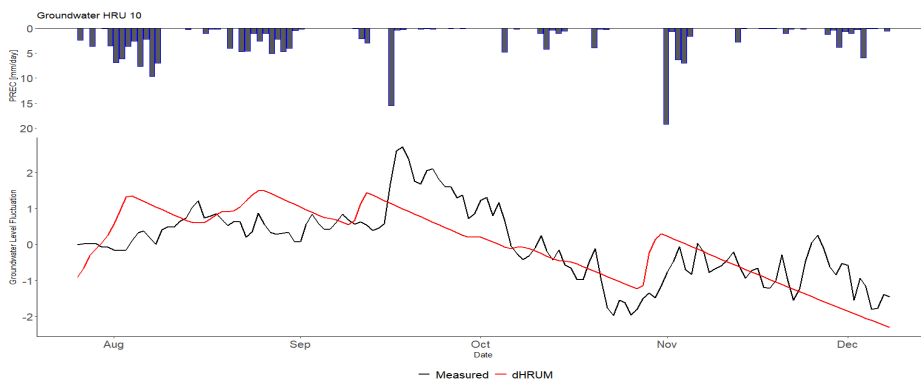


Fig. 45: Variations of GW level in HRU number 10 in KL\_S\_FG catchment

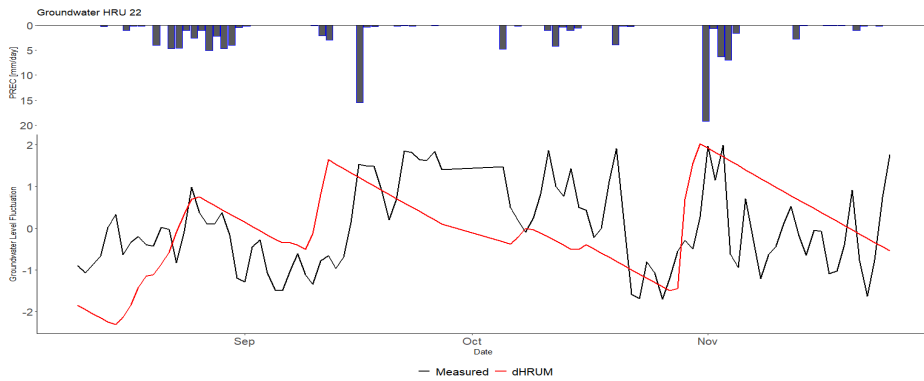


Fig. 46: Variations of GW level in HRU number 22 in KL\_S\_FG catchment

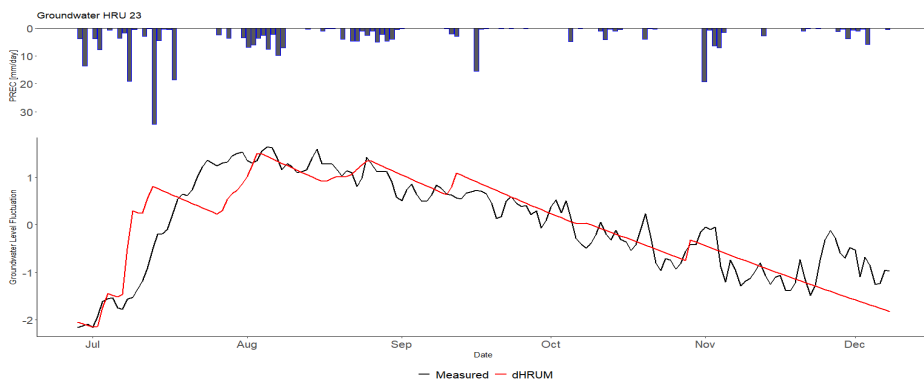


Fig. 47: Variations of GW level in HRU number 23 in KL\_S\_FG catchment

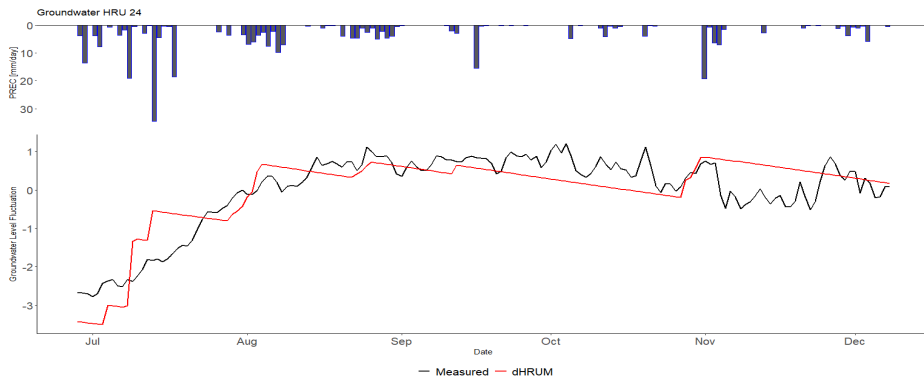


Fig. 48: Variations of GW level in HRU number 24 in KL\_S\_FG catchment

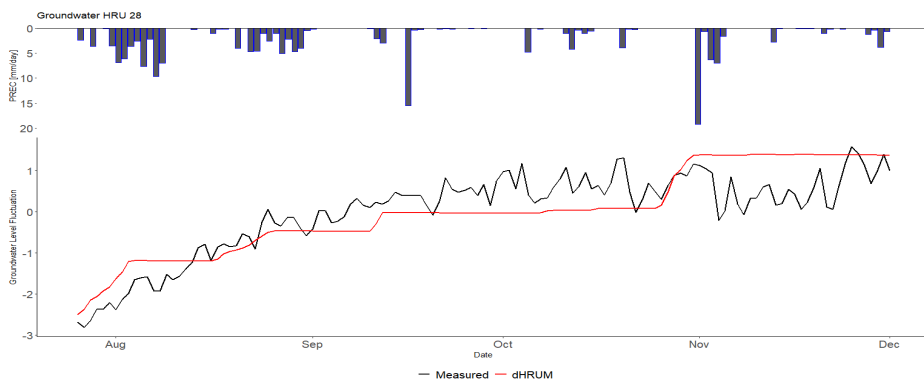


Fig. 49: Variations of GW level in HRU number 28 in KL\_S\_FG catchment

### Calibration Results Using SM

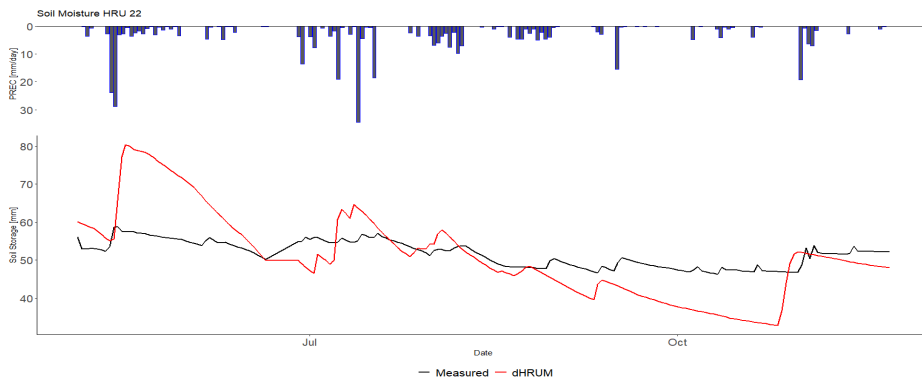


Fig. 50: Variations of SM storage in HRU number 22 in KL\_S\_FG catchment

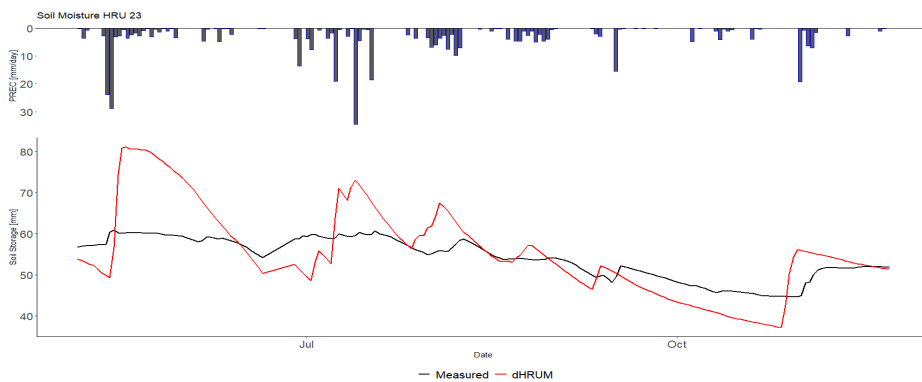


Fig. 51: Variations of SM storage in HRU number 23 in KL\_S\_FG catchment

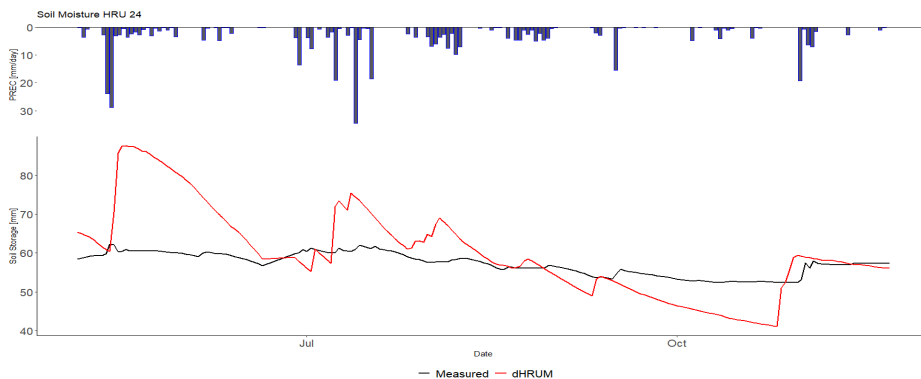


Fig. 52: Variations of SM storage in HRU number 24 in KL\_S\_FG catchment

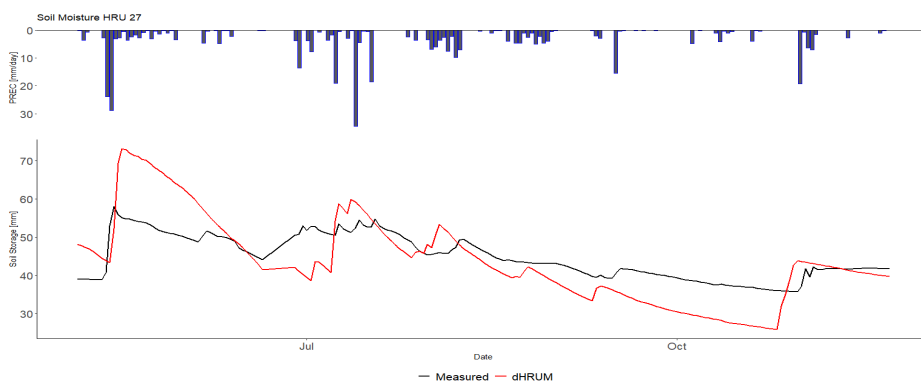


Fig. 53: Variations of SM storage in HRU number 27 in KL\_S\_FG catchment

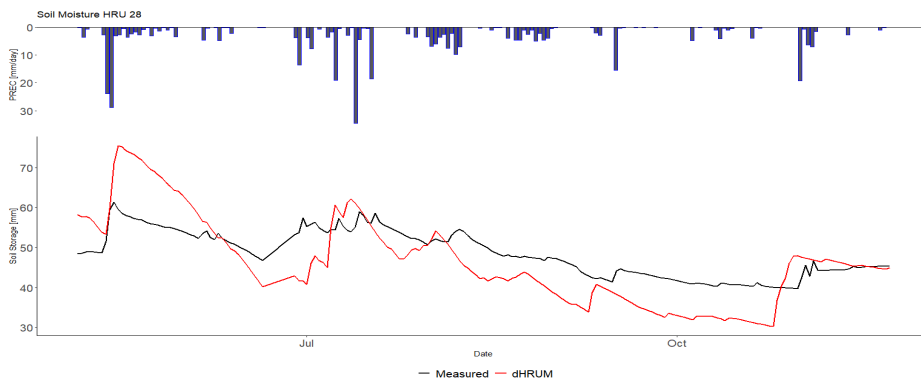


Fig. 54: Variations of SM storage in HRU number 28 in KL\_S\_FG catchment

### Calibration Results Using Both GW and SM

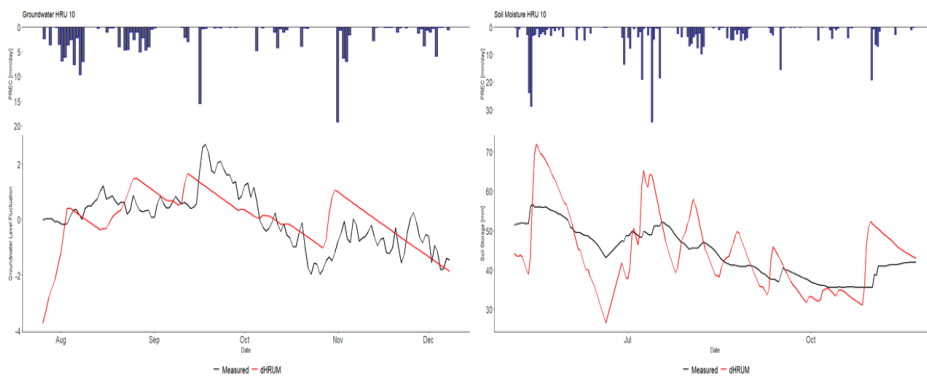


Fig. 55: Variations of GW and SM levels in HRU number 10 in KL\_S\_FG catchment

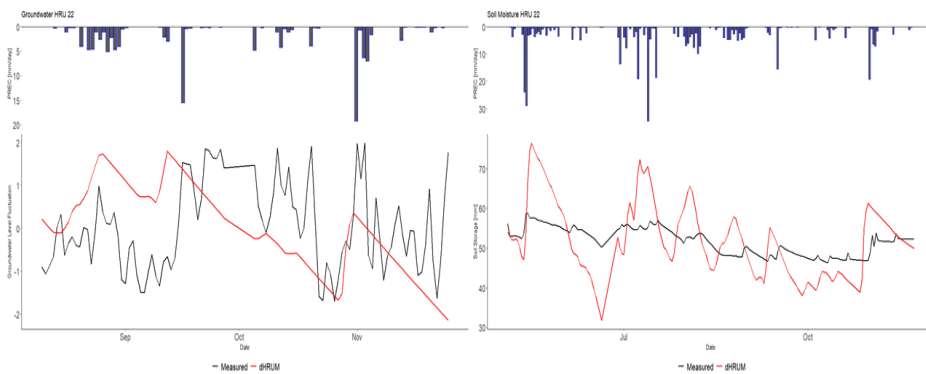


Fig. 56: Variations of GW and SM levels in HRU number 22 in KL\_S\_FG catchment

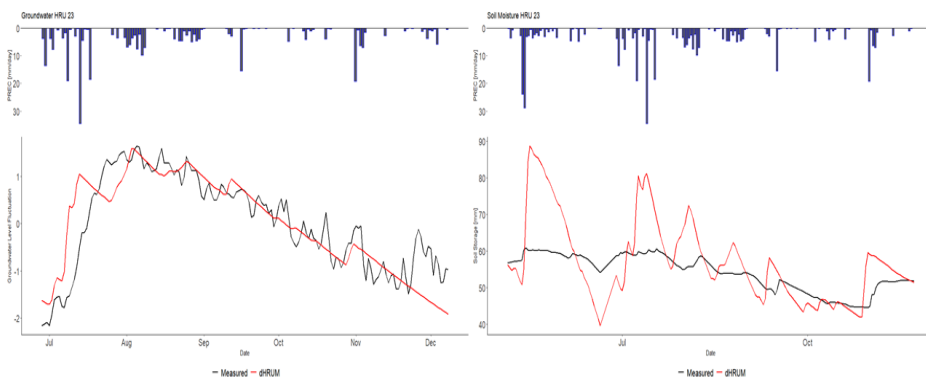


Fig. 57: Variations of GW and SM levels in HRU number 23 in KL\_S\_FG catchment

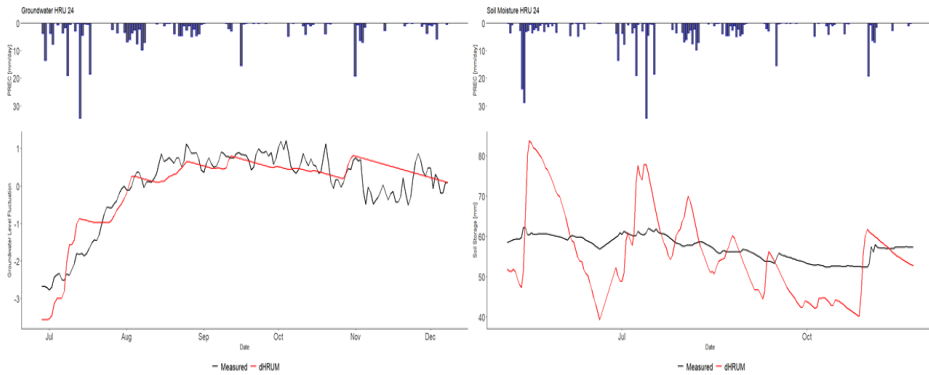


Fig. 58: Variations of GW and SM levels in HRU number 24 in KL\_S\_FG catchment

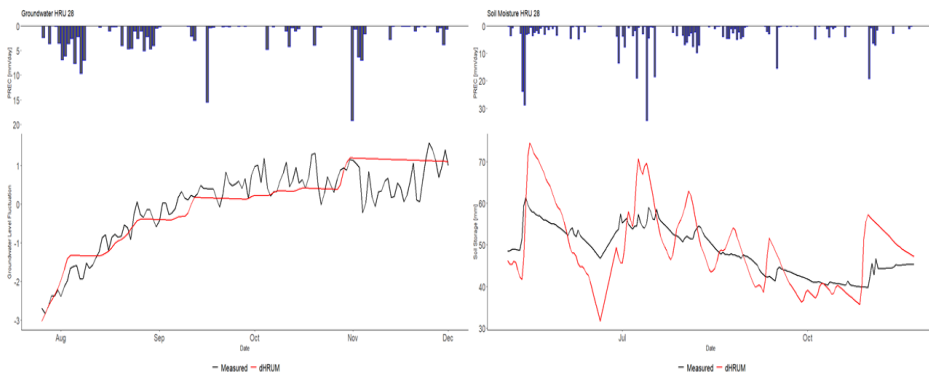


Fig. 59: Variations of GW and SM levels in HRU number 28 in KL\_S\_FG catchment